Performance Test of a Steam-Assisted Elevated Flare with Passive FTIR - Detroit

Final Report
November 23, 2010

Marathon Petroleum Company, LP
Detroit Refinery
1300 South Fort Street
Detroit, MI 48217

Testing Conducted
July 8 - 20, 2010

Prepared by
Clean Air Engineering, Inc.
Project No: 10971

Table of Contents

Acknowledgements

The Primary Authors for this report were:

Bill Ewing – Marathon Petroleum Company

Daniel Roesler – Clean Air Engineering

Scott Evans – Clean Air Engineering

This report would not have been possible without extensive input and feedback from others involved with this project. We wish to acknowledge the following people for their invaluable contributions to this project and this report.

Emily Barron – Marathon Petroleum Company

Ruth Cade – Marathon Petroleum Company

Bryan Duryee – Marathon Petroleum Company

Keith Boyd – Marathon Petroleum Company

Crystal Davis – Marathon Petroleum Company

Dr. Robert Spellicy – Industrial Monitor and Control Corporation

Mark Sloss – Industrial Monitor and Control Corporation

Jim Franklin – John Zink Company, LLC

1.0 Background and Summary

1.1 Overview

As required by a Clean Air Act Section 114 request for testing a refinery steam-assisted flare, Marathon Petroleum Company (MPC) conducted performance testing of the Complex 3 and 4 (CP) flare at the Detroit, MI refinery. This test was the second performance test on steam-assisted flares by MPC, following the test in Texas City, TX, in 2009.[1] The main objective of the test was to better understand the impacts of steam on the overall performance of the flare in terms of combustion efficiency (CE). The performance tests were conducted using a Passive Fourier Transform Infrared Spectroscopy (PFTIR) instrument developed and operated by Industrial Monitor and Control Corporation (IMACC). This report contains the Detroit test results and compares them to the Texas City test results.

Figure 1.1-1: Complex 3 and 4 Flare Tip

The purpose and major benefit of a steam injection system is to significantly reduce the amount of smoke (visible emissions) that would otherwise be created by combustion. In a typical system, steam is injected into the flare combustion zone to deliver educted air as well as mixing energy. Over-steaming is a generic description of an undesirable operating condition possible in steam-assisted flare systems. In an over-steaming scenario, it is possible that the amount of steam and educted air introduced into the combustion reaction zone diminishes, rather than promotes, the efficiency of the combustion process if introduced in large enough quantities.

[1] PERFORMANCE TEST OF A STEAM-ASSISTED ELEVATED FLARE WITH PASSIVE FTIR, Marathon Petroleum Company, Texas City, TX, May 2010

The operating envelope of a flare is bounded by excess visible emissions (i.e., too little steam) and excess emissions of volatile organic compounds (VOCs) (i.e., too much steam). The efficiency of any particular steam injection system with respect to smoke suppression is easily measured by monitoring steam rates and visually observing smoking performance. However, the ability to measure or even identify excess emissions caused by over-steaming is a more difficult task. Standard emissions estimation techniques have generally assumed a 98% combustion efficiency or higher when calculating VOC emissions from flares.

Regulatory requirements for flares are contained in 40 CFR §60.18 and §63.11. These requirements were developed from a series of flare emissions tests led by the United States Environmental Protection Agency (US EPA) from 1983 – 1986.[2,3,4] The requirements include maintaining a flare pilot, operating with a minimum net heating value of 300 BTU/scf in the vent gas, operating at exit velocities of less than 60 ft/s (or 400 ft/s depending upon the vent gas net heating value), and operating with a limited amount of visible emissions. However, a flare can be operated in compliance with these requirements and still be over-steamed.

Prior to the recent refinery tests of flare performance, including the US EPA tests in the mid-1980s, were conducted on pilot-scale test flares at moderate to high vent gas loads. However, a flare typically operates at low vent gas loads (i.e. high turndown) under normal conditions until a process upset or other operating condition requires the operator to flare waste gas. Thus, the flare normally operates at high turndown for the majority of the operating year, a condition for which there is little to no available performance data.

In the past, measuring the combustion products from a flare was difficult and dangerous. Recent technological advances, however, have produced remote sensing instruments capable of indicating the presence of combustion products such as carbon dioxide, carbon monoxide, and select hydrocarbons without the safety hazards introduced by physically sampling a flare plume. One such instrument is the PFTIR, which characterizes a plume's chemical make-up (carbon dioxide, carbon monoxide, and total hydrocarbons) in units of concentration × pathlength. Using this technology, the absolute concentration cannot be determined, but the product of concentration × pathlength (e.g., ppmv × meters), can be used in combustion efficiency calculations. The PFTIR is a relatively new tool that has not yet been blind-validated against extractive sampling results for flare plume testing. The Texas Commission on Environmental Quality (TCEQ) evaluated the PFTIR against extractive FTIR in 2004[5], and the PFTIR was first

[2] EVALUATION OF THE EFFICIENY OF INDUSTRIAL FLARES: TEST RESULTS, United States Environmental Protection Agency, Office of Air Quality Planning and Standards, EPA-600/2-84-095, May 1984

[3] EVALUATION OF THE EFFICIENY OF INDUSTRIAL FLARES: FLARE HEAD DESIGN AND GAS COMPOSITION, United States Environmental Protection Agency, Office of Air Quality Planning and Standards, EPA-600/2-85-106, May 1985

[4] EVALUATION OF THE EFFICIENY OF INDUSTRIAL FLARES: H2S GAS MIXTURES AND PILOT ASSISTED FLARES, United States Environmental Protection Agency, Office of Air Quality Planning and Standards, EPA-600/2-86-080, May 1986

[5] PASSIVE FTIR PHASE 1 TESTING OF SIMULATED AND CONTROLLED FLARE SYSTEMS, Texas Commission on Environmental Quality, June 2004

used for refinery flare testing at MPC Texas City in 2009. Recent testing conducted by TCEQ and the University of Texas did subject the PFTIR to blind testing however, the results of this study were not available at the time of the issuance of this report. Several accuracy, precision, and variability checks were performed during the Detroit test to challenge the PFTIR measurement technique.

1.2 Results

The PFTIR performance test conducted on MPC's Detroit CP flare produced valuable insights into the efficiency performance of the flare under a variety of conditions. Tests were conducted while flaring gases containing a base gas mixture, refinery fuel gas, propylene, hydrogen, and nitrogen mixtures. Figure 1.2-1 shows the S/VG ratios tested for each test series.

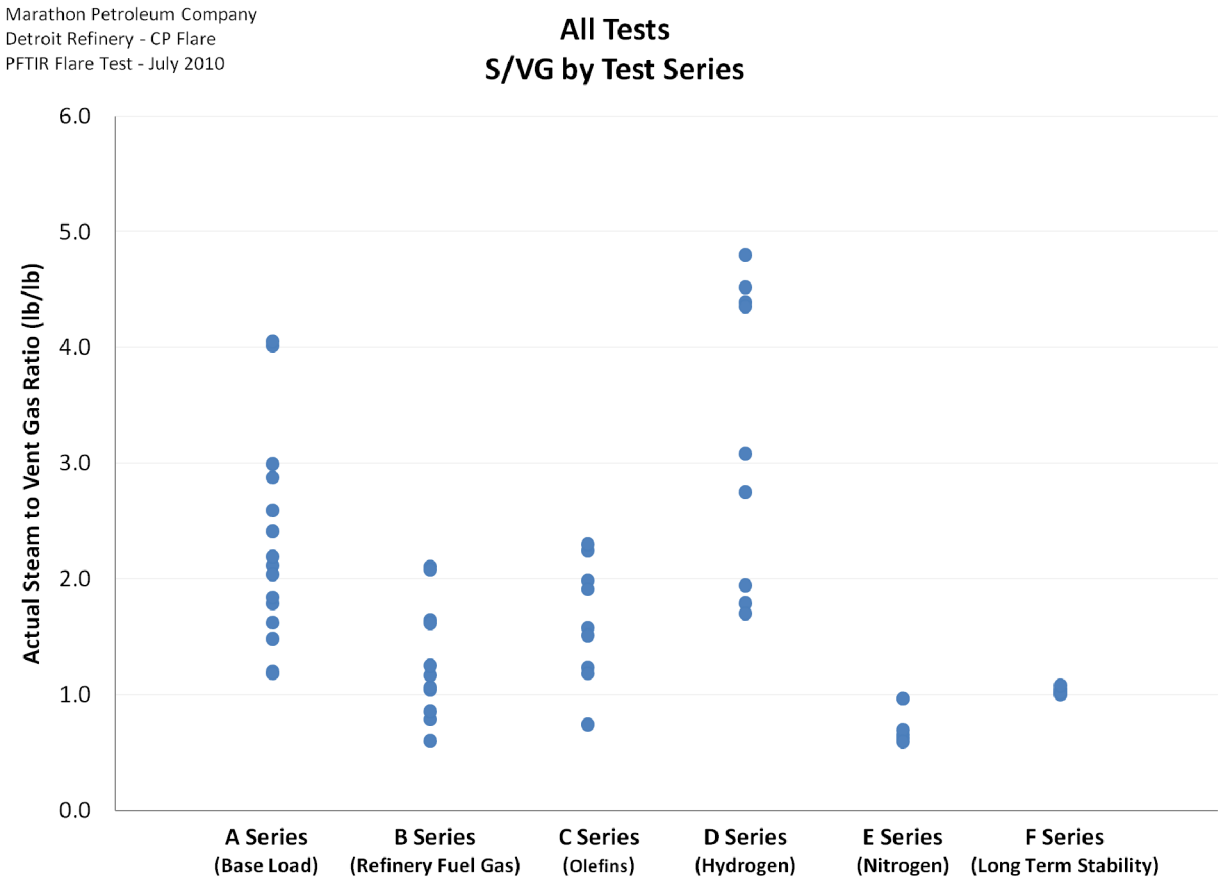

Figure 1.2-1: S/VG Ratios by Test Series

For the base load, refinery fuel gas, and propylene test series, steam was increased from the point of incipient smoke to a point just before snuffing the flare. For these test series, CE remained relatively constant at a high level until the steam to vent gas (S/VG) ratio reached a critical point after which, CE declined with increasing steam. Figures 1.2-2 and 1.2-3 show this trend in a lb/lb and scf/scf basis. Note that the variability of combustion efficiency also increased with increased S/VG.

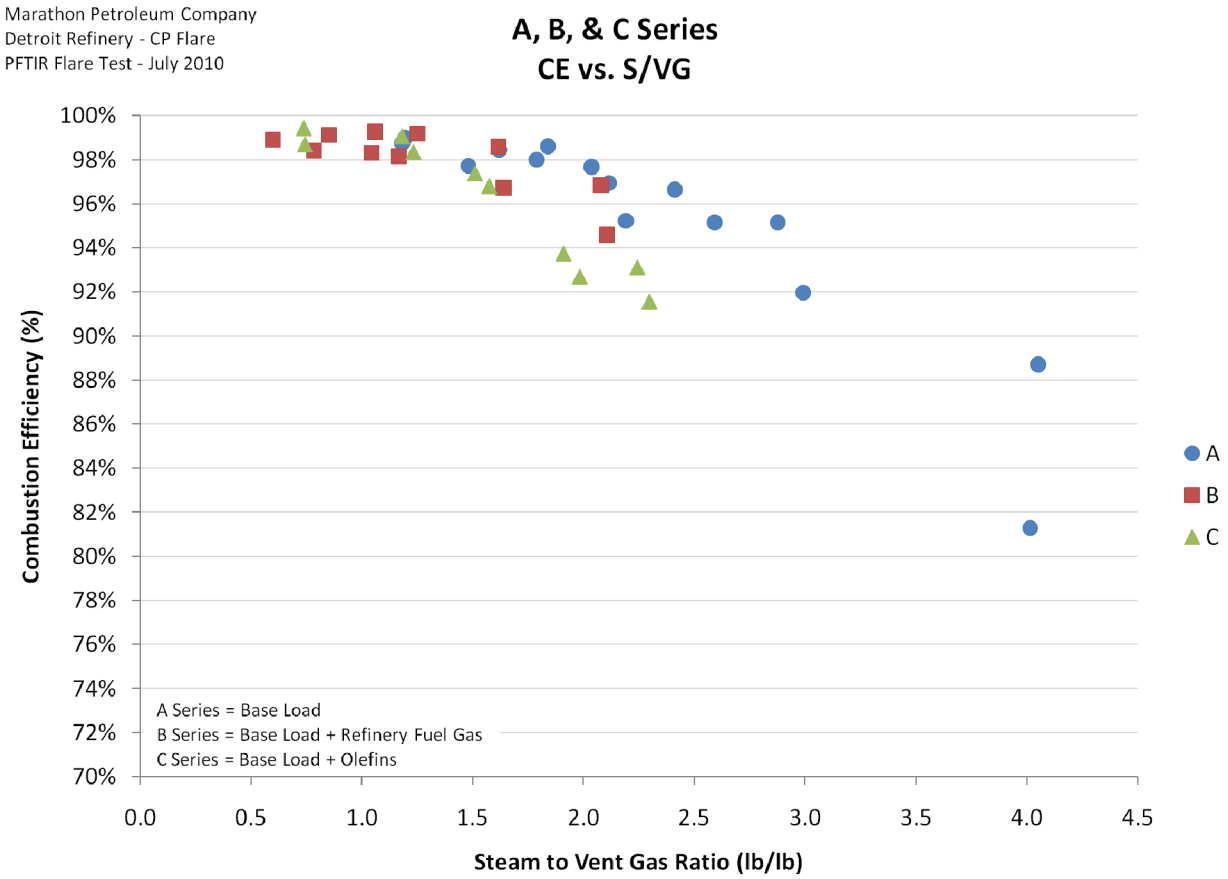

Figure 1.2-2: Combustion Efficiency vs. S/VG (lb/lb): Test Series A, B, and C

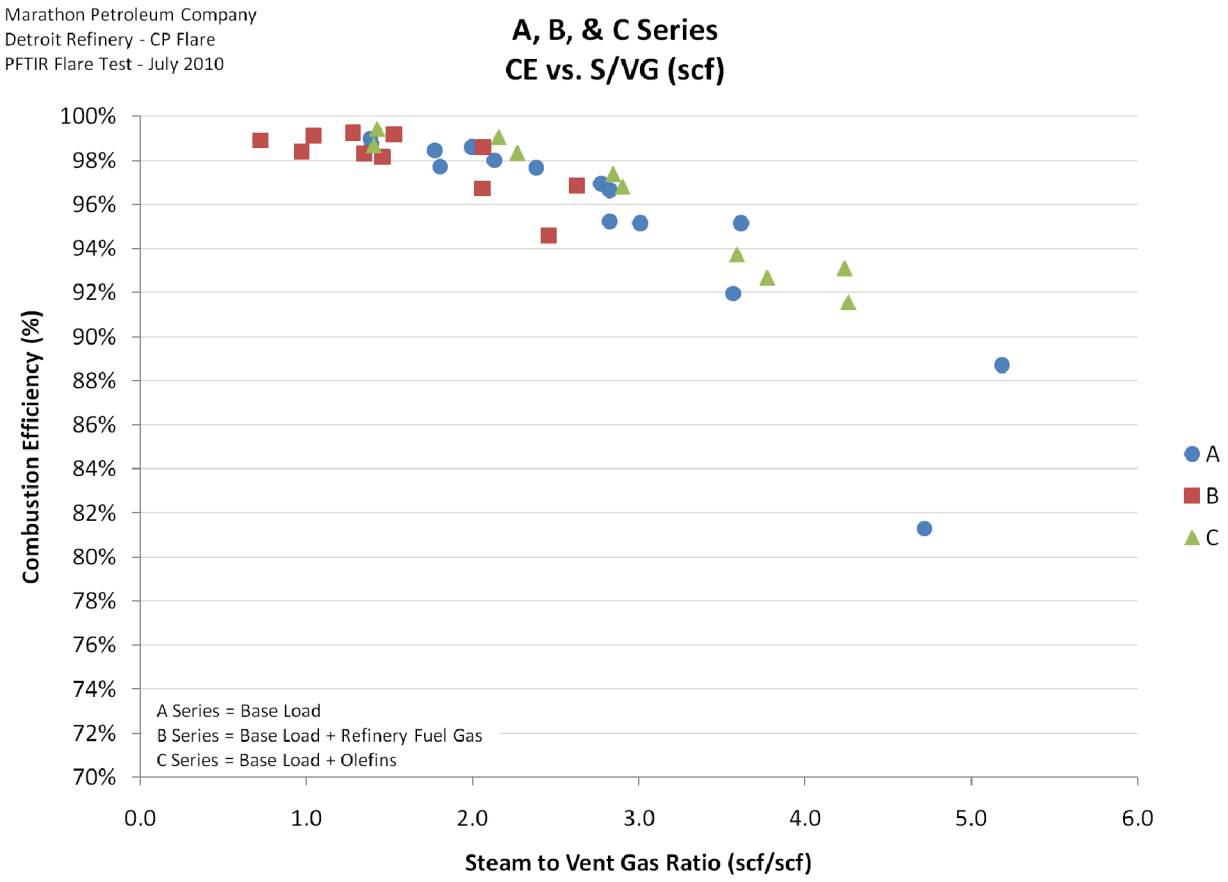

Figure 1.2-3: Combustion Efficiency vs. S/VG (scf/scf): Test Series A, B, and C

A slightly different test protocol was used when conducting the hydrogen and nitrogen test series. Both the vent gas composition and the flare steam rate were varied. For the hydrogen test series, the percent hydrogen in the vent gas was sequentially increased. For each hydrogen level the steam rate was varied. Due to the small number of data points for this condition, any conclusions are highly tentative. However, this test series may indicate that hydrogen does not have a significant effect at low S/VG ratios. However, at higher S/VG ratios the rate of combustion efficiency decline may be less with higher hydrogen vent gas content. Figure 1.2-4 shows the results from the hydrogen test series. Test series A is also shown because the base load normally contains about 20% hydrogen. More detail on these tests is found in Section 3.1.2.

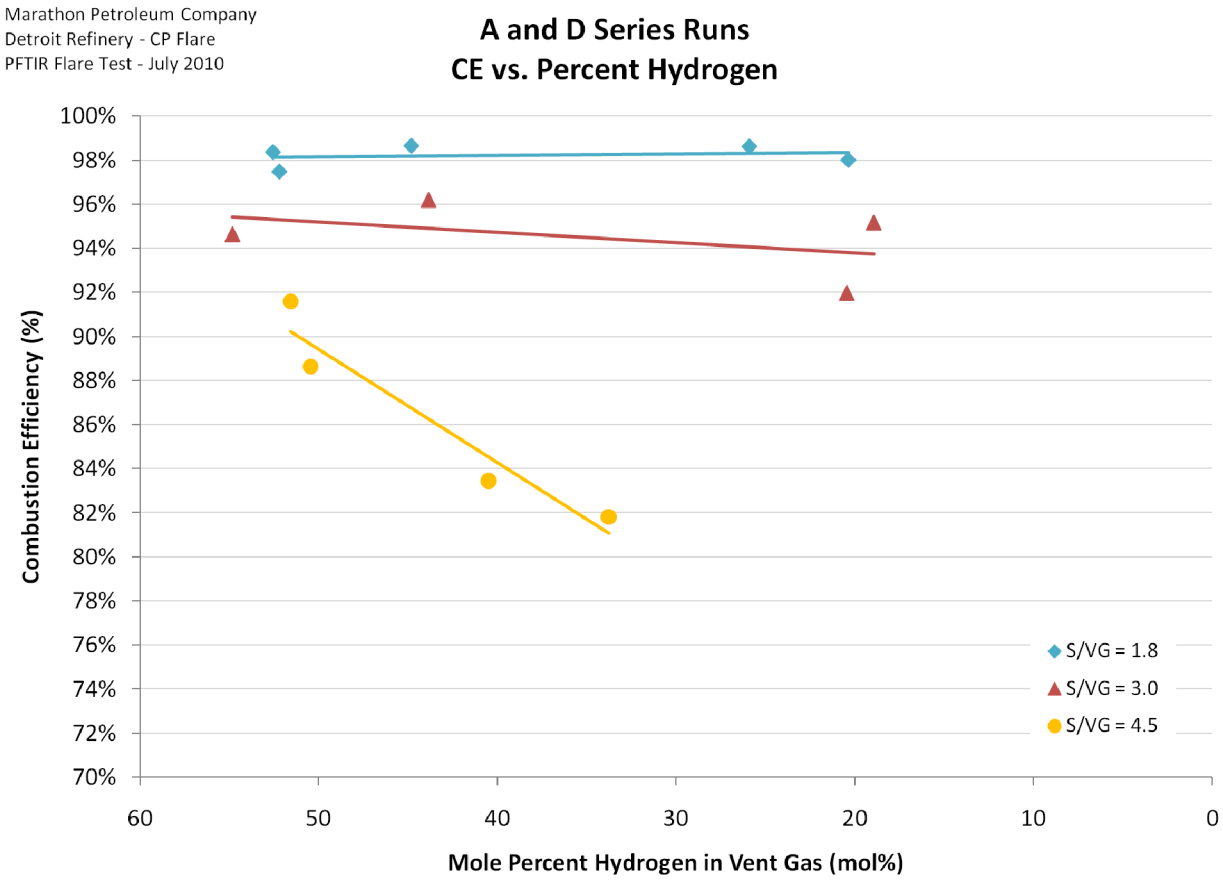

Figure 1.2-4: Combustion Efficiency vs. % Hydrogen: Test Series D (Hydrogen)

For the nitrogen test series, nitrogen was added sequentially to the vent gas to decrease the vent gas net heating value with the inert gas then runs were performed at two different steam rates. This test series showed decreasing combustion efficiencies with increasing nitrogen content. Figure 1.2-5 shows the combustion efficiency decreasing as combustion zone gas net heating value declines. Further detail on these tests is found in Section 3.1.3.

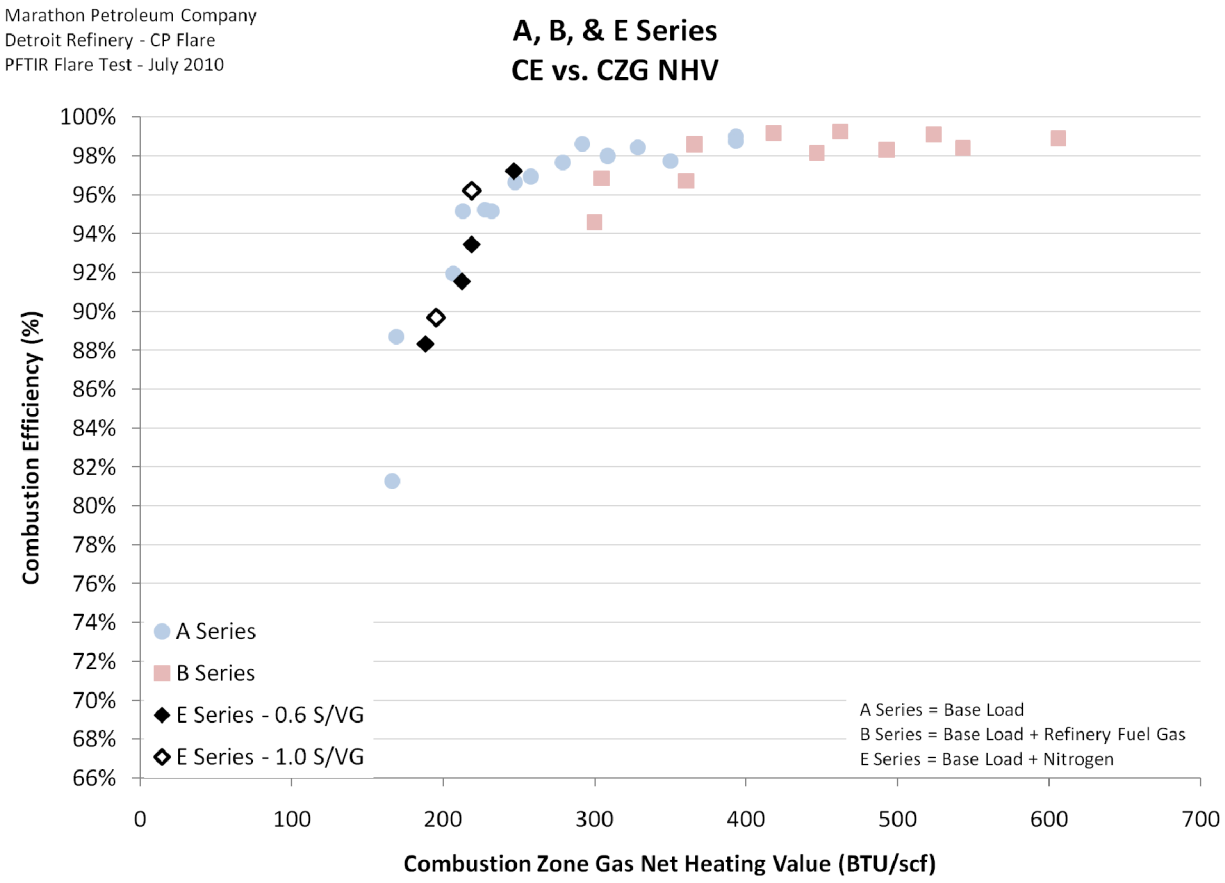

Figure 1.2-5: Combustion Efficiency vs. CZG NHV: Test Series E (Nitrogen)

The performance test data also yielded insights into variables that could potentially be used as parametric monitoring points to ensure high efficiency during high turndown operation. As seen in Figure 1.2-5, the Combustion Zone Gas Net Heating Value (CZG NHV) is a calculated term representing the net heating value of all components in the combustion zone. The combustion zone is directly above the flare tip and is the point at which all materials combine for combustion. The CZG NHV is therefore the resultant heat content from the mixture of the vent gas from the flare header, the pilot gas, and the total steam. The CZG NHV showed a correlation to combustion efficiency, with efficiency declining at about 250 BTU/scf for the base load and refinery fuel gas test series and at about 425 BTU/scf for the propylene Test Series. Figure 1.2-6 shows the relationship between combustion efficiency and CZG NHV.

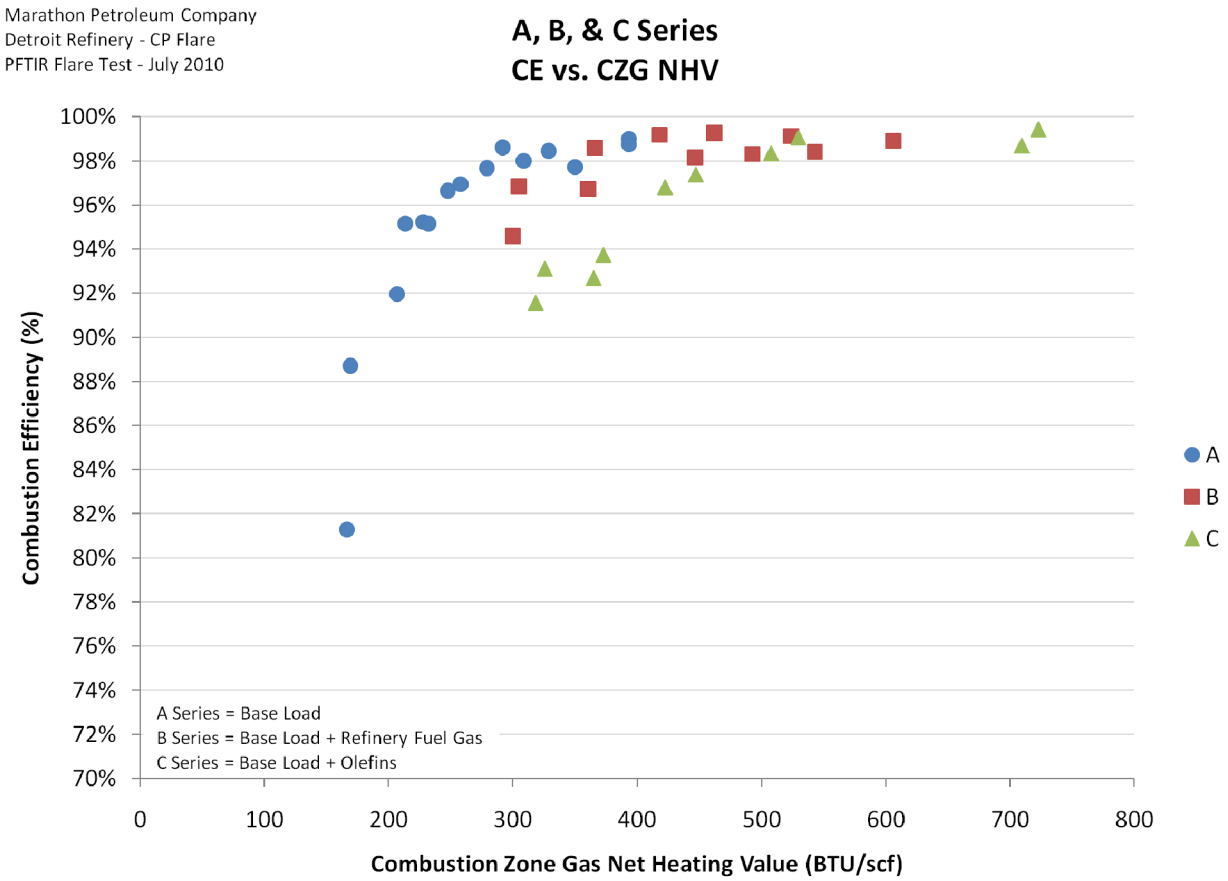

Figure 1.2-6: Combustion Efficiency vs. CZG NHV: Test Series A, B, and C

The combustion efficiency results are similar to the results from the 2009 Texas City flare performance test. The trends for the base load, refinery fuel gas, and propylene test series show approximately the same inflection points in both the Detroit Texas City tests. Unlike Texas City, which did not have favorable wind conditions for the hydrogen and nitrogen test series, Detroit wind conditions were much more favorable for the hydrogen and nitrogen test series.

Based on the data collecting during the two test programs conducted at Marathon facilities, we believe the PFTIR test method is capable of identifying general flare performance trends. However, additional research is needed to characterize the overall precision and bias of the method. Based on analysis of the Long Term Stability tests, method precision improved for the Detroit test as compared to the Texas City test. One reason for this may be that the PFTIR instruments used for the Detroit test employed more advanced detectors and data reduction software than the PFTIR used in the Texas City test. Method protocols were also improved based on lessons learned in Texas City.

As an overall accuracy check, an FCCU stack was measured by the PFTIR prior to testing and the results compared to the certified CEMS installed on the stack. The primary PFTIR used in the Detroit test showed good agreement in absolute concentration (ppm) compared to CEMS concentrations of carbon dioxide and carbon monoxide. The secondary PFTIR, however, showed scattered and inconsistent PFTIR readings compared to the CEMS data. This turned out to be a hardware problem with the secondary PFTIR. As a result, no data from the secondary PFTIR are included in the test results. However, this affects only three test runs.

There are many factors that could influence the measured efficiency of a flare, including those associated with the flare operation and design. Other factors contributing to variability in CE measurement data include atmospheric conditions, flame movement/plume tracking, instrument specific factors such as calibration and alignment, and variability in the measurement technique itself. Another potential cause of observed data variability may be that the flare plume itself is not homogeneous. Pockets of differing compositions may exist within the plume resulting in a plume cross-section with varying composition.

2.0 Test Program Overview

2.1 Objectives of Test Program

The overall objectives of the Detroit test program were as follows:

1. Evaluate the impacts of combustion efficiency over a range of operating scenarios by changing both flare vent gas composition and steam rates.

2. Evaluate key variables such as Combustion Zone Gas Net Heating Value (CZG NHV), actual steam to vent gas ratio (S/VG), and comparison of S/VG ratios predicted by API 521 to actual S/VG ratios (S/S521) as performance indicators that may assist in maintaining flare operation at high efficiency conditions.

3. Compare the flare performance results from the Detroit and Texas City tests and note any relationships between the two sets of data.

4. Evaluate the precision and bias of the PFTIR for measuring flare combustion efficiency in field conditions. Challenge PFTIR measurements against sources of known concentrations in the field.

2.2 Testing Organization

The test was conducted with the assistance of both Clean Air Engineering and Industrial Monitoring and Controls Corporation (IMACC).

Clean Air Engineering	IMACC
500 W Wood St.	800 Paloma, Suite 100
Palatine, IL 60067	Round Rock, TX 78645

Because the test required personnel from MPC's operations, maintenance, engineering, and environmental staff, a cross-functional team was formed between IMACC, Clean Air Engineering, and MPC in order to staff, monitor and record test results. A list of personnel that participated in the project is included in Appendix A.4.

2.3 Flare System Components

2.3.1 Purpose

A flare is one of the most important safety devices in use at a refinery. Its purpose is to safely combust gases generated by emergency or upset conditions within a process unit. As a result, a flare must function over a large and variable range of operating scenarios. These vary from typical stand-by operation at minimum flow conditions to efficiently combusting gases generated from a full power outage or other process safety relief scenario.

Like the Texas City flare test, the Detroit test focused on the stand-by (i.e., high turndown) operating range. Not only does this range encompass the majority of flare operating time, but it is also the range where documented performance test data are scarce.

2.3.2 Flare Tip

The MPC Detroit Complex 3 and 4 (CP) flare is an elevated (125 ft.) steam-assisted flare that was constructed in 1961-62. The most recent physical change to the flare was replacement of the flare tip in October, 2005. The flare tip was manufactured by NAO, Inc. and has two points of steam addition: center steam and ring steam. The ring steam has alternating high and low points of injection around the flare tip exit. Table 2.3-1 lists key design specifications of the CP flare.

Detroit CP Flare		
Flare Tip Details		
Flare Tip Manufacturer	NAO Inc.	
Flare Tip Installation Date	October 2005	
Flare Tip Size	20 in diameter (16" effective diameter)	
Flare Tip Model Number	20" NFF-RC	
Summary of Flare Design Information		
Parameter	***Value***	***Units***
Design Purge Rate (min)	180	scfh
Design Purge Rate (max)	600	scfh
Pilot Rate (per pilot, 3 total)	45	scfh
Minimum Center Steam	300	lb/hr
Minimum Ring Steam	300	lb/hr
Minimum Total Steam	600	lb/hr
Maximum Hydraulic Capacity (i.e. max vent gas rate)	241,000	lb/hr

Table 2.3-1: Detroit CP Flare Specifications

The CP flare serves as relief for Complex 3 and Complex 4 at the MPC Detroit refinery. The typical base load for stand-by flare operation is approximately 500 – 600 lb/hr, or less than 0.25% of the hydraulic capacity (approximately a 400:1 turndown factor). Base load includes flare header gas from Complex 3 and 4, seal purges from rotating equipment, sample station vents, and various process vents from refinery equipment. The flare was operated with a constant center steam of 300 lb/hr and variable ring steam for the Detroit CP flare performance test.

2.3.3 Flare Automatic Steam Control System

MPC implemented an automatic steam control system prior to the performance test. This system consists of flow instruments for both the total steam rate and vent gas rate, as well as a smaller trim steam control valve for the ring steam. A gas chromatograph was installed to characterize vent gas composition. Table 2.3-2 lists the specific components of the steam control system.

Parameter	Technique	Vendor	Model
Flare Gas Volumetric/ Mass Flow	Ultrasonic Time of Flight	GE Panametrics	DigitalFlow GF868
Steam Mass Flow	Ultrasonic Time of Flight	GE Panametrics	DigitalFlow GS868
Flare Gas Composition and NHV	Gas Chromatography	Siemens	Maxum II
Flare Gas Molecular Weight	Ultrasonic Time of Flight	GE Panametrics	DigitalFlow GF868

Table 2.3-2: Automatic Steam Control System Components

Flare Gas Flow Rate, Temperature, and Molecular Weight
A General Electric (GE) Panametrics ultrasonic flow meter measures the flare gas flow rate, temperature, and molecular weight. This instrument cannot distinguish between components of the same molecular weight. For instance, it cannot distinguish propane from carbon dioxide (both having a molecular weight of 44 lb/lbmol). Since the steam control requirements would be very different between the compounds, the molecular weight measurement cannot be used independently in the control logic.

The ultrasonic meter is spanned for a maximum flow range of the flare system. Manufacturer's specifications indicate reasonable accuracy at low flow conditions. The ultrasonic flow meter was field calibrated by manufacturer representatives prior to testing.

Flare Gas Composition
A Siemens Maxum II Gas Chromatograph monitors the flare vent gas composition and heat content (BTU/scf). This analyzer provides an analytical data point approximately once every 15 minutes.

Steam Flow Parameters
Steam flow is measured by a GE Panametrics ultrasonic flow meter. Prior to testing, steam control valve positioners were calibrated and checked for proper operation.

2.4 Flare Test Program

2.4.1 Steam Demand and API 521

The Detroit flare performance test plan was designed to evaluate over-steaming under a variety of flaring conditions. Steam demand at a flare can vary for any number of reasons, including:

- Compositional changes in vent gas – Saturated hydrocarbons such as methane and ethane require less steam for smokeless combustion than olefinic hydrocarbons like propylene or butene. Non-hydrocarbons (i.e., hydrogen) or inerts (i.e., nitrogen) require little to no steam for smokeless combustion; however, the amounts present may influence combustion efficiency performance.

- Mixing – Well-mixed combustion reactants require less steam for smokeless performance.

- Steam pressure at tip nozzles – Subsonic steam flow conditions, typical during stand-by operation, require more steam to produce the same smokeless capacity at given conditions.

- Wind conditions – Strong winds may push the combustion gas zone away from ring steam nozzles, causing injected steam to not fully mix with the combustion gas. The momentum flux ratio (MFR) may indicate the extent to which non-mixing steam is present.

API 521 "Pressure-relieving and Depressuring Systems" is a design practice issued by the American Petroleum Institute. API 521 suggests that a certain amount of steam is required for smokeless (Ringlemann 0) performance based upon the chemical composition of hydrocarbons in the vent gas. However, the API 521 steam ratios are not related to combustion efficiency, but are meant to be a guide for the design of steam delivery systems for smoke suppression under worst-case design release scenarios. Proprietary commercial steam injection systems are of widely varying designs and may have different degrees of effectiveness in smoke suppression than what is suggested by API 521.

One of the objectives of the MPC Detroit flare performance test was to determine if API 521 Table 11 could also serve as an operational guide or target, which may provide adequate steam and smokeless operation. Table 2.4-1 is a reproduction of API 521 Table 11. As the intent of API 521 Table 11 was to serve as a design guide under relief loads, it was unknown if the same ratios would hold true for low flow operation as for high flow operation. If so, then the amount of steam recommended by API 521 could serve as a "minimum" target, and represent the amount of steam necessary to provide smokeless flare operation under all operating ranges. A multiple above the minimum API 521 ratio could then be utilized to establish an upper bound preventing over-steaming. The mathematical representation of this concept is known as the "S/S521" ratio, which represents the amount of actual steam applied in excess of the minimum recommended by API 521 Table 11.

Gases being fired	Steam required[a] kg (lb) of steam per kg (lb) of hydrocarbon gas
Paraffins	
Ethane	0.10 to 0.15
Propane	0.25 to 0.30
Butane	0.30 to 0.35
Pentane plus	0.40 to 0.45
Olefins	
Ethylene	0.40 to 0.50
Propylene	0.50 to 0.60
Butene	0.60 to 0.70
Diolefins	
Propadiene	0.70 to 0.80
Butadiene	0.90 to 1.00
Pentadiene	1.10 to 1.20
Acetylenes	
Acetylene	0.50 to 0.60
Aromatics	
Benzene	0.80 to 0.90
Toluene	0.85 to 0.95
Xylene	0.90 to 1.00

[a] The suggested amount of steam that should be injected into the gases being flared in order to promote smokeless burning (Ringlemann 0) can be determined from this table. The given values provide a general guideline for the quantity of steam required. Consult the flare vendor for detailed steam requirements.

Table 2.4-1: API 521 Table 11 Suggested Steam Rates

By plotting the API 521 predicted steam demand for saturates, olefins/aromatics, and diolefins based upon their molecular weight, linear relationships emerge. Figure 2.4-1 shows these linear relationships. MPC's test program uses the linear relationship of the olefin/aromatic curve as the basis representing the amount of minimum steam API 521 Table 11 would require to achieve smokeless combustion. This is represented mathematically as:

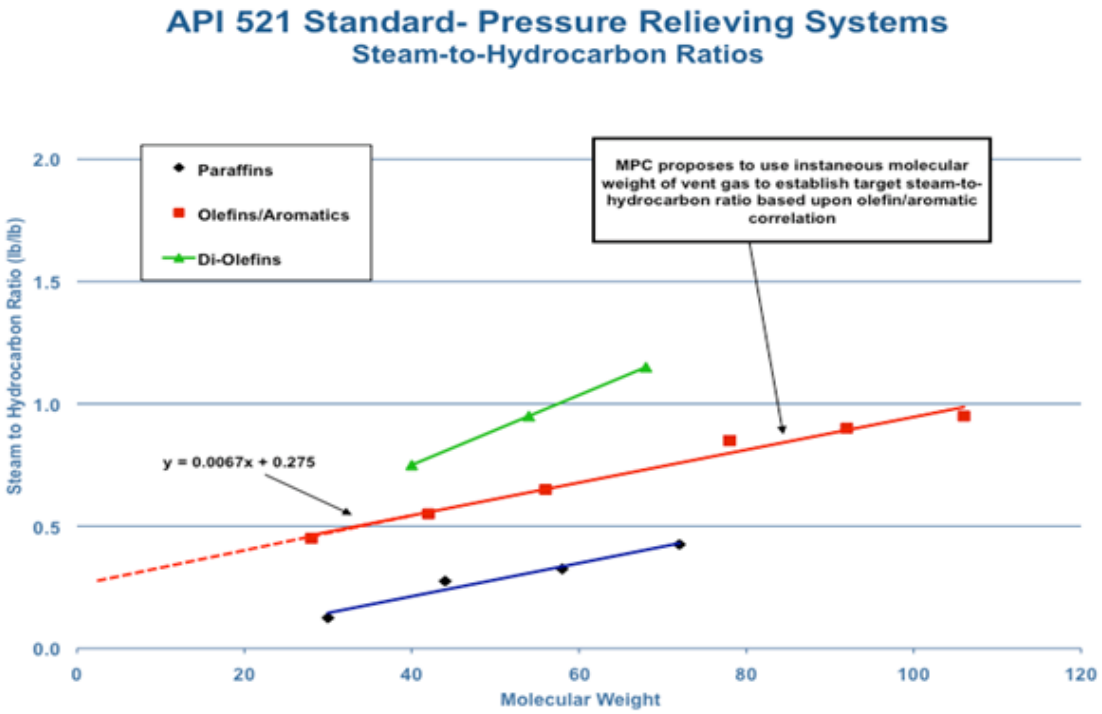

Figure 2.4-1: API 521 Steam-to-Hydrocarbon Ratios

Another key parameter used in evaluating over-steaming is the combustion zone gas net heating value (CZG NHV). The CZG NHV is the Lower Heating Value, expressed in BTU per standard cubic foot (BTU/scf), of the mixture of gases introduced into the combustion zone of the flare (i.e., at the flare tip). This value represents the resulting heat balance using the inputs of vent gas, pilot gas, and steam.

2.4.2 Test Conditions

Three test series (A, B, and C) were conducted by setting a vent gas composition and vent gas flow rate. Within the test series, the steam flow was varied to achieve a range of S/VG ratios. Test series D and E were special series that varied both the vent gas composition and S/VG ratios. Long term stability test series F held the vent gas composition, vent gas flow rate, and S/VG ratio constant. The rationale for each test series is as follows:

Test A To simulate normal base load with typical flow conditions for the flare. This test represented day-to-day operation.

Test B To demonstrate flare performance with a higher flow rate of hydrocarbons by adding refinery fuel gas (RFG) having a low S/VG for smokeless operation.

Test C To demonstrate flare performance at flow rates similar to test series B with addition of unsaturates (olefins in the form of a 95% propylene / 5% propane mix) that would require a higher S/VG for smokeless operation than the RFG added in test series B.

Test D To demonstrate flare performance when operating at higher levels of hydrogen than typically found in the base load. Hydrogen has been shown to have exceptional combustion characteristics but has low volumetric heat content (270 BTU/scf). The hydrogen source for this test was the Reformer at a purity of approximately 85 – 90%. NOTE: The base load contains nominal amounts of hydrogen from 20% to 30%.

Test E To study the effect of nitrogen rich vent gas streams on combustion efficiency.

Test F This was the Long Term Stability (LTS) test. The purpose of this test was to demonstrate the repeatability of PFTIR measurements over an extended period. This test may also provide information on the effects of uncontrolled variables such as wind on the overall test result. The LTS tests will be conducted under test series B conditions at an S/VG of 1.0. Every effort was made to ensure the process conditions were held as constant as possible from run to run.

The Michigan Department of Natural Resources and Environment (MDNRE) mandated that the Detroit West Plant flare be operated within the approved operating limits as stated in the Title V air permit due to community involvement. Therefore, steam could only be reduced to the incipient smoke point and could only be increased to a point at which the flare would not be extinguished by excessive steam.

2.4.3 PFTIR Locations

At the previous MPC Texas City flare performance test, wind direction was a major source of delay because only one PFTIR was used from a single ground location. To prevent wind delays at the Detroit test, two PFTIRs were placed at perpendicular ground locations so at least one instrument would always have an adequate cross-sectional view of the flare plume. One location was in a contractor parking lot ("lot location") and the other location was on the main road through the Complex 3 and 4 part of the refinery ("road location"). Figure 2.4-2 shows a map of the PFTIR locations in relation to the flare. One PFTIR was mounted inside a trailer and placed at the lot location. The other PFTIR was mounted on a tripod and placed at the road location. Section 4.2 gives more detail about each location.

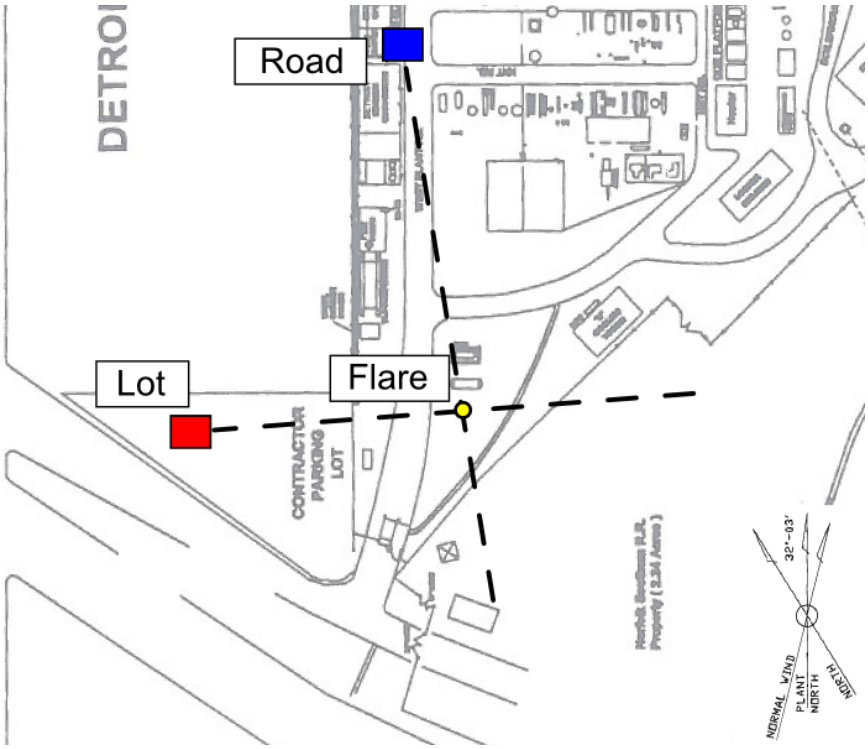

Figure 2.4-2: Map of Locations in Relation to Flare

2.4.4 Run Length and Replicates

The default run length for test series A, B, and C was 30 minutes. However, with the consent of the US EPA, this default was changed during the test program. At the conclusion of the first 30-minute run for each test condition the run was divided into 10-minute segments and analyzed. If each of the average combustion efficiencies for the first, second, and third 10-minute sections did not vary from the entire 30 minute average combustion efficiency by more than 0.5% absolute, the remainder of the runs for that test condition for the day were shortened to 20 minutes. For test series D, the default run time was 10 minutes. For test series E, the default run time was 15 minutes. For test series F, the default run time was 30 minutes.

Also, the initial test plan called for three replicate measurements at each test condition for the A, B, and C tests. With the consent of EPA, this requirement was changed during the test program. Two replicates (repeated runs with the same operating conditions) were performed at each S/VG set point for test series A, B, and C. However, if the average combustion efficiencies of the first two replicates differed by more than 5% absolute, a third replicate was performed. Test series D, E, and F did not require any replicates.

2.5 Passive FTIR

An IMACC PFTIR was used to determine the gas composition of the flare plume. A detailed description of the instrument and testing procedure are found in Section 4.0 with further detail in Appendix A.2.

The Passive FTIR operates on the principle of spectral analysis of thermal radiation emitted by hot gases. Passive means that no "active" infrared light source is used. Instead, the hot gases of the flare are the infrared source. The spectrometer is a receiver only. This approach is possible because the infrared emission spectra of hot gases have the same patters or "fingerprints" as their absorption spectra. Consequently, observing a flare plume with an infrared instrument allows for identification and quantification of species through emission spectroscopy just as in absorption spectroscopy.

Two instruments were used for this test program. They were placed at approximately 90° from one another in order to ensure a good view of the flare plume regardless of wind direction. Section 2.4.3 describes the locations of these instruments. Dr. Robert Spellicy of Industrial Monitor and Control Corporation (IMACC) oversaw the PFTIR operation and data analysis. IMACC also developed the instrument hardware and analytical software. The PFTIRs used at the Detroit test included dual-color detectors (InSb-MCT). This detector configuration has increased sensitivity over a larger frequency range than the single color detector used for the Texas City test (MCT only).

2.6 Video Cameras

During the test program, a total of seven video cameras recorded flare activity from the lot and road locations (see Section 2.4.3 for location information). At the beginning of the test program, four infrared cameras and two visible light cameras were used. However, one of the infrared cameras became unusable after the first day, so it was replaced by another type of infrared camera for the remainder of the test program. The types of cameras used during the test program are listed in Appendix A.6.

3.0 Summary of Results

3.1 Summary and Key Data Trends by Test Series

Test series A, B, and C were analyzed individually and as a group to study the effect of steam on combustion efficiency of a flare with hydrocarbon vent gases. Test series D and E were separately analyzed because they were primarily performed to study the effect of hydrogen and nitrogen on the combustion efficiency of the flare.

3.1.1 Combustion Efficiency with Increasing Steam Rates

For each test series presented below, relationships between combustion efficiency and three calculated variables are presented: actual steam to vent gas ratio (S/VG), actual steam to API521 recommended (S/S521), and combustion zone gas net heating value (CZG NHV). The lowest S/VG set point was always the incipient smoke point for test series A, B, and C.

3.1.1.1 Test Series A – Typical Base Load Conditions

Test series A represents typical base load conditions at the Detroit CP flare. The base load vent gas typically has a flow rate of 500 – 600 lb/hr and is composed of 60 – 70% hydrocarbons and 15 – 25% hydrogen. Section 5.2.1 contains more detailed process conditions for test series A.

Only two S/VG set points required a third replicate. Due to wind restrictions, combustion efficiency for the first replicate for condition A6 (S/VG≈2.4) was measured with the secondary PFTIR at the road location. Due to hardware issues with this instrument, the data is not reported and the run was marked invalid. The second replicates for A8 (S/VG≈3.0) and A9 (S/VG≈4.0) did not contain enough valid PFTIR readings (fewer than 5 valid readings each), so those two conditions were repeated a third time. Also, to create a more complete trend between 1.0 and 2.0 S/VG, two additional runs -- A2 (S/VG≈ 1.5) and A3 (S/VG≈1.8) -- were added at 15-minutes each. A total of 15 valid runs were completed for test series A. Table 3.1-1 lists the test conditions for each run.

Run	S/VG	Run Time	Notes
A1-1	1.2	30 min	Incipient smoke point
A1-2	1.2	30 min	Incipient smoke point
A2-1	1.5	15 min	Added to test series
A2-2	1.6	15 min	Replicate of added run
A3-1	1.8	15 min	Added to test series
A3-2	1.8	15 min	Replicate of added run
A4-1	2.1	30 min	
A4-2	2.0	30 min	
A5-1	2.2	30 min	S/VG close to other runs, added extra runs instead of replicates (A2)
A6-1	2.4	30 min	Invalid run, secondary (road location) PFTIR only, no combustion efficiency data
A6-2	2.4	30 min	
A7-1	2.6	30 min	S/VG close to other runs, added extra runs instead of replicates (A3)
A8-1	3.0	30 min	
A8-2	3.0	30 min	Invalid run, only 4 combustion efficiency readings
A8-3	2.9	30 min	
A9-1	4.0	30 min	
A9-2	4.2	30 min	Invalid run, only 1 combustion efficiency reading
A9-3	4.0	30 min	

Table 3.1-1: Test Conditions for Test Series A (Base Load)

Figure 3.1-1 shows the relationship between combustion efficiency and S/VG. A clear trend of decreasing combustion efficiency is present at S/VG above about 2.7, but the trend begins to scatter at higher ratios. As the flare began to snuff at higher S/VG, the flare plume became more inconsistent and sometimes pulsed. This made aiming the PFTIR more difficult because the plume was no longer cone-shaped or column-shaped but was instead hourglass-shaped.

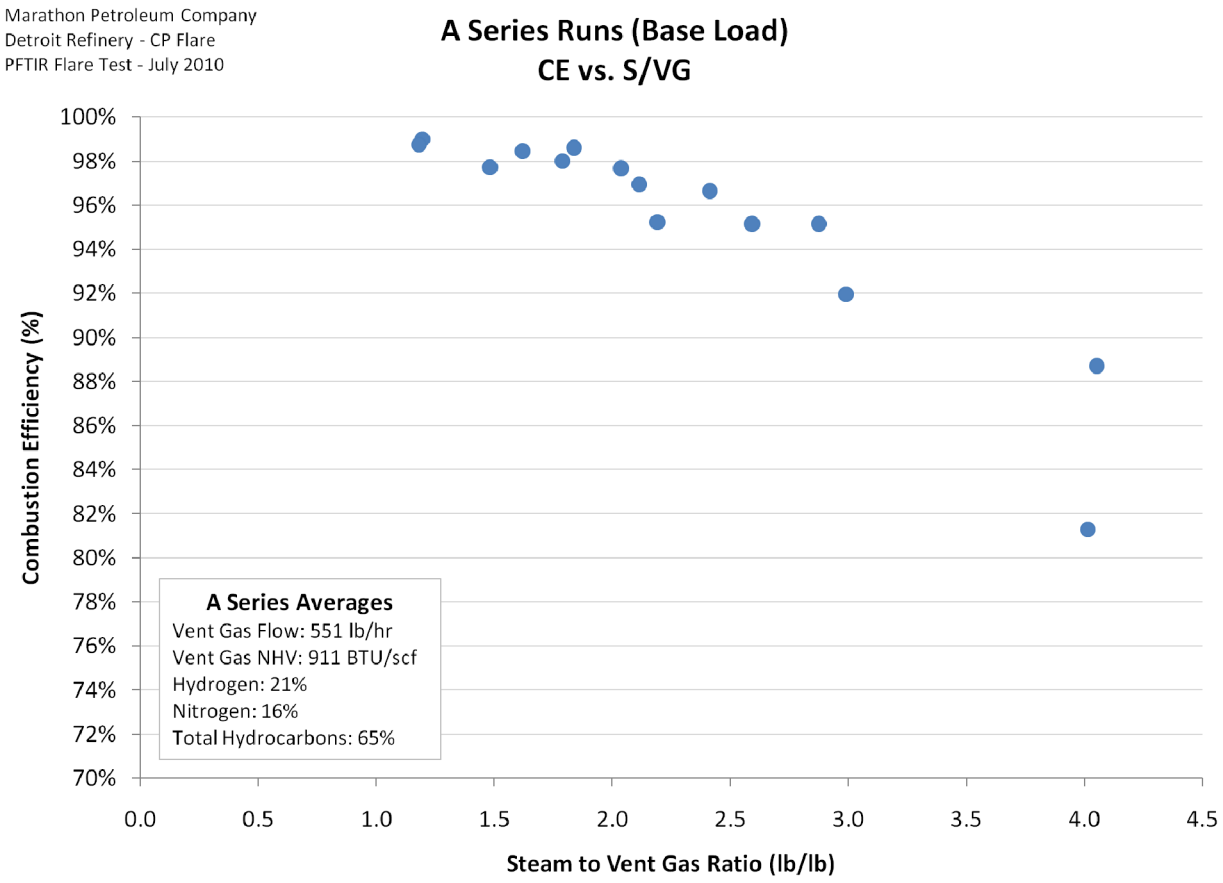

Figure 3.1-1: CE vs. S/VG for Test Series A (Base Load)

Figure 3.1-2 shows the relationship between combustion efficiency and S/S521. A decrease in combustion efficiency appears above an S/S521 of 6.0. The incipient smoke point is near an S/S521 of 3.0.

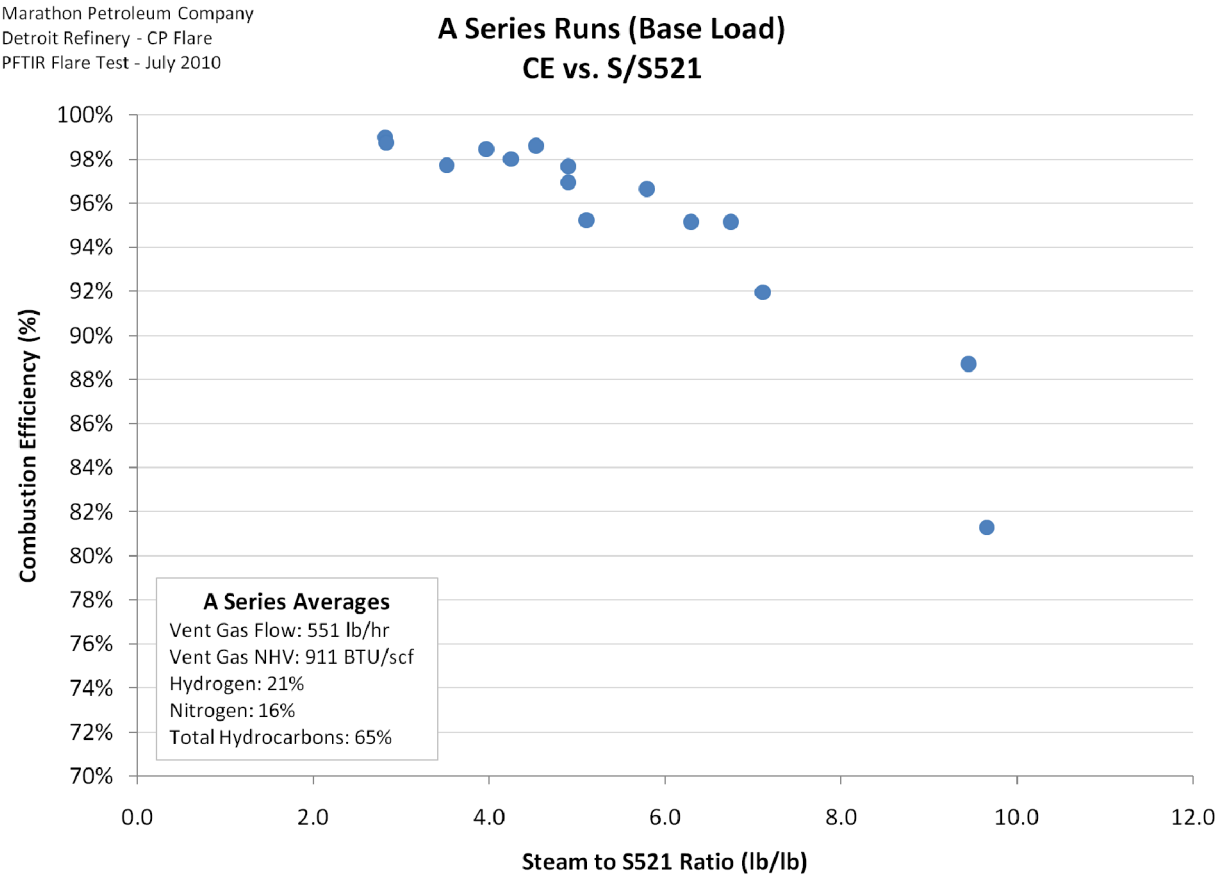

Figure 3.1-2: CE vs. S/S521 for Test Series A (Base Load)

Figure 3.1-3 shows the relationship between combustion efficiency and CZG NHV. A clear trend of decreasing combustion efficiency is present as CZG NHV falls below about 250 BTU/scf.

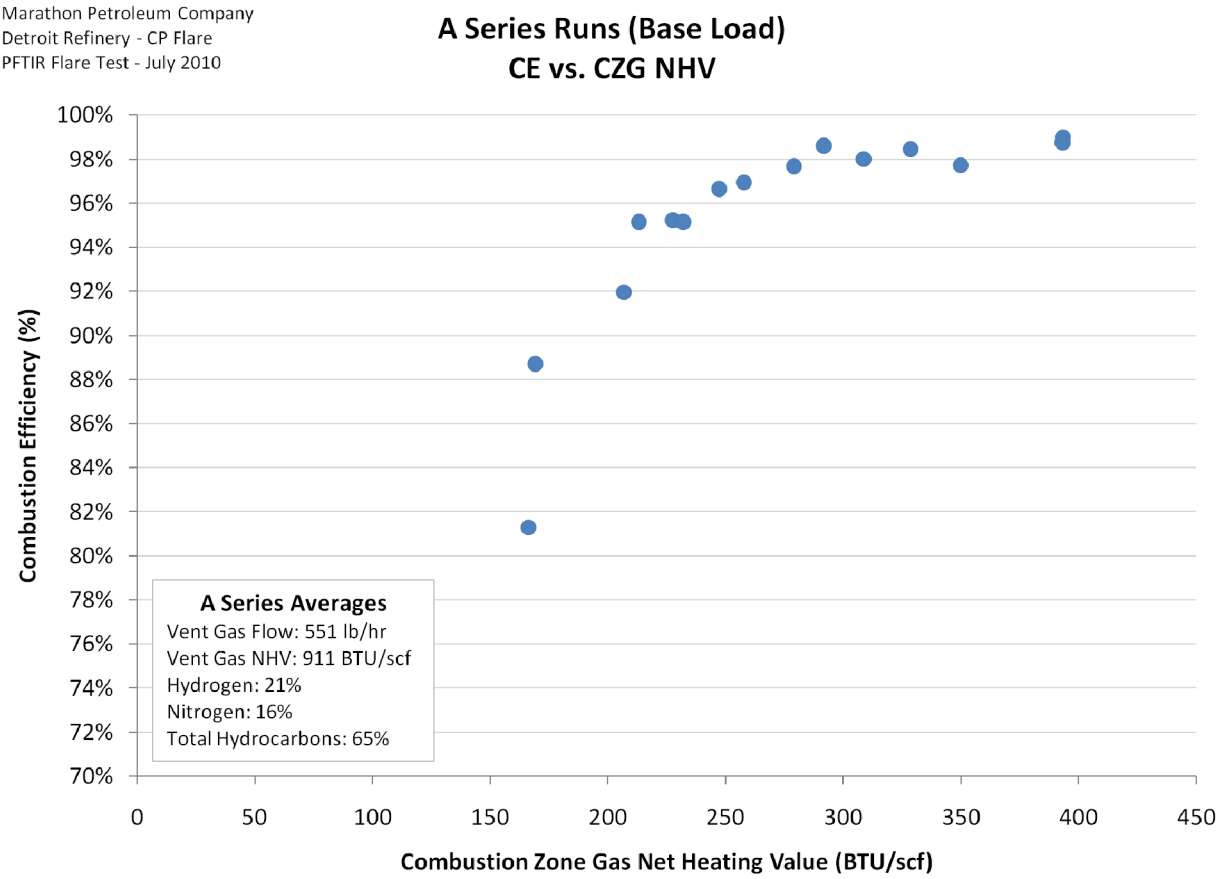

Figure 3.1-3: CE vs. CZG NHV for Test Series A (Base Load)

3.1.1.2 Test Series B – Refinery Fuel Gas

The purpose of test series B was to simulate a base load but at higher velocity. To accomplish this, about 1,000 lb/hr refinery fuel gas was added to the normal base load of about 500-600 lb/hr.. The vent gas was composed of 60 – 70% hydrocarbons and 20 – 30% hydrogen. Section 5.3.1 contains more detailed process conditions for test series B.

All six conditions required only two replicates in test series B. Combustion efficiency for the second replicate for B1 (S/VG≈0.6) was measured with the secondary PFTIR at the road location. Due to hardware issues with this instrument, the data is not reported and the run was marked invalid. A total of 11 valid runs were completed for this test series. S/VG set points higher than 2.1 were not attempted. Table 3.1-2 lists the test conditions for each run.

Run	S/VG	Run Time	Notes
B1-1	0.6	30 min	
B1-2	0.6	30 min	Invalid run, secondary (road location) PFTIR only, no combustion efficiency data
B2-1	0.8	30 min	
B2-2	0.8	30 min	
B3-1	1.0	30 min	
B3-2	1.1	30 min	
B4-1	1.2	30 min	
B4-2	1.2	20 min	
B6-1	1.7	30 min	S/VG for B5 close to B6, so skipped B5
B6-2	1.6	20 min	
B8-1	2.1	30 min	S/VG for B7 close to B8, so skipped B7
B8-2	2.1	20 min	

Table 3.1-2: Test Conditions for Test Series B (Refinery Fuel Gas)

Figure 3.1-4 shows the relationship between combustion efficiency and S/VG. Replicates are tightly grouped, and a trend of decreasing combustion efficiency begins to appear above 1.5 S/VG. Higher S/VG set points may have been beneficial to further complete the trend, but concern about the flare snuffing prevented attempts above 2.1 S/VG. Although the combustion efficiency had not begun to rapidly decrease at 2.1 S/VG, the thermal video feeds showed the flame nearing a snuff point.

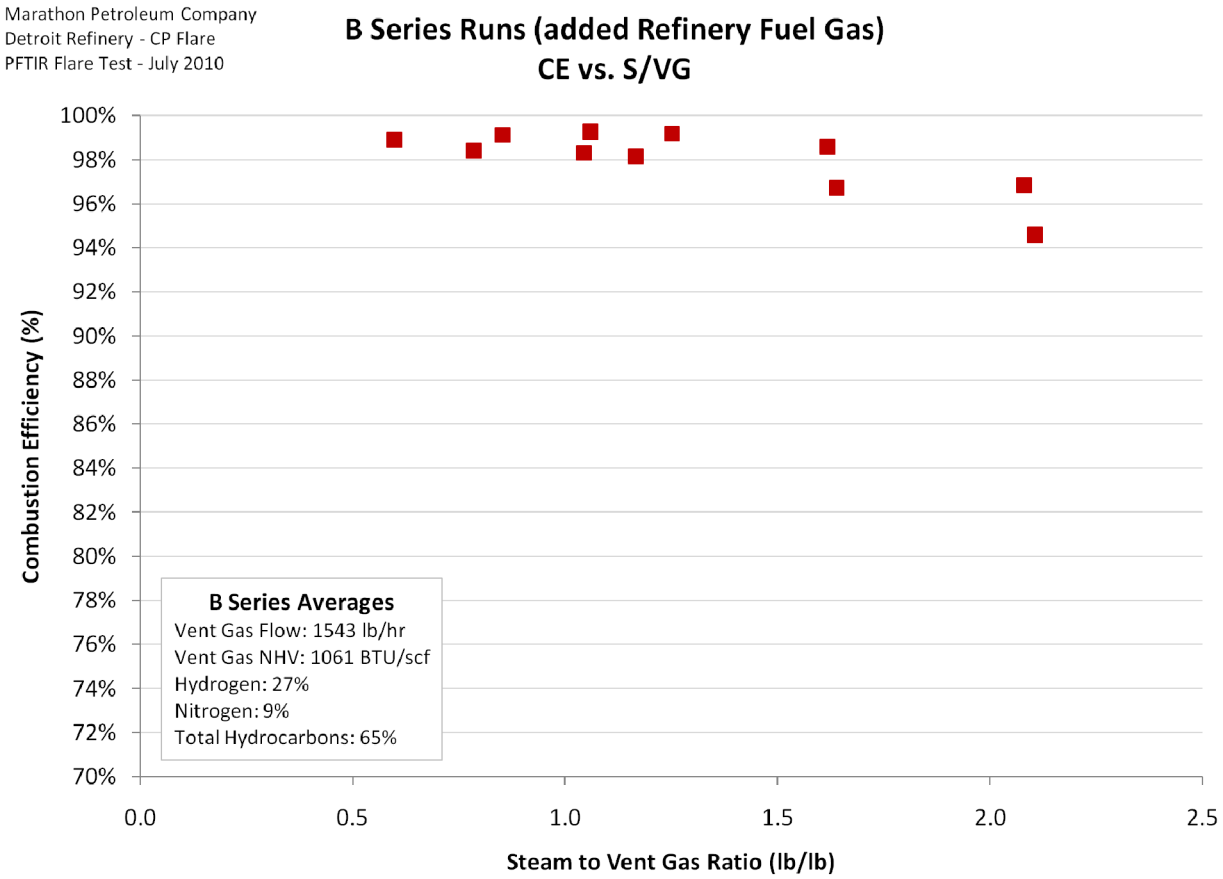

Figure 3.1-4: CE vs. S/VG for Test Series B (Refinery Fuel Gas)

Figure 3.1-5 shows the relationship between combustion efficiency and S/S521. A trend of decreasing combustion efficiency appears above an S/S521 of 4.5. The incipient smoke point is near an S/S521 of 1.5, which is lower than test series A.

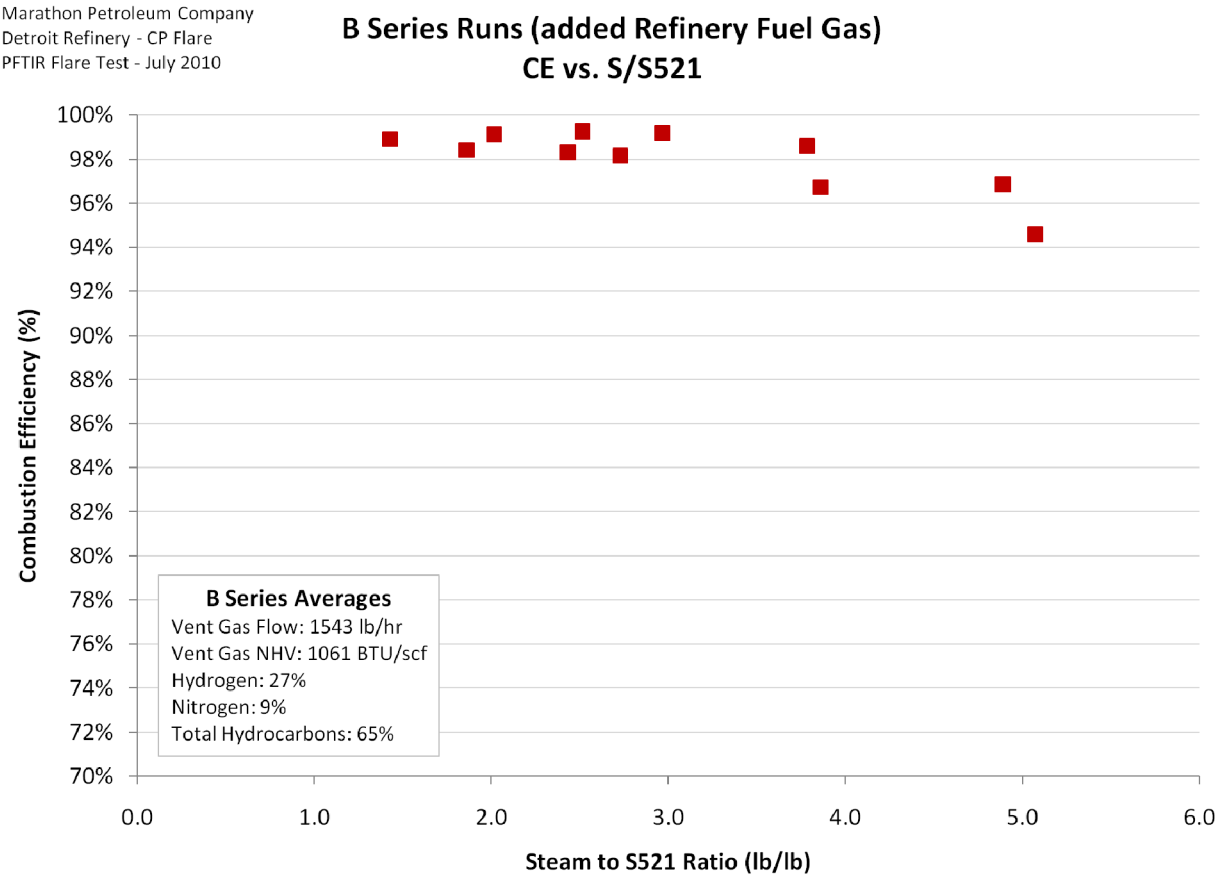

Figure 3.1-5: CE vs. S/S521 for Test Series B (Refinery Fuel Gas)

Figure 3.1-6 shows the relationship between combustion efficiency and CZG NHV. A trend of decreasing combustion efficiency is present as CZG NHV falls below about 300 BTU/scf.

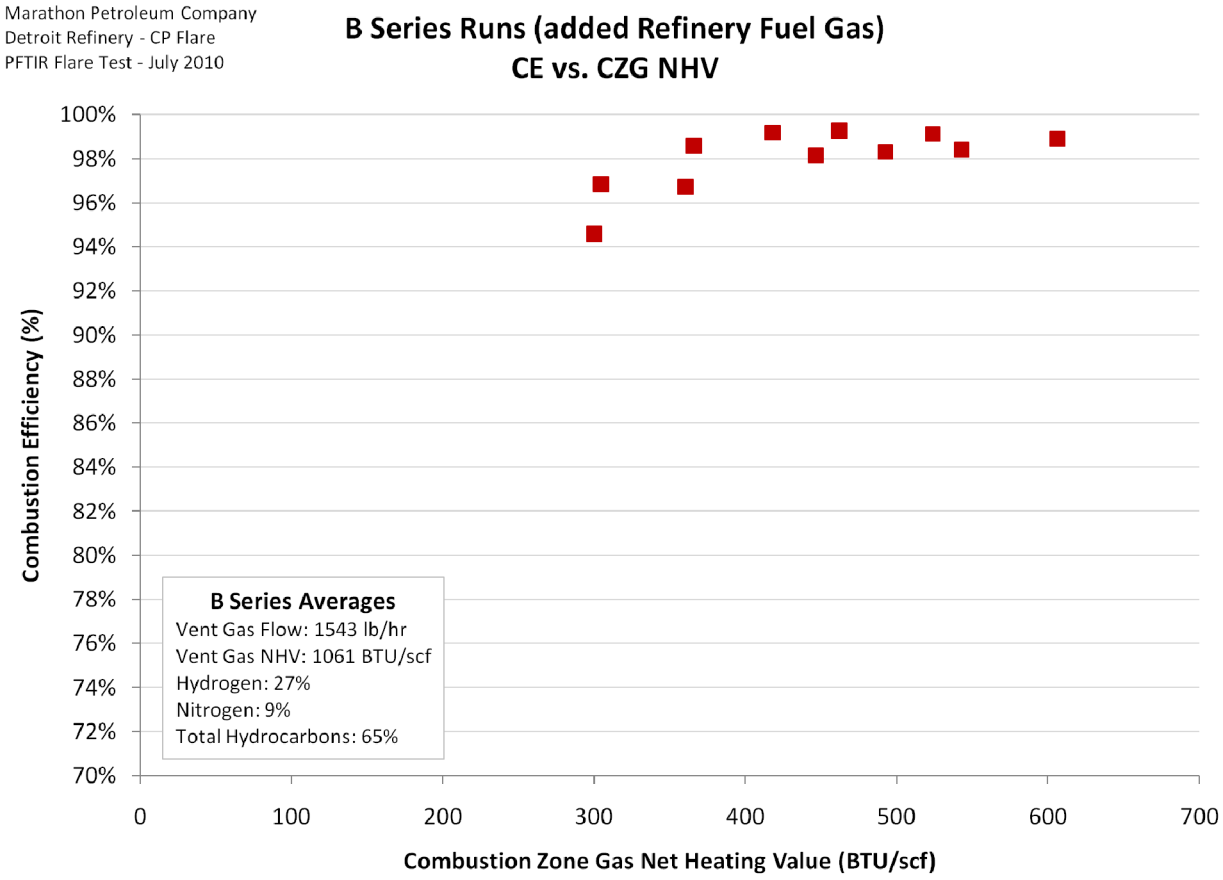

Figure 3.1-6: CE vs. CZG NHV for Test Series B (Refinery Fuel Gas)

3.1.1.3 Test Series C – Propylene Olefins

The purpose of this test series was to determine the effect of higher molecular weight compounds on the flare operating envelope. Test series C represents typical base load conditions with added propylene. The base load vent gas typically has a flow rate of 500 – 600 lb/hr, and 1,100 lb/hr of a 95% propylene / 5% propane mix was added to the vent gas. The vent gas was composed of 85 – 90% hydrocarbons and 5 – 10% hydrogen. Section 5.4.1 contains more detailed process conditions for test series C.

All five conditions required only two replicates in test series C. A total of 10 valid runs were completed for test series C. Like test series B, S/VG set points higher than 2.3 were not attempted. Table 3.1-3 lists the test conditions for each run.

Run	S/VG	Run Time	Notes
1-1	0.7	30 min	
1-2	0.7	30 min	
2-1	1.2	30 min	
2-2	1.1	20 min	
3-1	1.6	20 min	Paused during run due to change in vent gas constituents
3-2	1.5	20 min	
4-1	2.0	20 min	
4-2	1.9	20 min	
5-1	2.2	11 min	Paused then ended run due to change in vent gas constituents
5-2	2.3	20 min	

Table 3.1-3: Test Conditions for Test Series C (Propylene)

Figure 3.1-7 shows the relationship between combustion efficiency and S/VG. Replicates are tightly grouped and a trend of decreasing combustion efficiency begins to appear above 1.5 S/VG. Like test series B, higher S/VG set point may have been beneficial to further complete the trend, but concern about the flare snuffing prevented attempts above 2.3 S/VG. Although the combustion efficiency had not begun to rapidly decrease at 2.3 S/VG, the thermal video feeds showed the flame nearing a snuff point. The trend of decreasing combustion efficiency does compare to test series A and B results, but it appears to have a shifted S/VG inflection point.

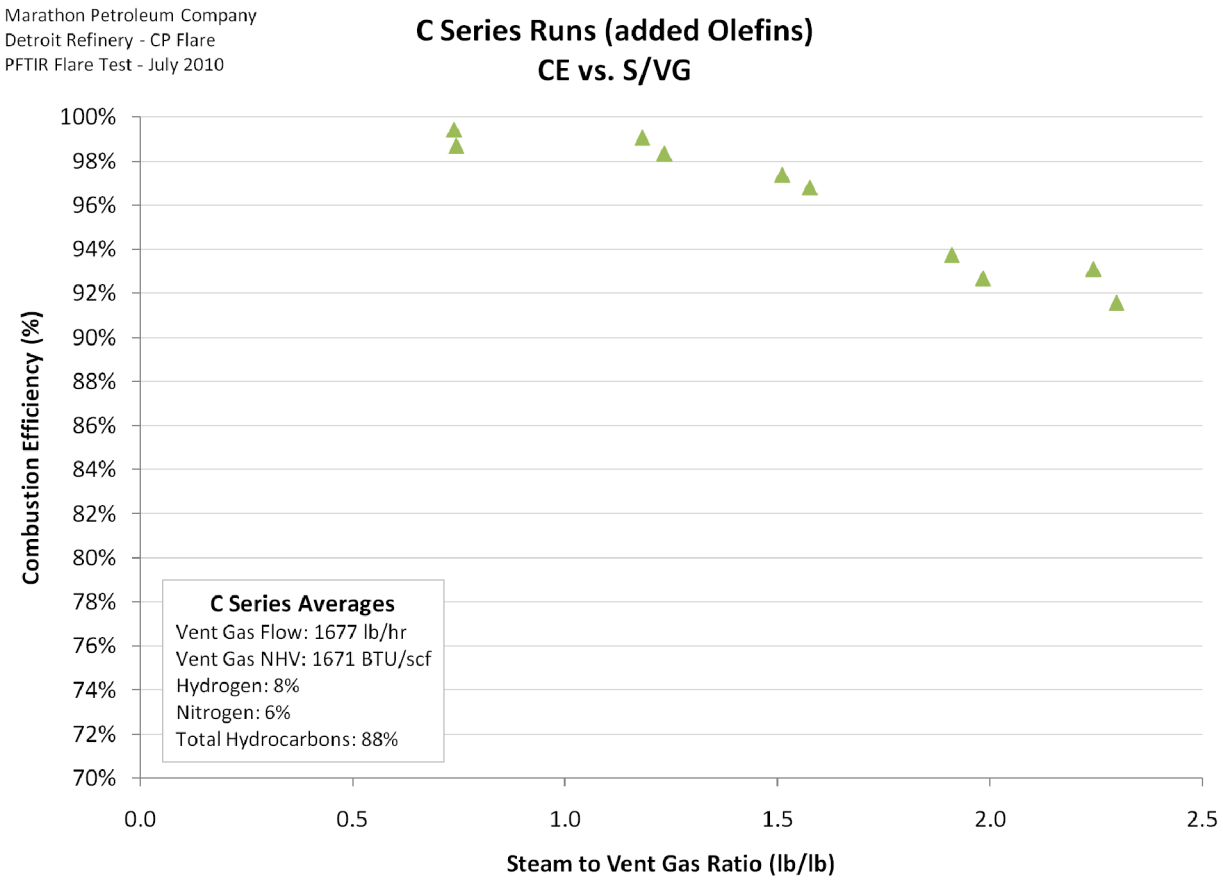

Figure 3.1-7: CE vs. S/VG for Test Series C (Propylene)

Figure 3.1-8 shows the relationship between combustion efficiency and S/S521. A trend of decreasing combustion efficiency appears above an S/S521 of about 3.5. The incipient smoke point is near an S/S521 of 1.5, which is comparable to test series B.

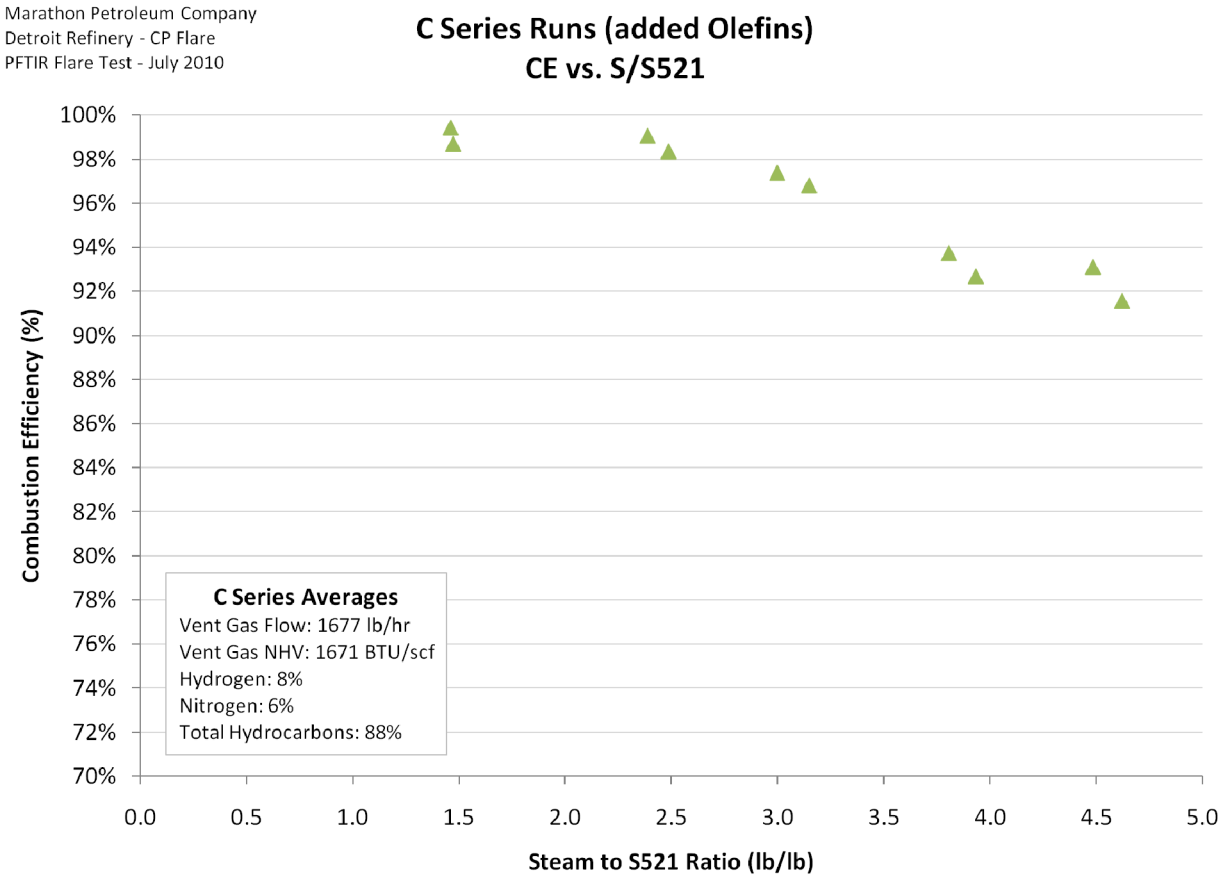

Figure 3.1-8: CE vs. S/S521 for Test Series C (Propylene)

Figure 3.1-9 shows the relationship between combustion efficiency and CZG NHV. A trend of decreasing combustion efficiency is present as CZG NHV falls below about 425 BTU/scf. This is noticeably higher than test series A and B.

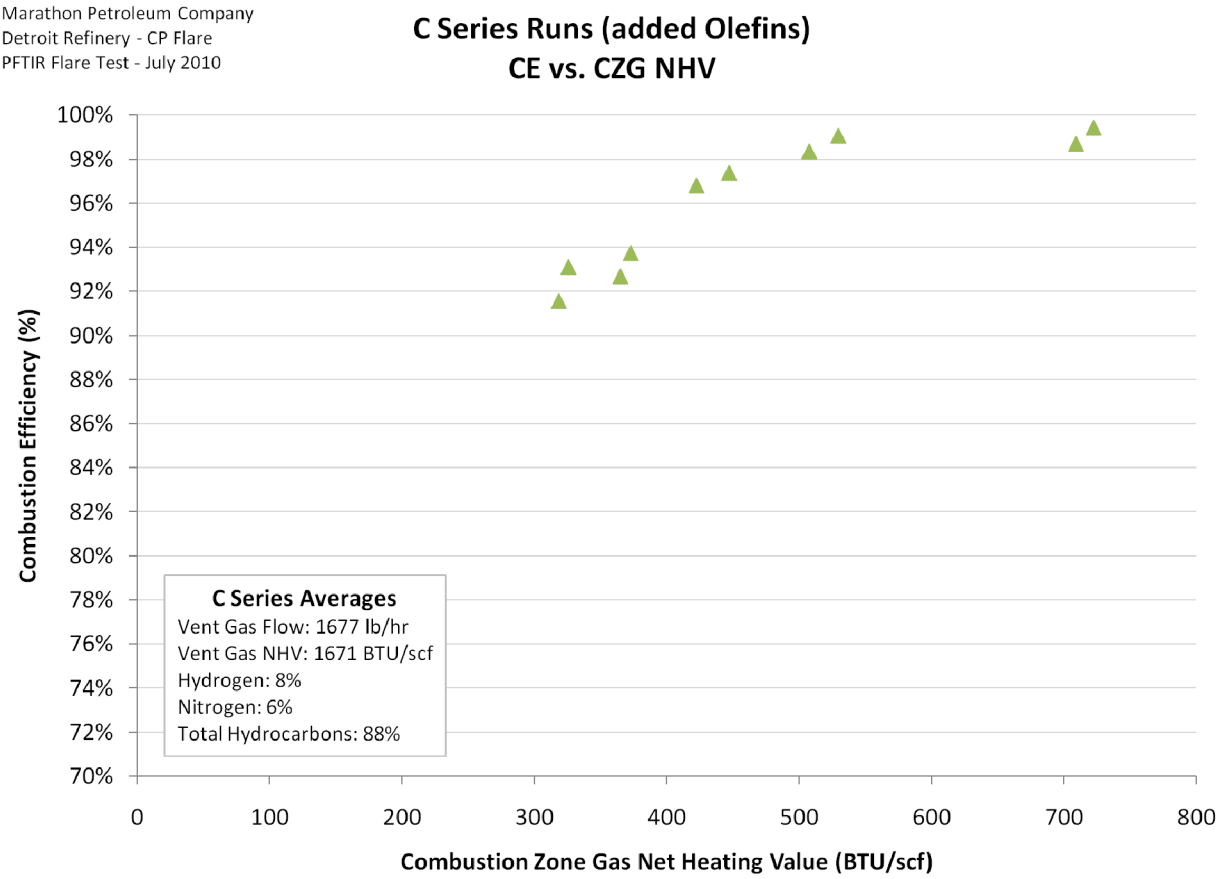

Figure 3.1-9: CE vs. CZG NHV for Test Series C (Propylene)

3.1.2 Observed Impacts of Hydrogen (Test Series D)

The purpose of the test series D was to determine the effects of hydrogen on the flare operating envelope. Hydrogen was added to the base load vent gas at three levels, where the base load contained approximately 20% hydrogen. Streams containing 54%, 52%, and 43% hydrogen were tested at a high steam ratio (4.5), a mid steam ratio (3.0), and a low steam ratio (1.8). These runs were conducted for 10 minutes each. Table 3.1-4 lists these test conditions. An extra 34% hydrogen stream run with high S/VG was added at the end of the test series to bridge the gap between the base load and the test series D runs. No replicates were required for test series D. Section 5.5.1 contains more detailed process conditions for test series D.

	Target S/VG		
Hydrogen	4.5	3.0	1.8
54%	D1-1 (Invalid run due to process instability)	D2-1	D3-1
52%	D4-1 D5-1 (actual S/VG=4.4)		D6-1
43%	D7-1	D8-1	D9-1
34%	D10-1 (added)		
21%		Test Series A	

Table 3.1-4: Test Conditions for Test Series D (Hydrogen)

The high S/VG set point run for the 54% hydrogen stream had a lower than expected hydrogen content reading because the added hydrogen had not yet fully stabilized in the vent gas. This run is not considered valid due to process instability. Also, the mid S/VG set point run for the 52% hydrogen stream had a higher than planned S/VG, but the process and PFTIR readings were stable so it was still considered a valid run, just with an S/VG closer to 4.5 than 3.0. A total of nine valid runs were completed for test series D.

Figure 3.1-10 shows the relationship between combustion efficiency and percent hydrogen in the vent gas. Test series A is added to represent a base load case with relatively low hydrogen content (~20%). Replicates for condition A3 were used for a S/VG of 1.8, and replicates for condition A8 were used for a S/VG of 3.0. Test series A did not reach a S/VG of 4.5. At the lower S/VG of 1.8, hydrogen has no effect on combustion efficiency. At the mid S/VG of 3.0, higher hydrogen runs have a slight increase in combustion efficiency. At the high S/VG of 4.5, however, there is a significant increase in combustion efficiency for higher hydrogen runs.

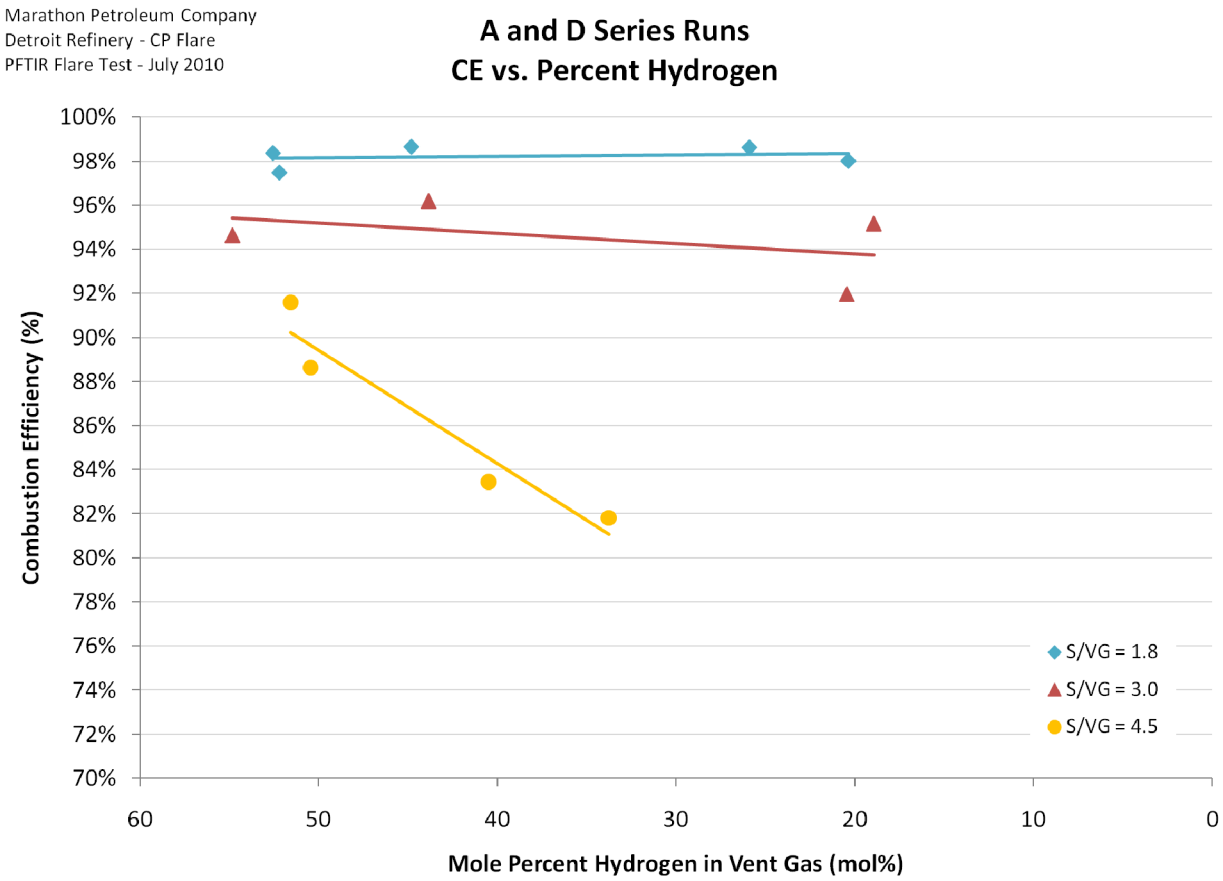

Figure 3.1-10: CE vs. Percent Hydrogen for Test Series D (Hydrogen)

Figure 3.1-11 shows the relationship between combustion efficiency and S/VG for the levels of hydrogen. The extra 34% hydrogen run is also included, and test series A has been added to show a base load of approximately 21% hydrogen. When at mid and lower S/VG ratios, combustion efficiency is not significantly impacted by hydrogen content. However, at higher S/VG ratios, CE tends to fall off more slowly with higher hydrogen concentrations.

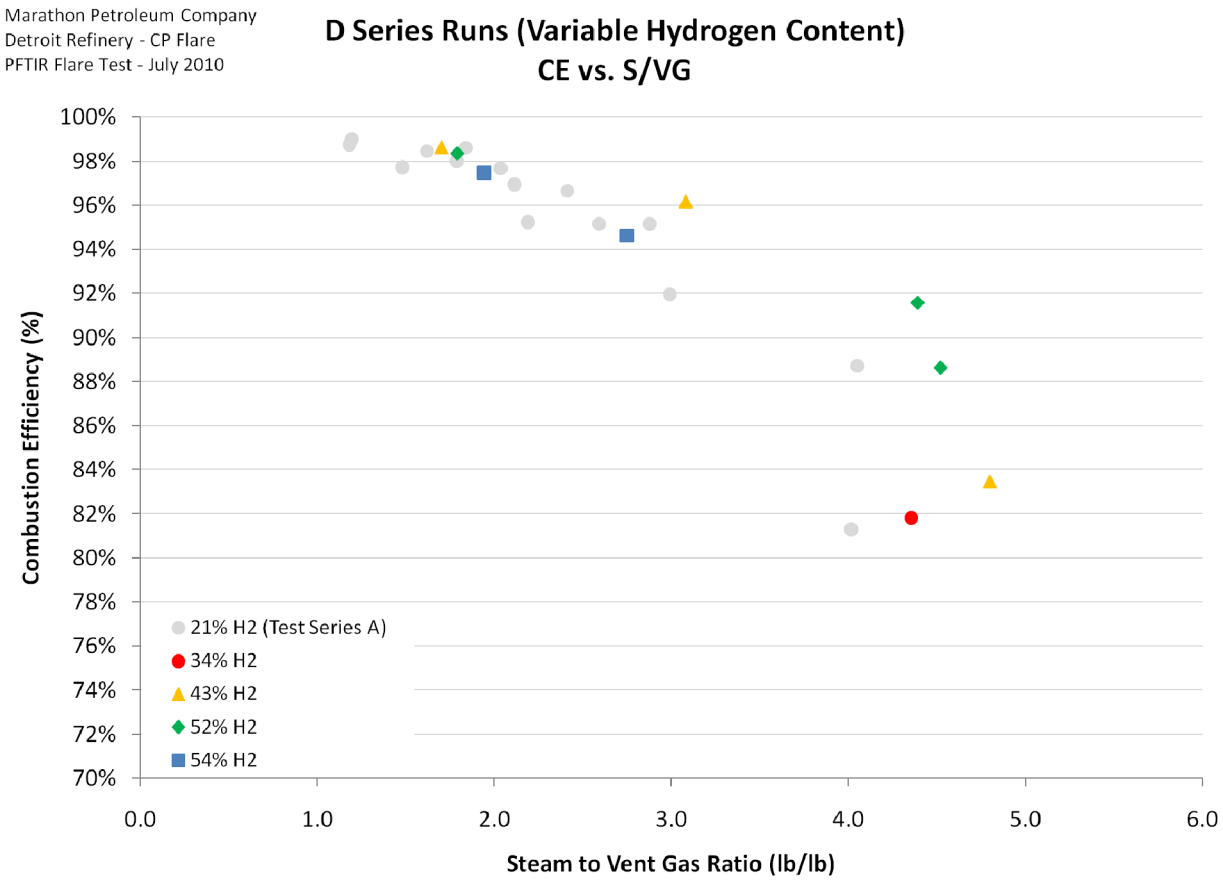

Figure 3.1-11: CE vs. S/VG for Test Series D (Hydrogen)

Figure 3.1-12 shows the relationship between combustion efficiency and S/S521, with test series A added to show a base load of approximately 21% hydrogen. The decrease in combustion efficiency above an S/S521 of 6.0 is also observed in the hydrogen runs. However, the extent to which the combustion efficiency decrease occurs is lessened by more hydrogen rich streams.

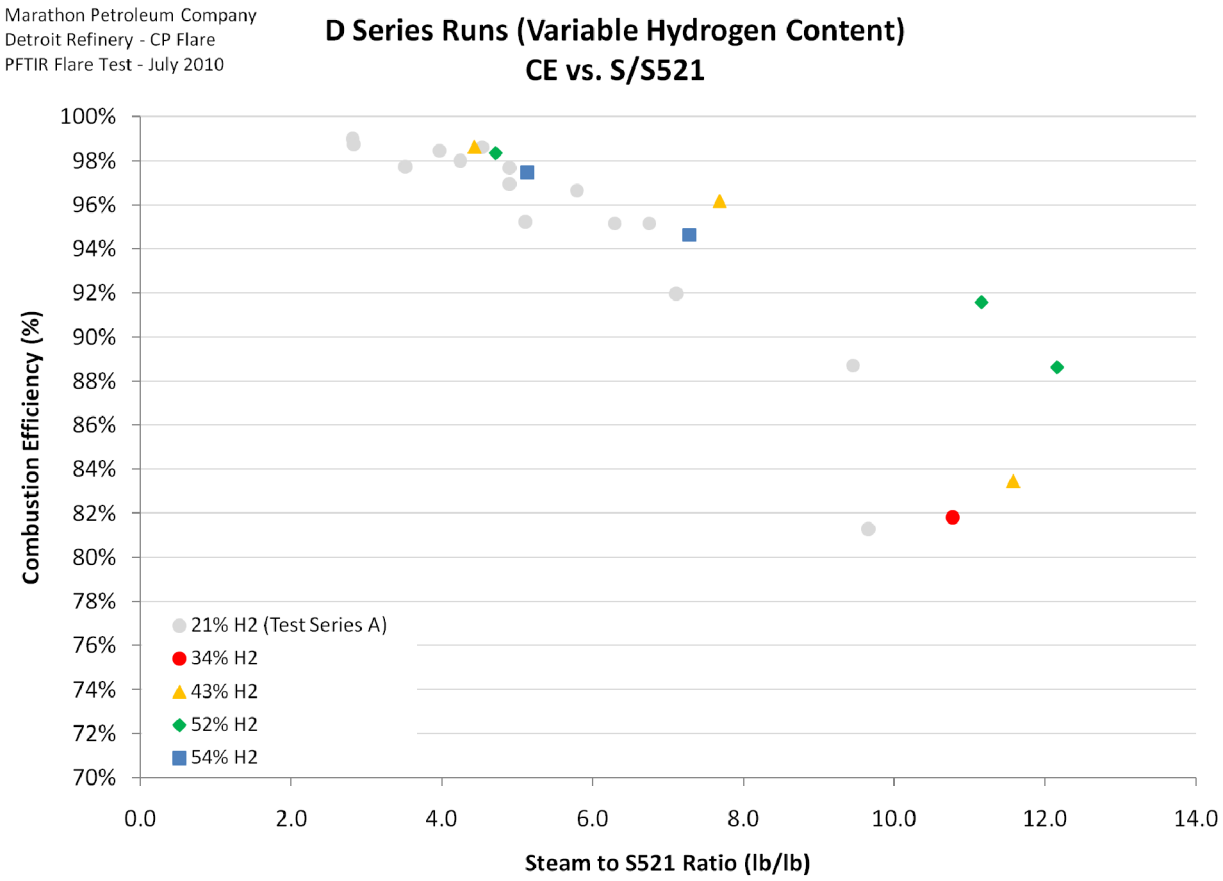

Figure 3.1-12: CE vs. S/S521 for Test Series D (Hydrogen)

Figure 3.1-13 shows the relationship between combustion efficiency and CZG NHV, with test series A added to show a base load of approximately 21% hydrogen. Although the curve appears continuous, the vertical distribution of combustion efficiencies for the same low CZG NHV (150-170 BTU/scf) shows higher hydrogen streams having higher combustion efficiencies than lower hydrogen streams.

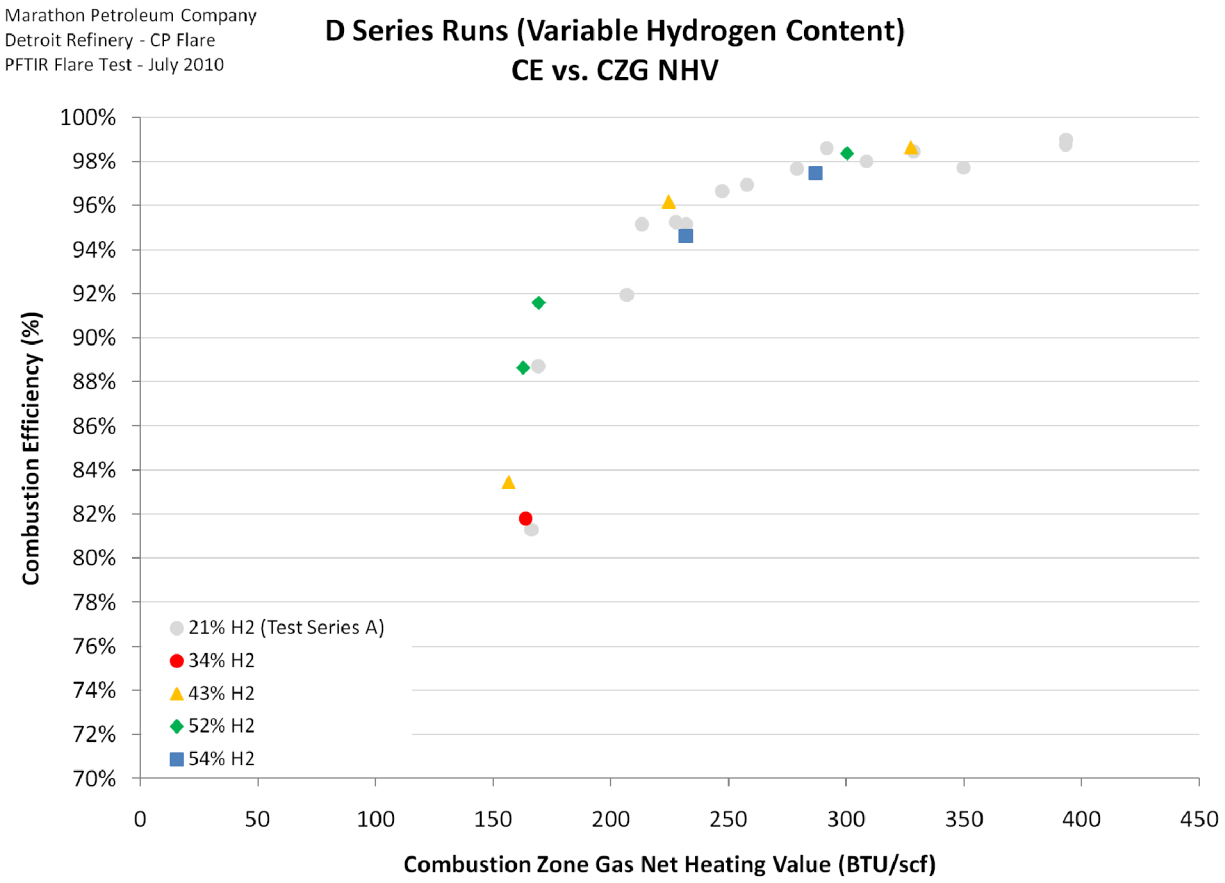

Figure 3.1-13: CE vs CZG NHV for Test Series D (Hydrogen)

In a petroleum refinery, there may be relief and/or operational scenarios that would divert highly concentrated hydrogen to a flare. At high combustion efficiencies hydrogen has little or no effect. It will not, for example, even at high concentrations, raise a 98% combustion efficiency to 99%. However, once combustion efficiency begins to drop off due to increased steam injection, hydrogen has the effect of reducing the rate of combustion efficiency decline.

3.1.3 Observed Impacts of Nitrogen (Test Series E)

The purpose of test series E is to determine the effects of nitrogen on the flare operating envelope. In particular we looked at the comparison of diluting the vent gas with nitrogen to diluting the vent gas with steam. It is not common to operate the flare at Detroit with nitrogen rich vent gas streams. However, purging tanks or loading trucks may require that nitrogen be vented to the flare.

Because nitrogen is non-combustible, it dilutes the combustion zone gas net heating value (CZG NHV) even when the vent gas flow rate is substantial and the S/VG is low. Test series E focused on flare performance at low S/VG with varying nitrogen composition. Specifically, two S/VG ratios (0.6 and 1.0) were tested while varying the vent gas nitrogen content. Table 3.1-5 lists these test conditions. Figure 3.1-14 shows the combustion efficiency results for each S/VG condition. The nitrogen content was increased until the CZG NHV was at or below 200 BTU/scf for the first run. After each run at each S/VG ratio, the nitrogen content was reduced to yield a higher CZG NHV. A total of seven runs were completed for test series E. Each run was 15 minutes, and no replicates were performed. Combustion efficiency for the E4-1 (N2≈66%) was measured with the secondary PFTIR at the road location. Because of hardware issues with this instrument the data is not reported and the run was marked invalid. Section 5.6.1 contains more detailed process conditions for test series E.

S/VG = 0.6			**S/VG = 1.0**		
Run	N_2 (%)	CZG NHV (BTU/scf)	Run	N_2 (%)	CZG NHV (BTU/scf)
E2-1	70%	188	E4-1 (invalid)	66%	161
E1-1	68%	212	E6-1	60%	183
E3-1	66%	223	E7-1	56%	213
E5-1	61%	279			

Table 3.1-5: Test Conditions for Test Series E (Nitrogen)

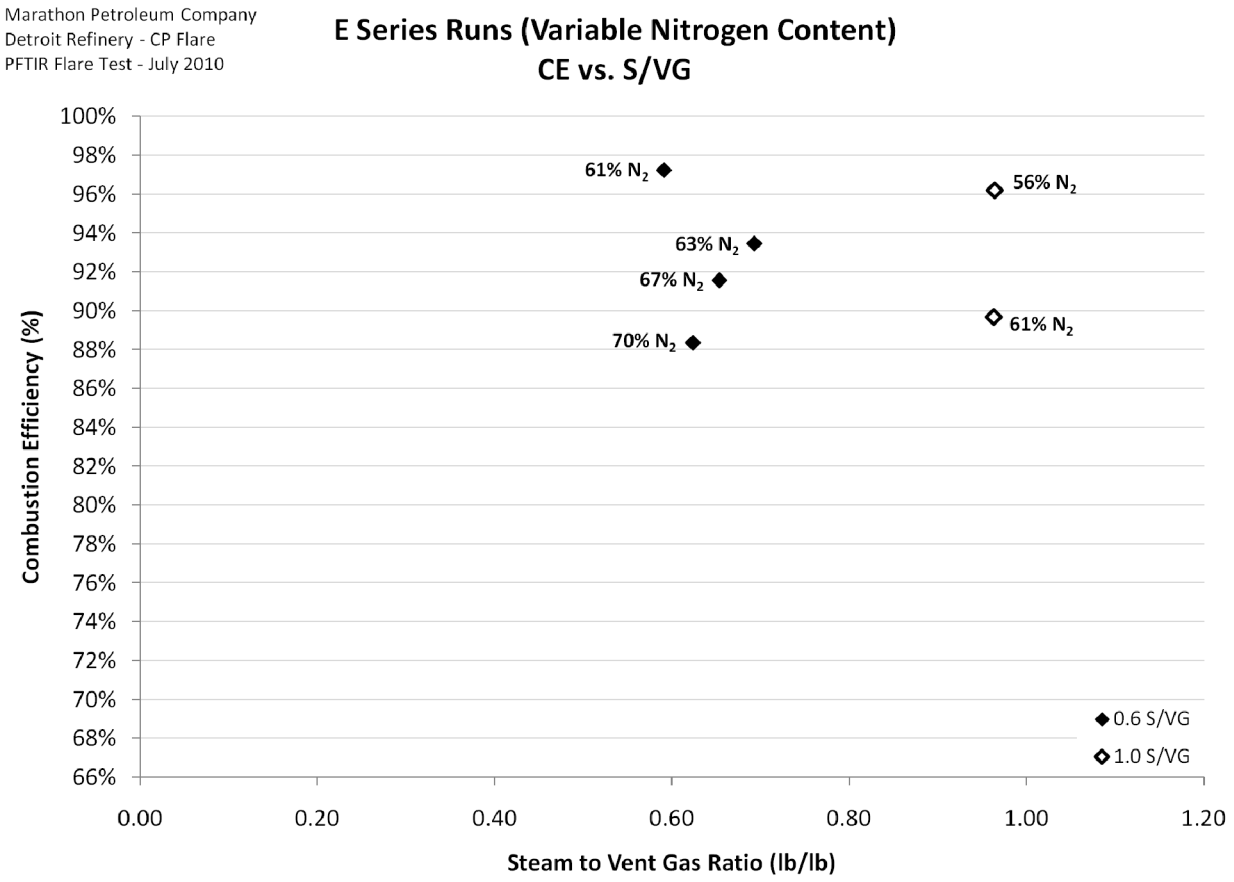

Figure 3.1-14: CE vs. S/VG for Test Series E (Nitrogen)

Figure 3.1-15 shows the relationship between combustion efficiency and CZG NHV at both S/VG set points. A clear trend of decreasing combustion efficiency with increasing nitrogen content (and thus lower CZG NHV) is present in both S/VG set points.

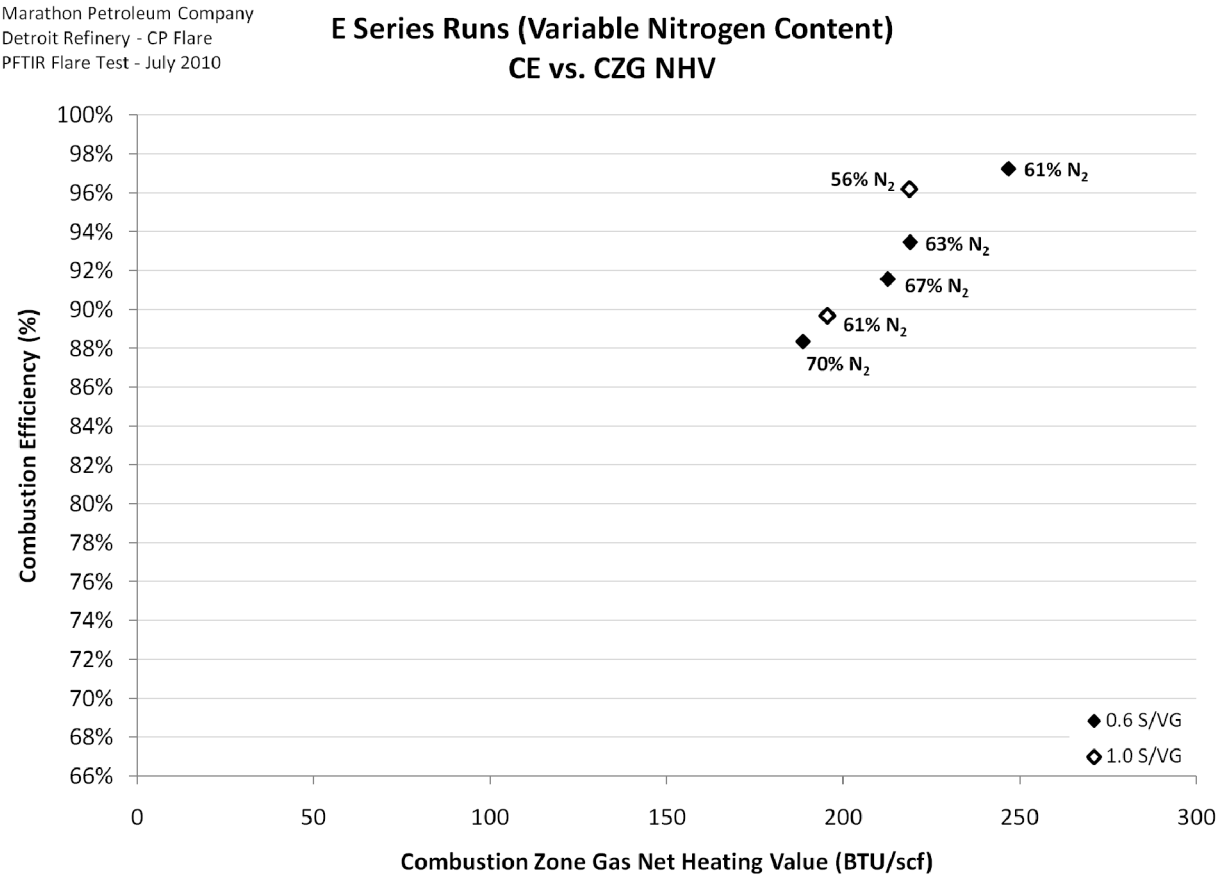

Figure 3.1-15: CE vs. CZG NHV for Test Series E (Nitrogen)

The results for combustion efficiency vs. CZG NHV in test series E are similar to the results in test series A and B. Figure 3.1-16 shows the relationship between combustion efficiency and CZG NHV for test series E with test series A and B added in the background. The trend of decreasing combustion efficiency as CZG NHV is decreased for test series E fits well with the same trend for test series A and B. Thus, the decrease in combustion efficiency when adding nitrogen appears to follow the same trend as when adding steam.

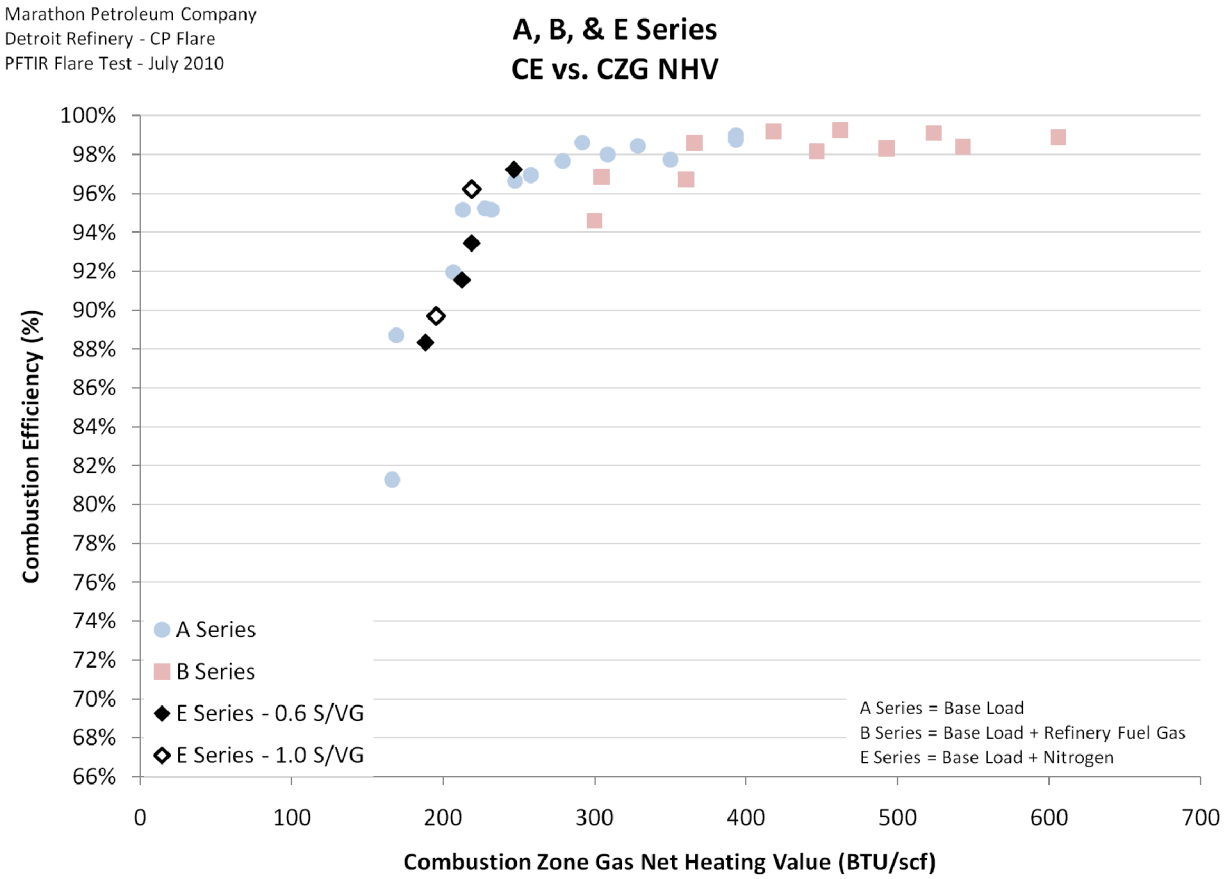

Figure 3.1-16: CE vs. CZG NHV for Test Series A, B, and E

3.2 Summary and Key Data Trends of Entire Data Set

3.2.1 Composite of All Hydrocarbons Tested

When comparing the combustion efficiency curves for test series A, B, and C, an overall trend emerges. Figure 3.2-1 shows the relationship between combustion efficiency and S/VG on a lb/lb basis for test series A, B, and C. For unsaturates such as propylene (test series C), the decreasing combustion efficiency trend appears to develop more rapidly with increasing S/VG than for base load or refinery fuel gas conditions (test series A and B).

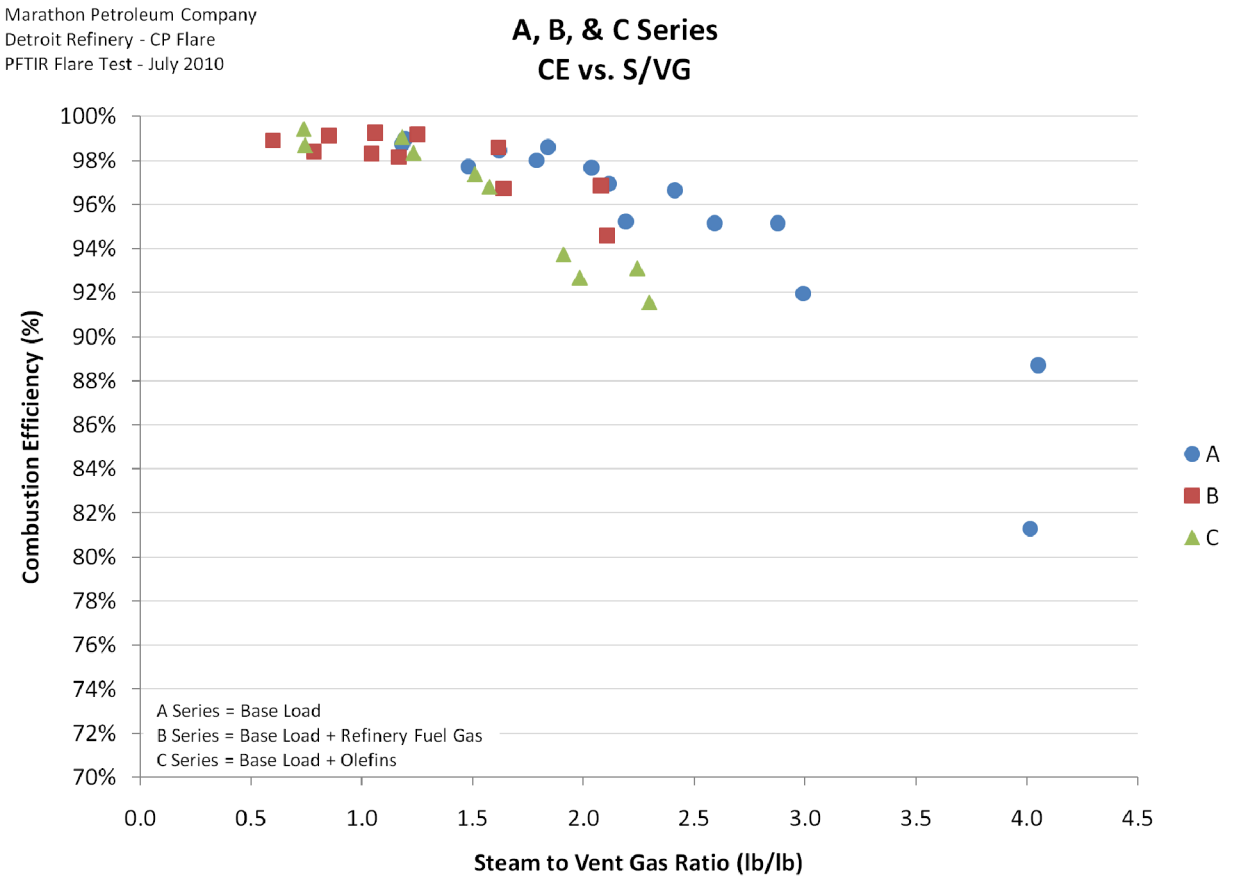

Figure 3.2-1: CE vs. S/VG (lb/lb) for Test Series A, B, and C

However, when S/VG is determined on a volumetric basis (scf/scf), the separation between test series A/B and test series C does not appear (See Figure 3.2-2). This indicates that the separation in test series C may be caused by a molecular weight effect. Further research is being conducted into this issue..

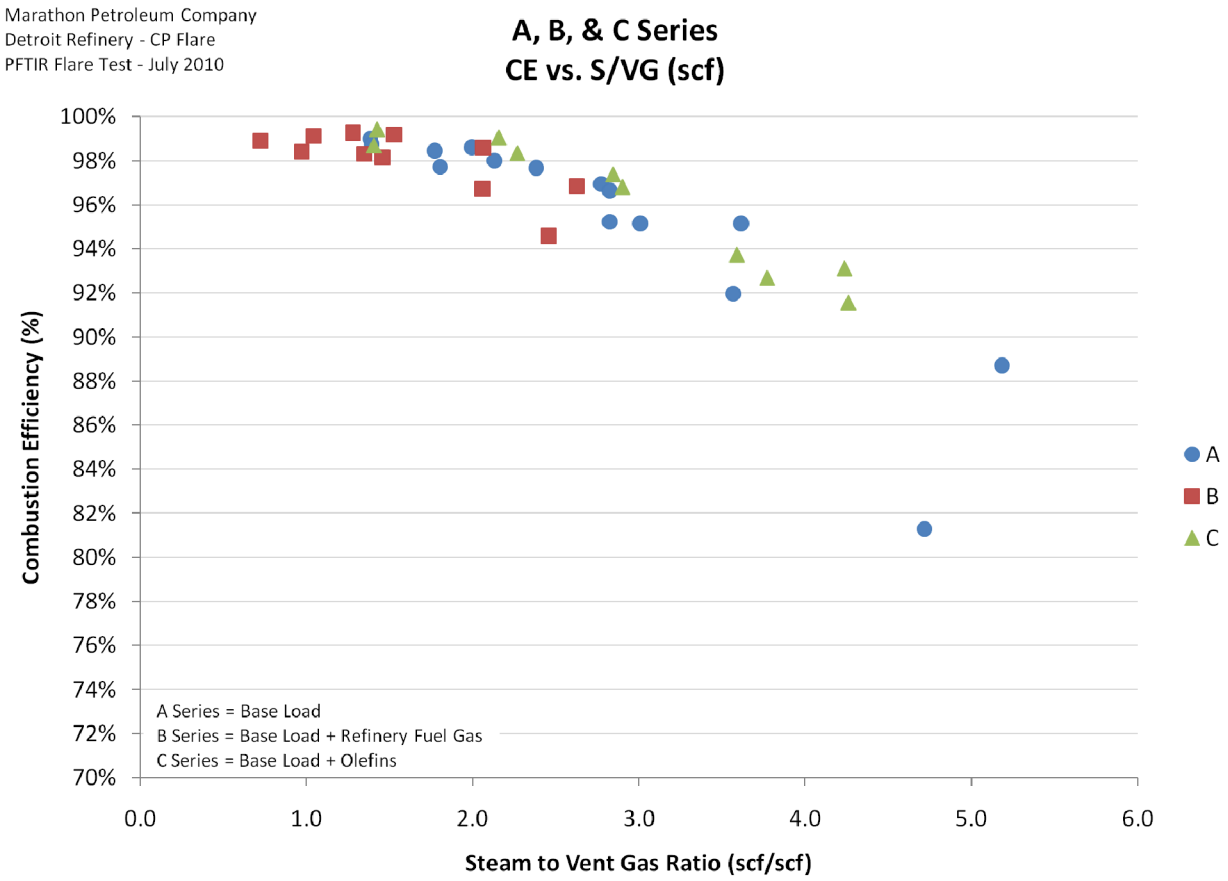

Figure 3.2-2: CE vs. S/VG (scf/scf) for Test Series A, B, and C

Figure 3.2-3 shows the relationship between combustion efficiency and S/S521 for test series A, B, and C. Test series A and B follow the same trend of maintaining high combustion efficiency until a S/S521 of 5.0-6.0. Test series C shows a steeper decline in combustion efficiency as S/S521 increases above 3.5. Because S521 takes into account molecular weight, S/S521 on a standard cubic foot basis does not change the observed trends.

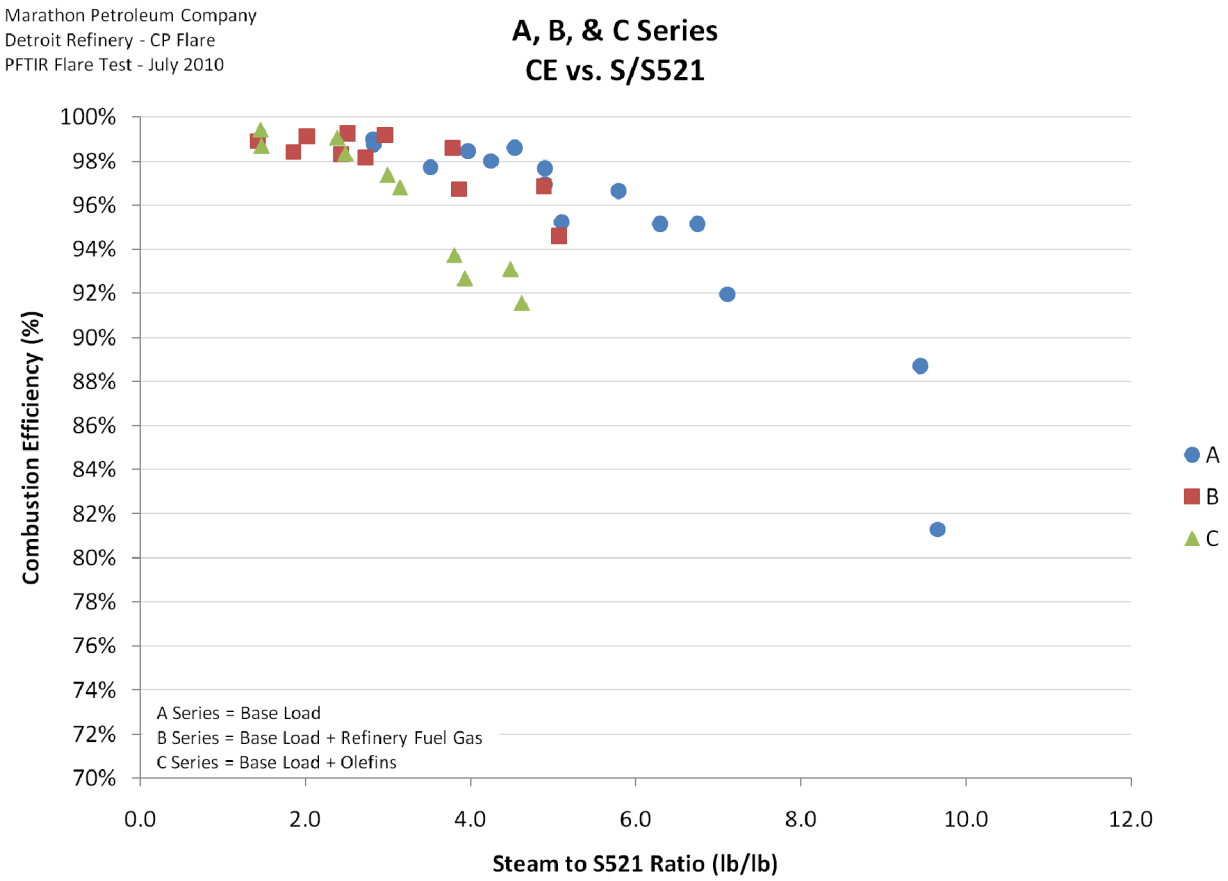

Figure 3.2-3: CE vs. S/S521 for Test Series A, B, and C

Figure 3.2-4 shows the relationship between combustion efficiency and CZG NHV for test series A, B, and C. Test series A and B follow the same trend of decreasing combustion efficiency below a CZG NHV of about 250 BTU/scf. Test series C combustion efficiency begins to decrease at a higher CZG NHV of about 425 BTU/scf.

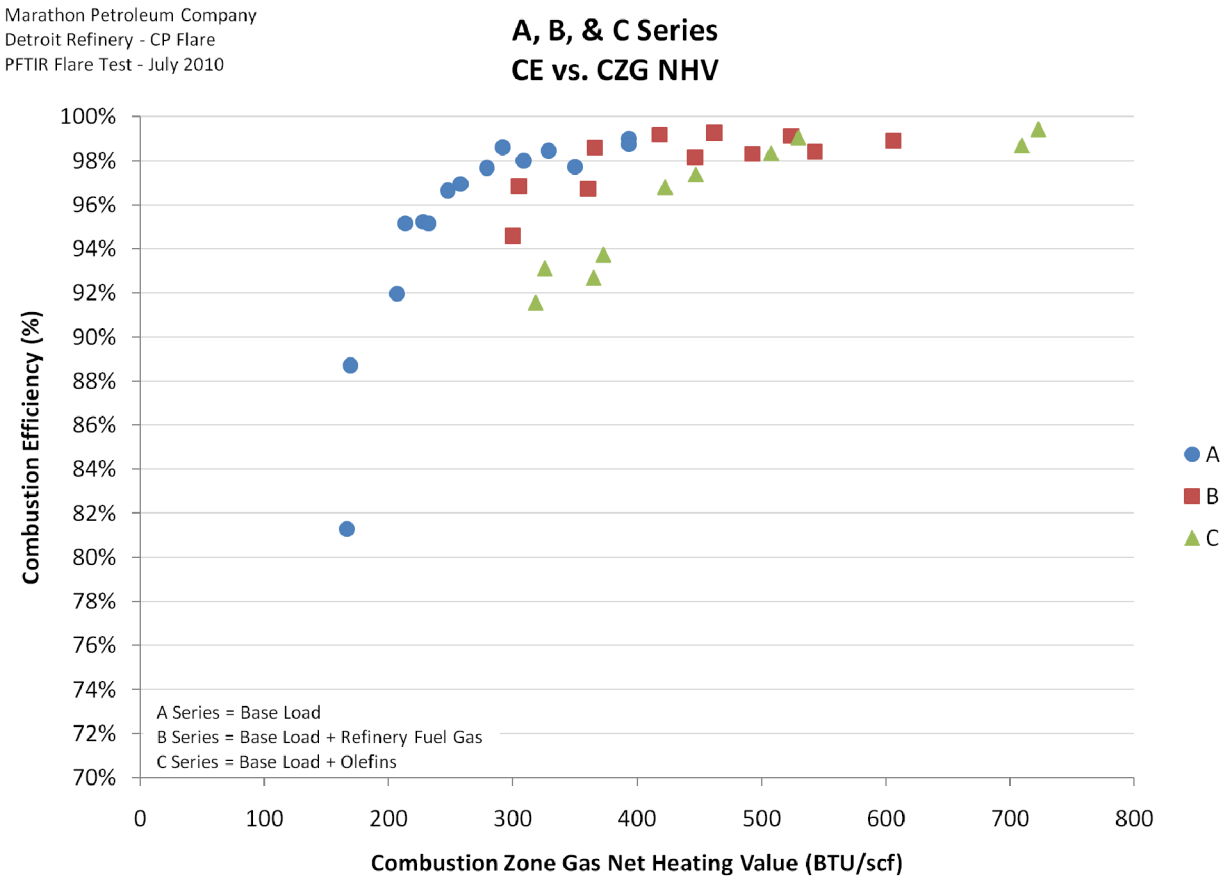

Figure 3.2-4: CE vs. CZG NHV for Test Series A, B, and C

3.2.2 Visible Emissions and Combustion Efficiency

Unlike the Texas City test, the Detroit test protocol did not allow for intentionally taking flare operation past the incipient smoke point or to extinguish the flare. Flare visual readings were still collected during the test program using the same scale as the Texas City test. Table 3.2-1 describes the flare visual rating scale.

The incipient smoke point is designated as the number 5 (the center of the scale), and represents the point at which the flare displays a "marbled" texture, indicative of small carbon soot particles forming in the combustion zone but quickly dissipating. No visible soot particles are present outside of the flame boundary at the incipient smoke point.

Flame ratings above 5 indicate increasing visible emissions extending beyond the flame boundary observed by an increasingly distinct trailing smoke plume. Flame ratings less than 5 indicate a visible flame decreasing in intensity until it becomes invisible. Ratings of 4 to 2 indicate a visible flame and a rating of 1 indicates a transparent or invisible flame. A flame rating of 0 indicates that the flare is extinguished with steam visually present.

Flame Rating	Flame Characteristic
0	Steam plume
1	Transparent
2	Mostly transparent, with occasional yellow flame.
3	Mostly yellow flame, with occasional transparency.
4	Yellow to orange flame.
5	Orange flame with some dark areas in the flame. (Incipient smoke point)
6	Orange flame with light smoke trail.
7	Clear steam at the flare tip, with an orange flame and a light smoke trail.
8	Orange flame with dark smoke trail leaving the flame.
9	Orange flame with heavy dark smoke trail leaving the flame.
10	Billowing black smoke

Table 3.2-1: Flare Visual Rating Scale

Figure 3.2-5 shows the relationship between combustion efficiency and visual rating for all runs. Most of the runs performed in the Detroit flare test had invisible flames and low visual ratings. For the runs that did have visible flames, combustion efficiency tended to be higher than for runs with invisible flames.

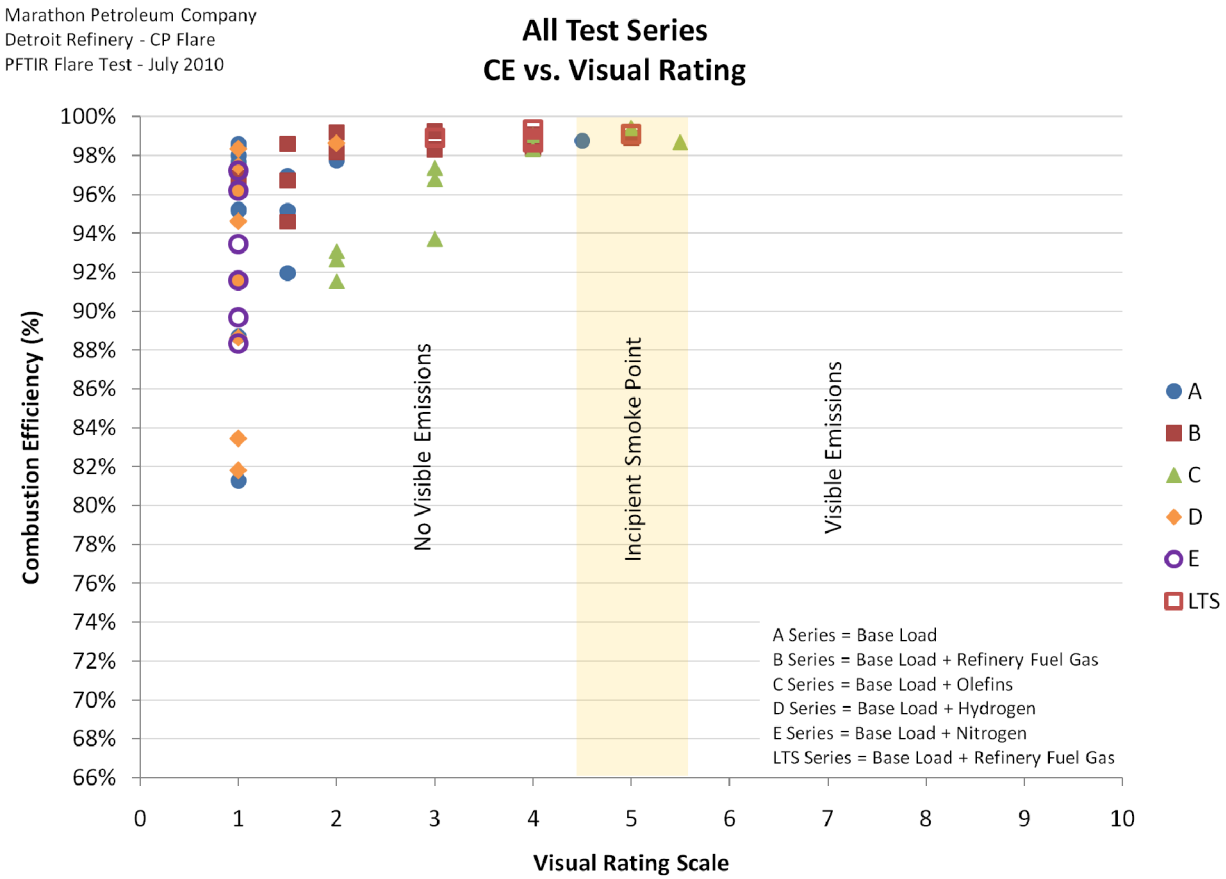

Figure 3.2-5: CE vs. Visual Rating for All Test Series

The range of the visual ratings observed for the Detroit test (1 to 6) was more limited than the range observed for the Texas City test (0 to 10) due to the limitations of the test protocol described above. However, within the 1 to 6 range, the Detroit test follows the same trend that appeared in the Texas City test results. The most consistently high combustion efficiencies appeared to be near the incipient smoke point (visual rating of 5). It is also possible to have an invisible flame that is still high combustion efficiency.

3.2.3 Comparisons to API 521 Table 11

The steam to hydrocarbon ratios for incipient smoke points in test series A, B, and C were always above the minimum recommended steam to hydrocarbon ratios listed in API 521 Table 11. Figure 3.2-6 lists shows where the incipient smoke point occurs for each test series in comparison to the API 521 Table 11 recommendation.

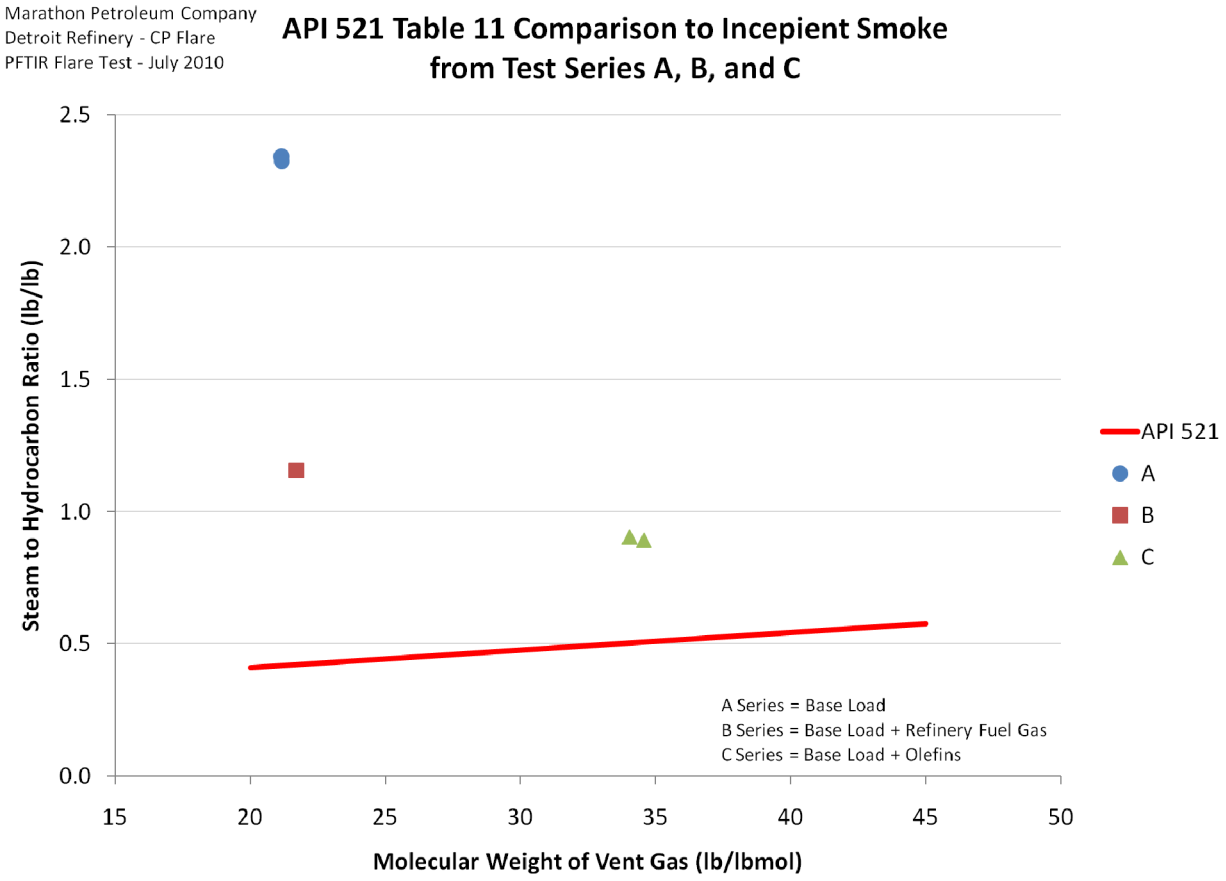

Figure 3.2-6: API 521 Table 11 Comparison to Test Series A, B, and C

3.3 Comparison with Texas City

The Texas City test was performed in 2009 on the Texas City Refinery Main Flare. The flare tip in Texas City was designed and manufactured by Callidus Technologies. The flare tip in Detroit was designed and manufactured by NAO Inc. Table 3.3-1 compares the specifications of the two tips.

	Detroit CP Flare	Texas City Main Flare
Tip Manufacturer	NAO Inc.	Callidus Technologies
Tip Model Number	20" NFF-RC	BTZ-IS^3/US-24-C
Effective Diameter	16"	23.25"
Maximum Vent Gas Rate	241,000 lb/hr	500,000 lb/hr
Base Load Vent Gas Rate	500-600 lb/hr	1,100-1,900 lb/hr
Steam Configuration	Center + Ring	Center + Lower + Upper
Avg Base Load Hydrogen	21%	15%

Table 3.3-1: Comparison of Detroit and Texas City Flare Specifications

For test series A (base load), the Detroit and Texas City tests have similar trends in combustion efficiency for S/VG (lb/lb), S/VG (scf/scf), S/S521, and CZG NHV. Figures 3.3-1 through 3.3-4 compare the trends for test series A in Detroit and Texas City.

For test series B (added refinery fuel gas), the Detroit and Texas City tests have mostly similar trends in combustion efficiency for S/VG (lb/lb), S/VG (scf/scf), S/S521, and CZG NHV. For the Texas City test, the combustion efficiency decreased rapidly below a S/VG (lb/lb) of 1.7. The Detroit test results do not show the same steep decrease in combustion efficiency above 1.7 S/VG (lb/lb). Figures 3.3-5 through 3.3-8 compare the trends for test series B in Detroit and Texas City.

For test series C (added olefins), the Detroit and Texas City results have very similar trends in combustion efficiency when using S/VG (scf/scf). However, for S/VG (lb/lb), S/S521, and CZG NHV, the Detroit and Texas City results have slightly different trends for combustion efficiency falloff. The increased molecular weight of the added olefins appears to impact only the mass-basis trends. Figures 3.3-9 through 3.3-12 compare the trends for test series C in Detroit and Texas City.

The overall trends observed with the test series performed at the Detroit flare performance test are similar to those from the 2009 Texas City flare performance test with the few previously mentioned exceptions. Figures 3.3-13 through 3.3-20 compare the combustion efficiency results from the Detroit test to the Texas City test results for all hydrocarbon test series: base load, added refinery fuel gas, and added olefins. Full view and zoomed in versions (>90% combustion efficiency) of the charts are shown.

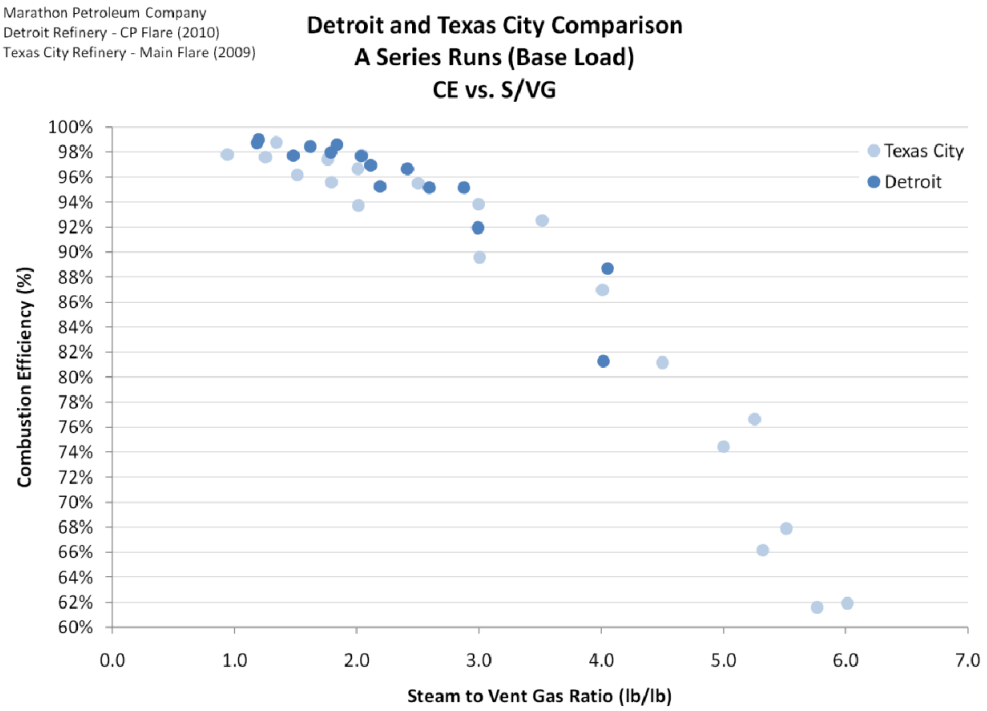

Figure 3.3-1: CE vs. S/VG (lb/lb) for Test Series A – TXC Comparison

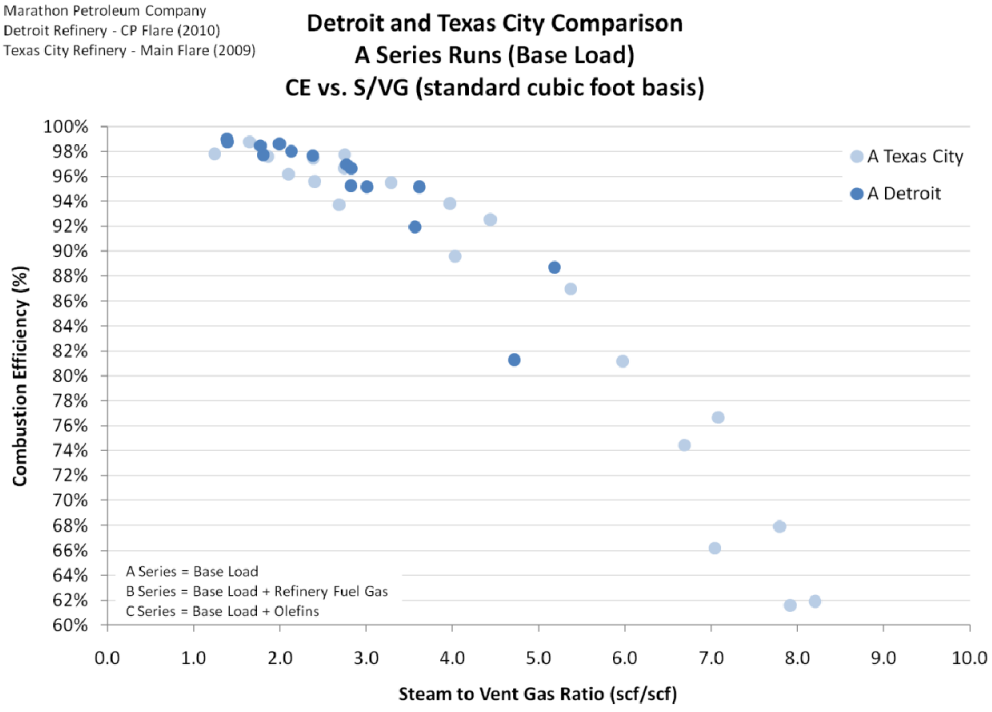

Figure 3.3-2: CE vs. S/VG (scf/scf) for Test Series A – TXC Comparison

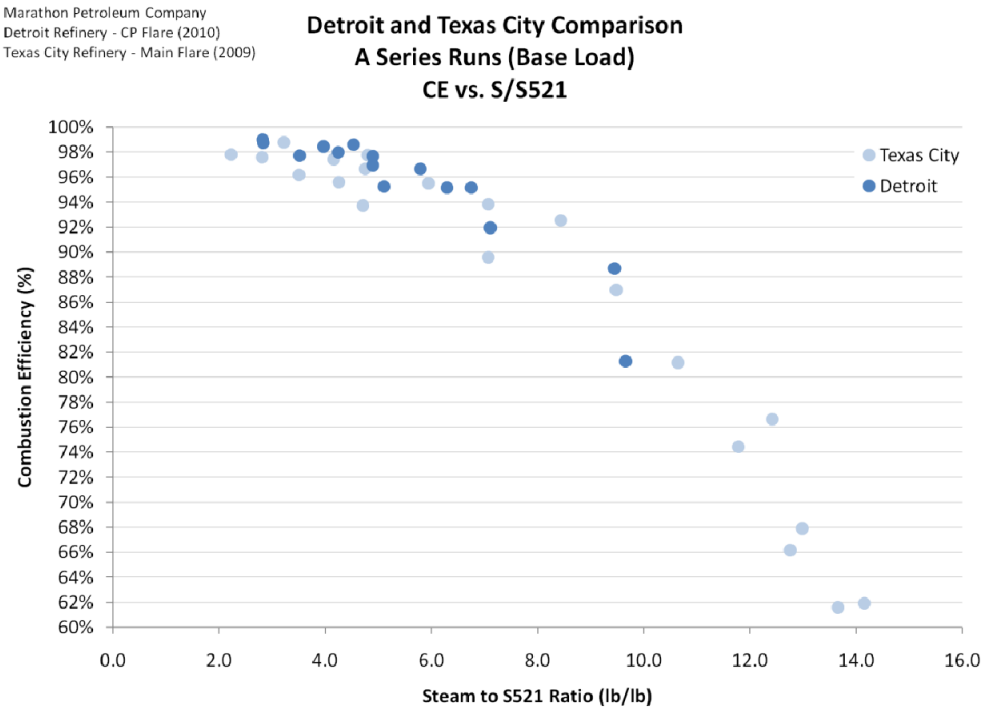

Figure 3.3-3: CE vs. S/S521 for Test Series A – TXC Comparison

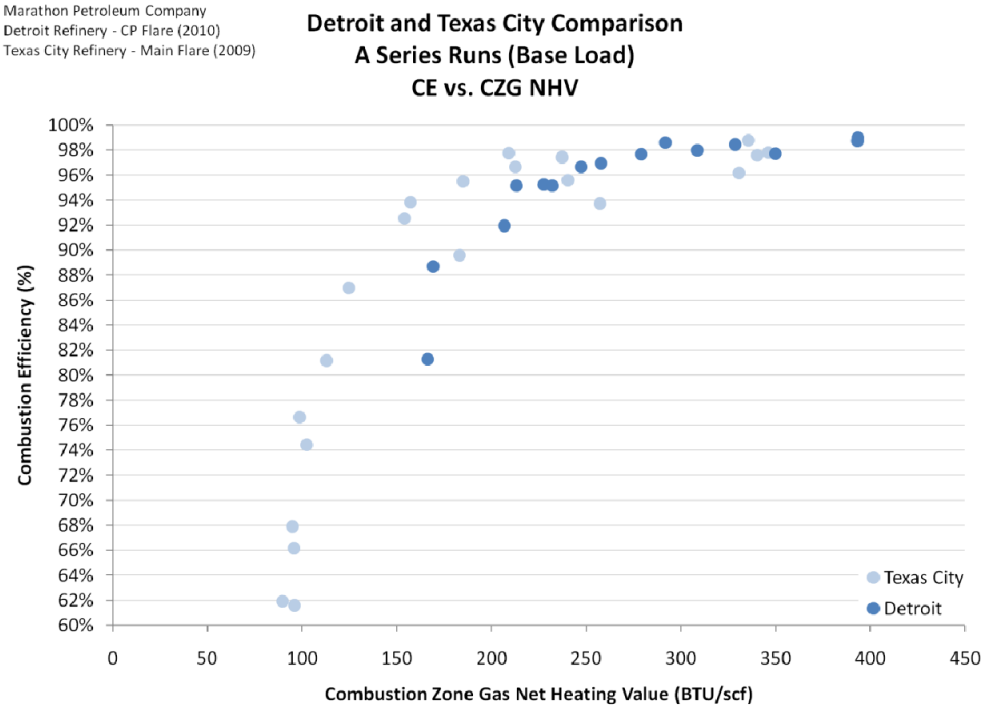

Figure 3.3-4: CE vs. CZG NHV for Test Series A – TXC Comparison

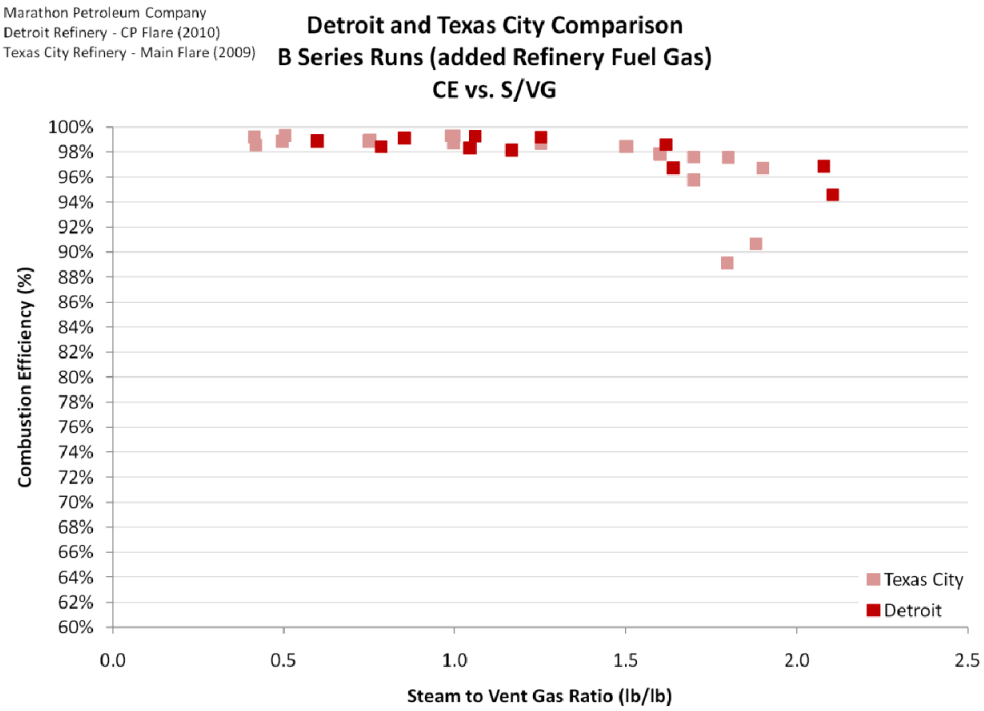

Figure 3.3-5: CE vs. S/VG (lb/lb) for Test Series B – TXC Comparison

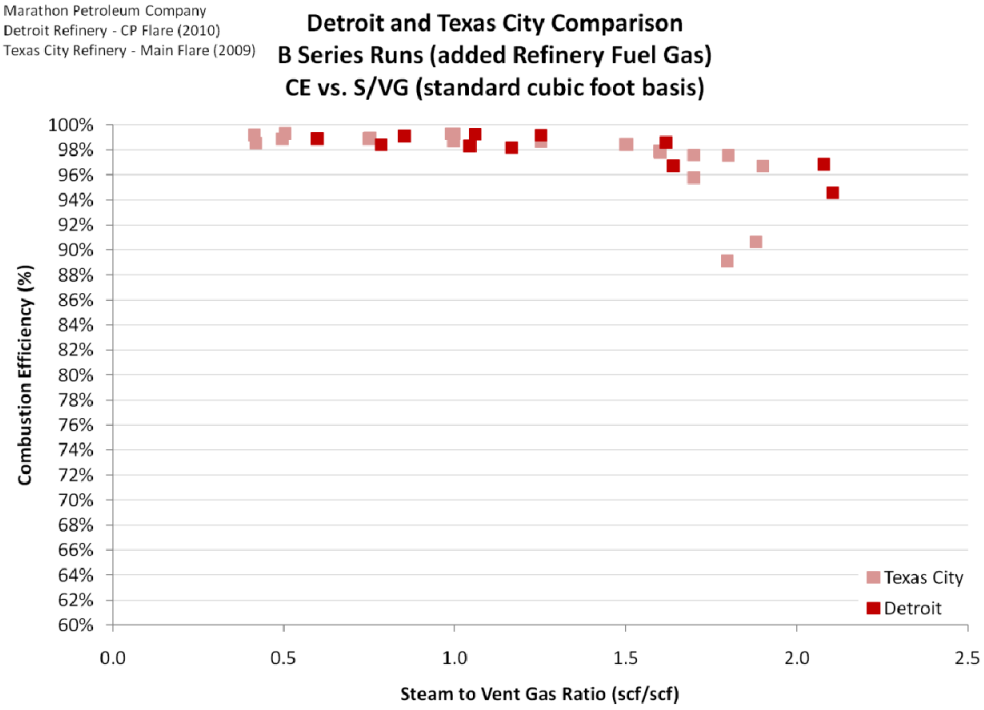

Figure 3.3-6: CE vs. S/VG (scf/scf) for Test Series B – TXC Comparison

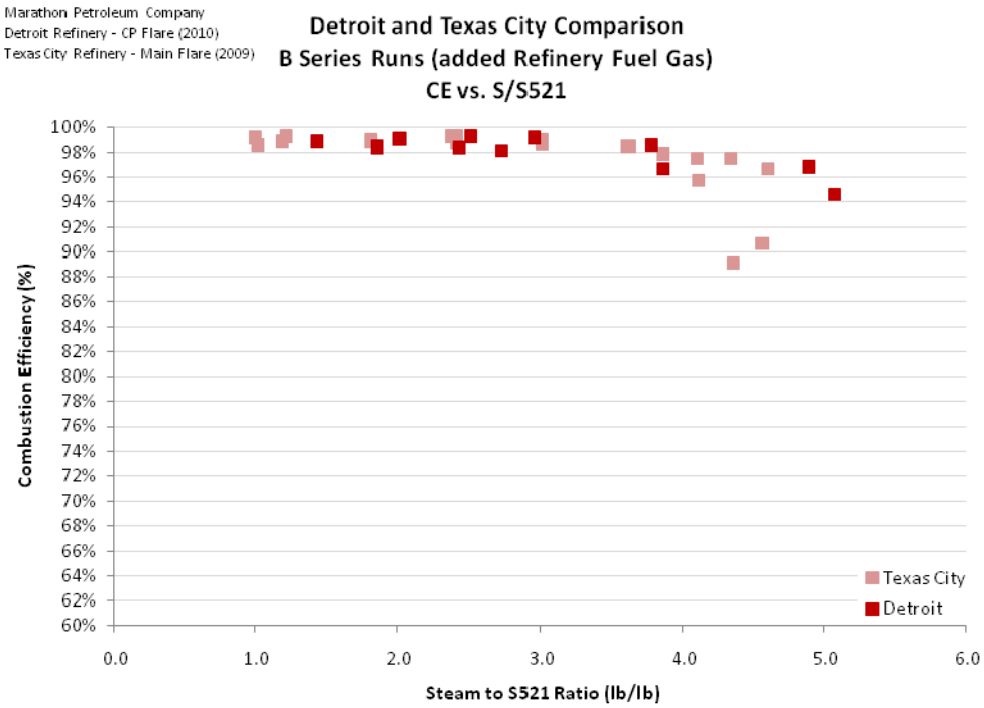

Figure 3.3-7: CE vs. S/S521 for Test Series B – TXC Comparison

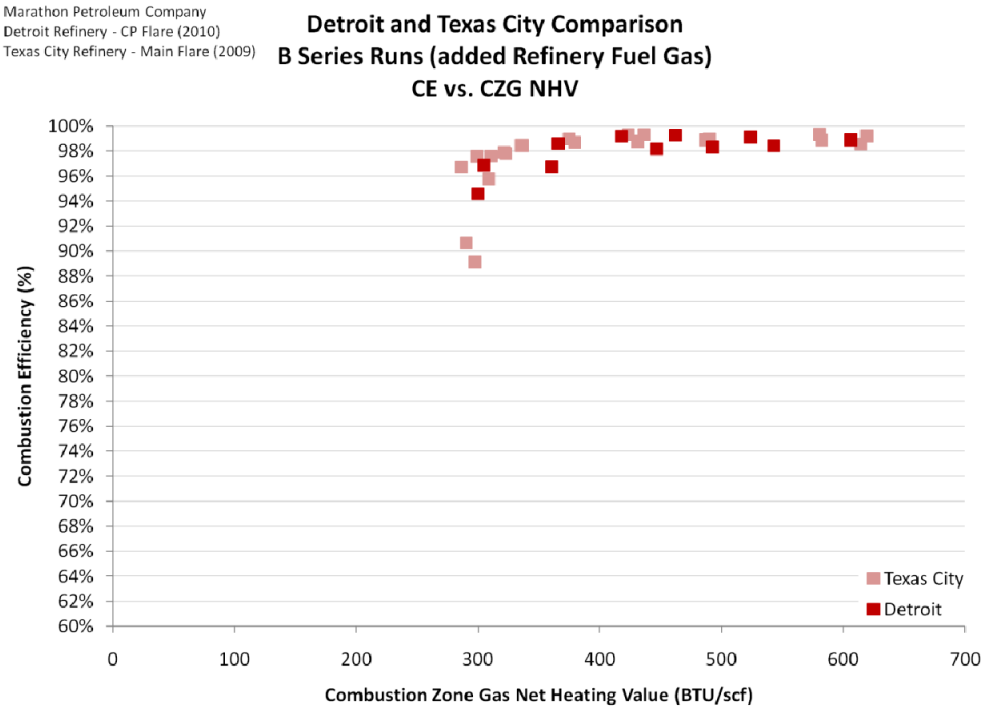

Figure 3.3-8: CE vs. CZG NHV for Test Series B – TXC Comparison

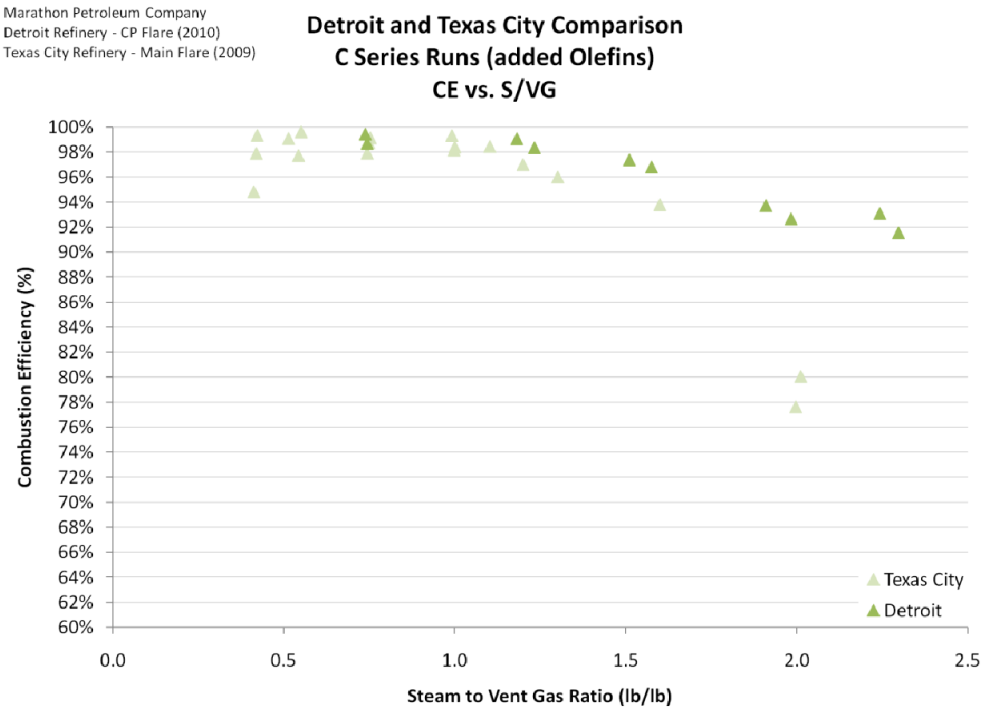

Figure 3.3-9: CE vs. S/VG (lb/lb) for Test Series C – TXC Comparison

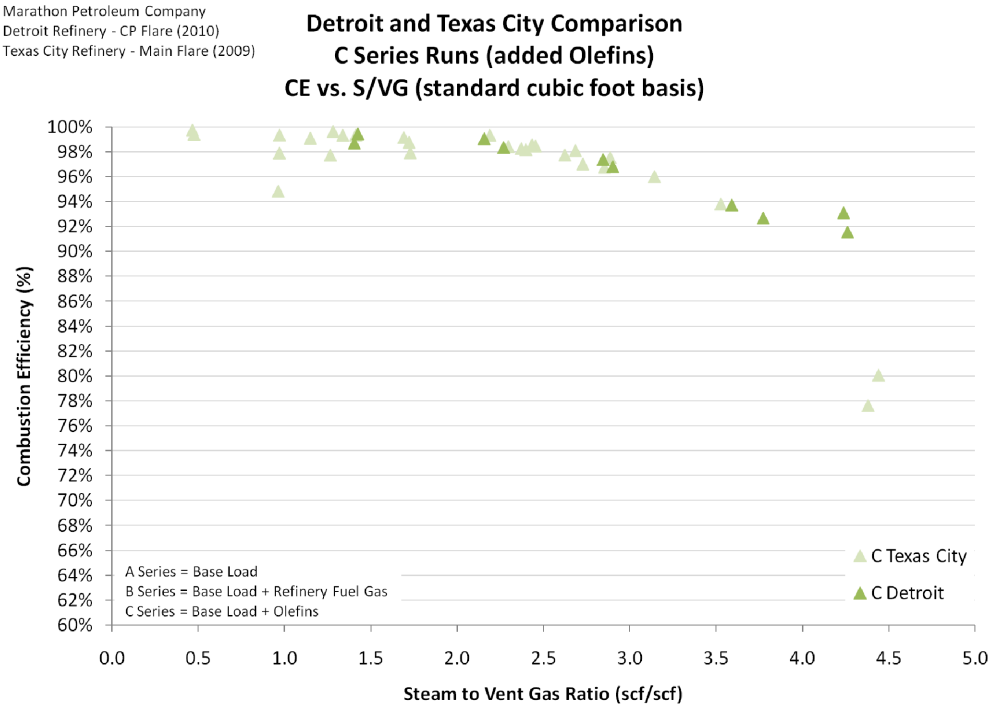

Figure 3.3-10: CE vs. S/VG (scf/scf) for Test Series C – TXC Comparison

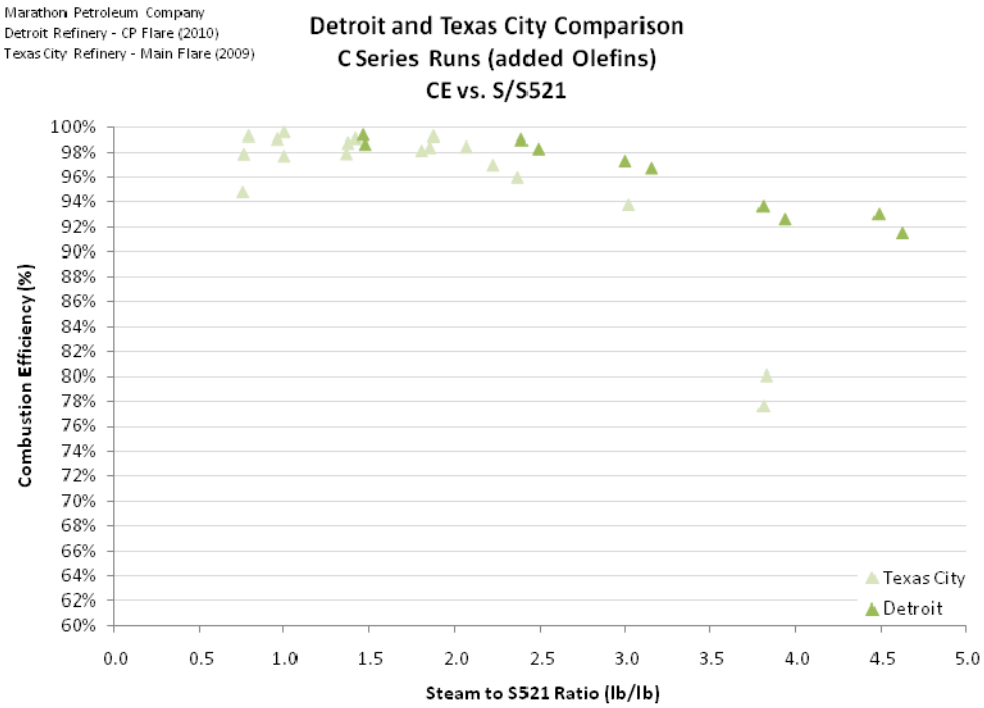

Figure 3.3-11: CE vs. S/S521 for Test Series C – TXC Comparison

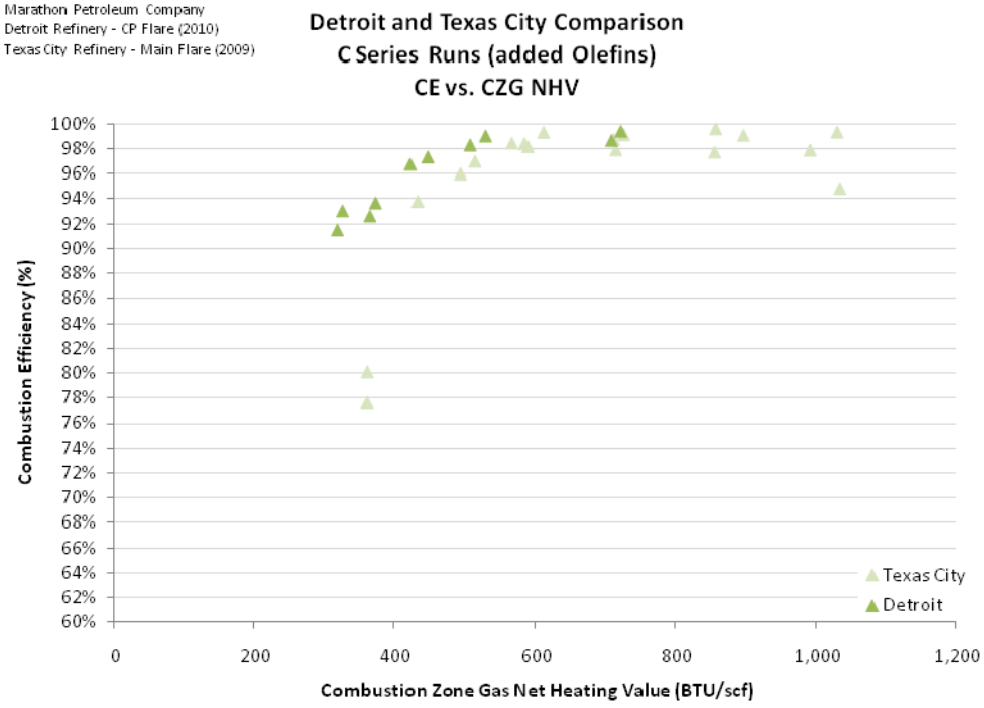

Figure 3.3-12: CE vs. CZG NHV for Test Series C – TXC Comparison

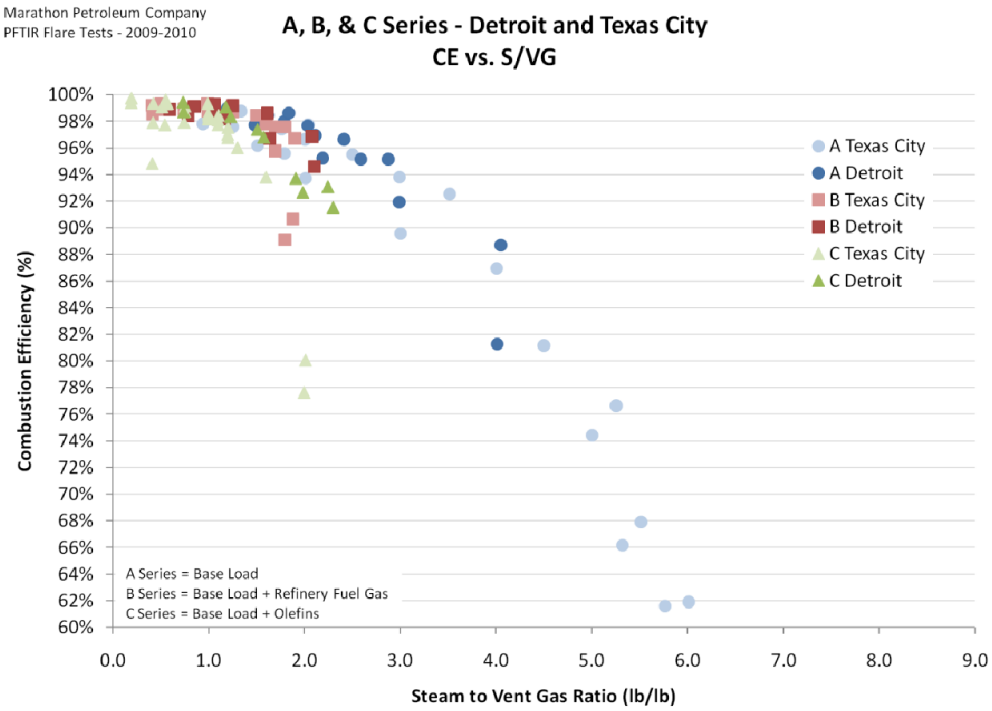

Figure 3.3-13: CE vs. S/VG (lb/lb) for Test Series A, B, and C – TXC Comparison

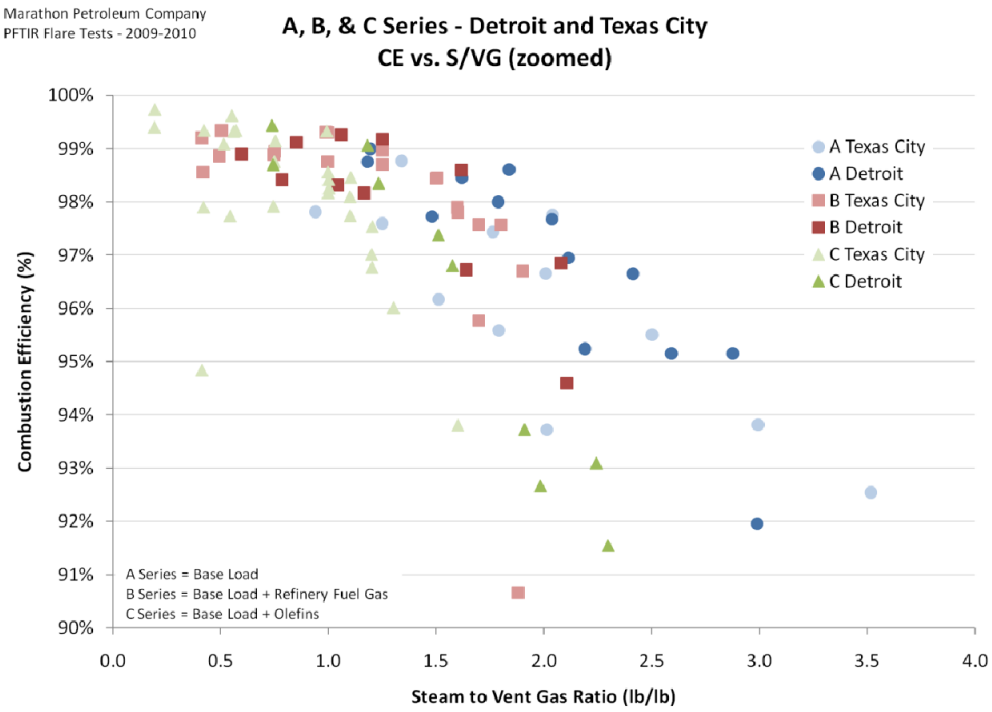

Figure 3.3-14: CE vs. S/VG (lb/lb) for Test Series A, B, and C (zoomed)

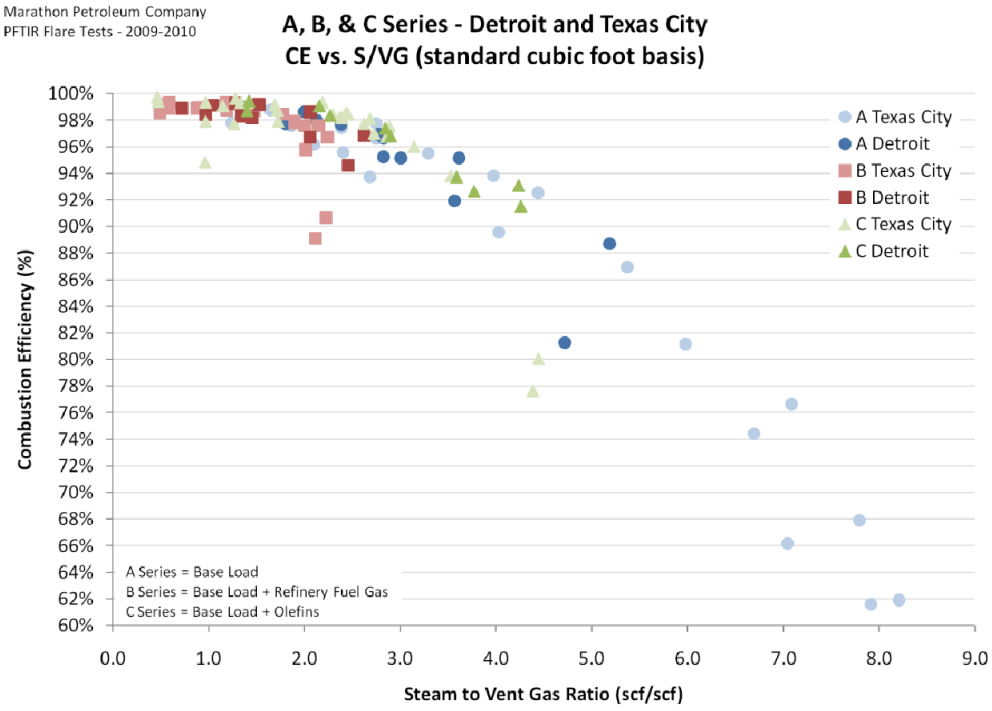

Figure 3.3-15: CE vs. S/VG (scf/scf) for Test Series A, B, and C – TXC Comparison

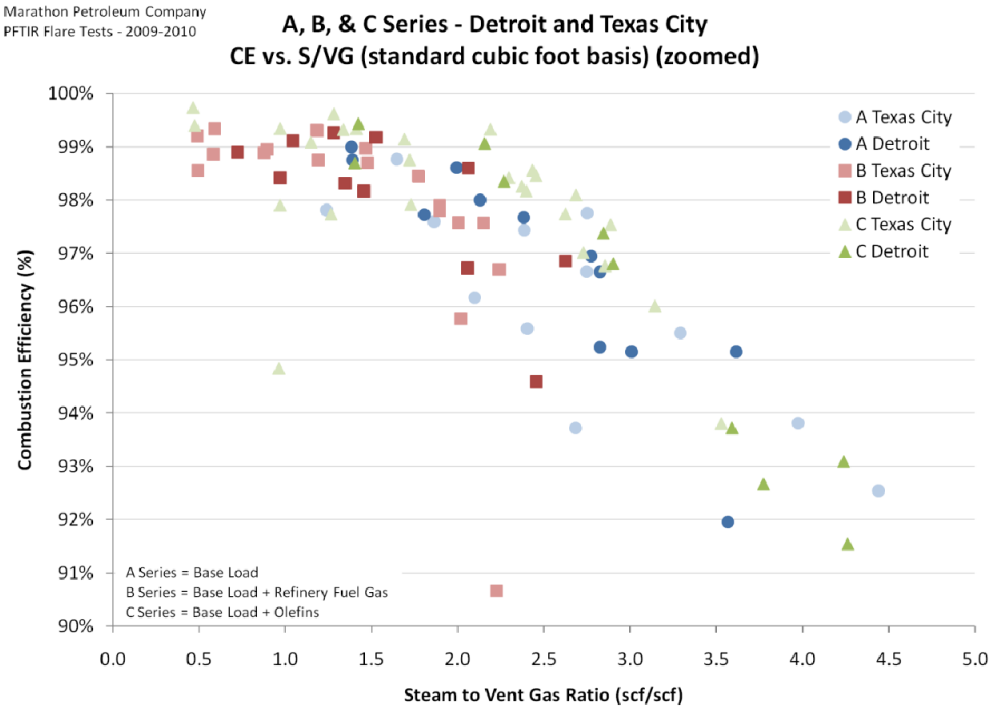

Figure 3.3-16: CE vs. S/VG (scf/scf) for Test Series A, B, and C (zoomed)

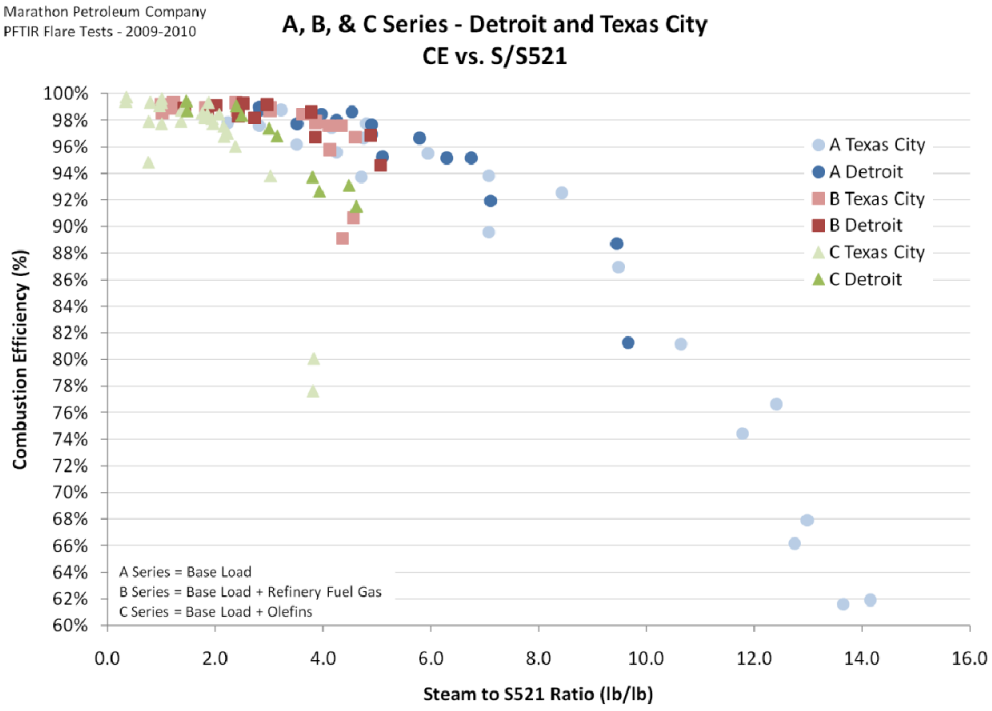

Figure 3.3-17: CE vs. S/S521 for Test Series A, B, and C – TXC Comparison

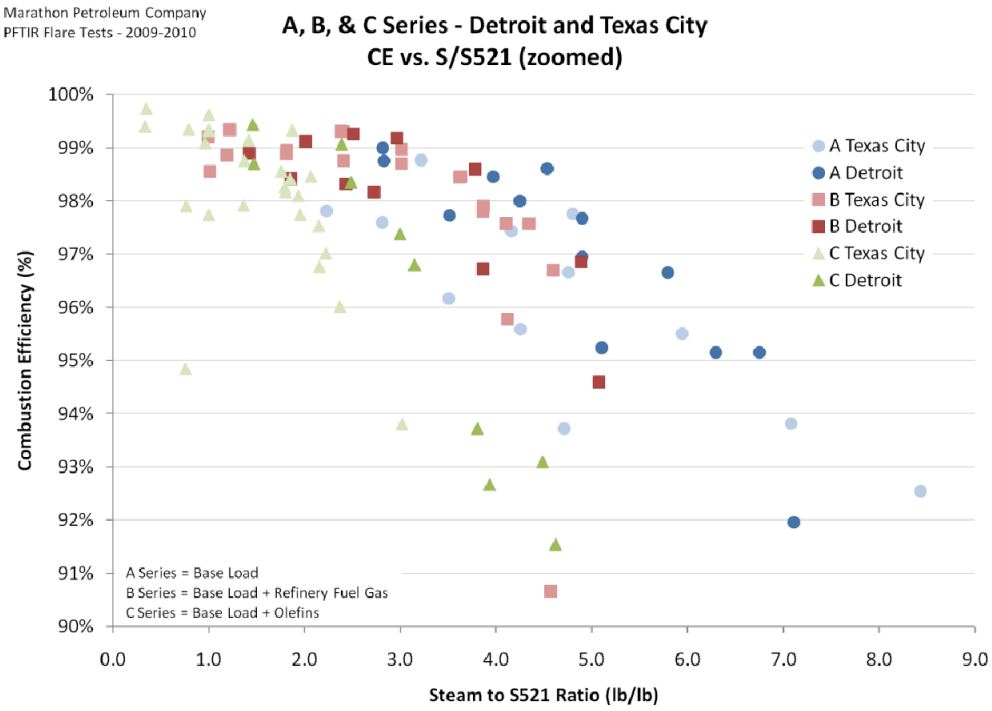

Figure 3.3-18: CE vs. S/S521 for Test Series A, B, and C (zoomed)

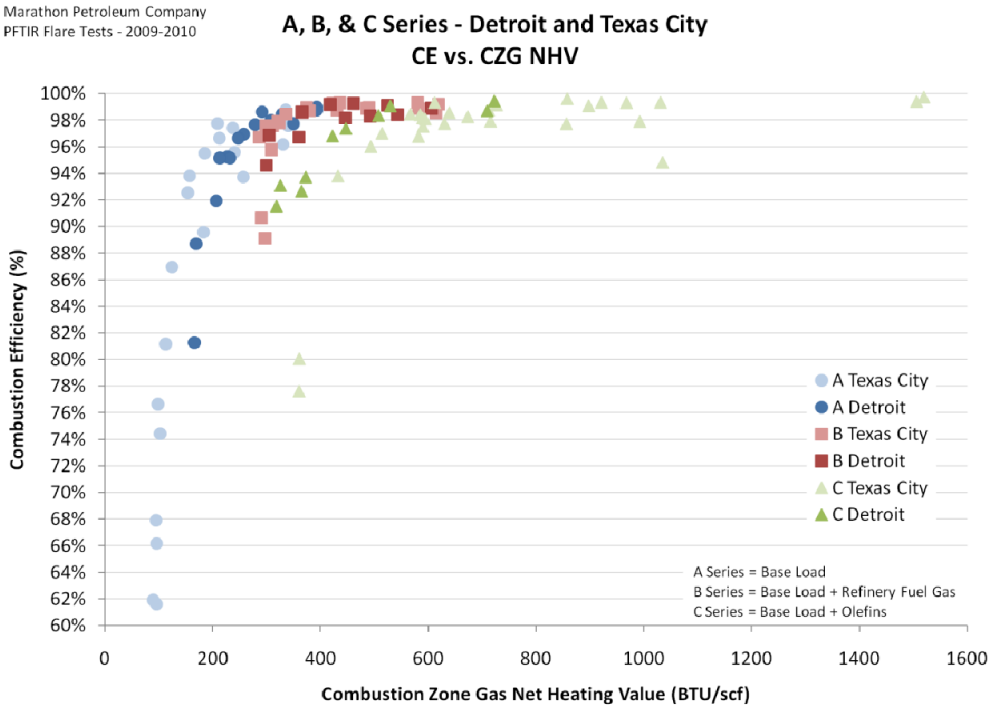

Figure 3.3-19: CE vs. CZG NHV for Test Series A, B, and C – TXC Comparison

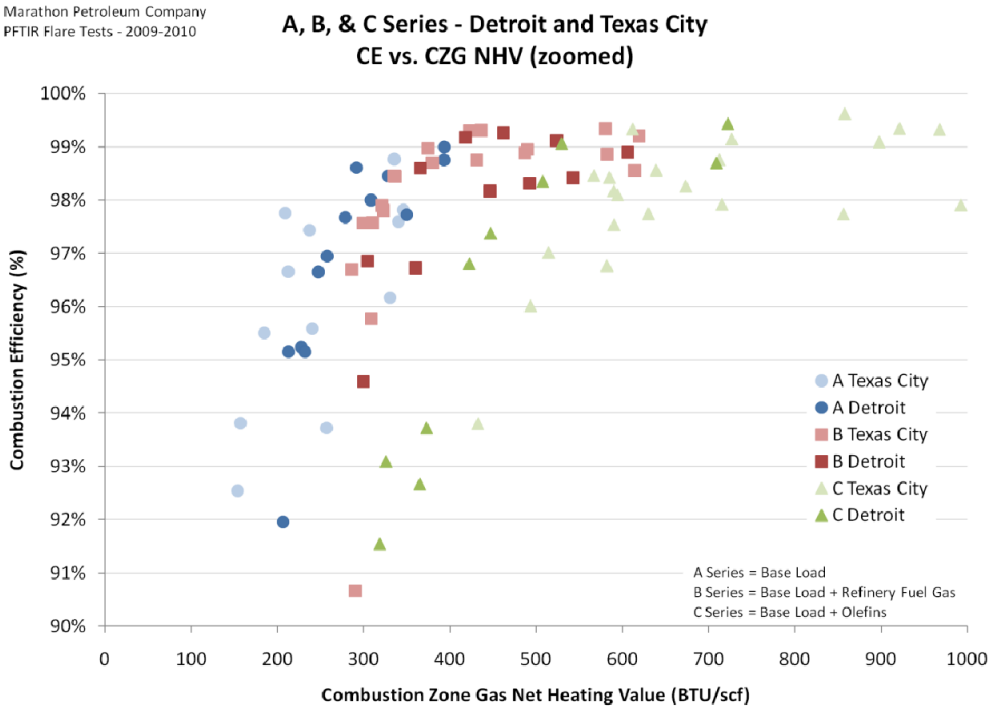

Figure 3.3-20: CE vs. CZG NHV for Test Series A, B, and C (zoomed)

3.4 Factors Influencing Test Results

3.4.1 Road PFTIR

During initial field hot cell checks (see Section 3.5.3.3) and FCCU tests (see Section 3.5.3.2), measurements from the Road PFTIR did not match the expected results. The Lot PFTIR measurements matched the expected results in the FCCU test, so the problem was isolated to the Road PFTIR. It was initially thought that the problem was calibration or software related. This meant the Road PFTIR could still collect spectra for tests, and the data could be reprocessed once the calibration or software issues were resolved. Because of these issues the Lot PFTIR was used as the primary PFTIR for all test runs. The Road PFTIR was only used when the Lot PFTIR did not have an acceptable view of the flare plume.

The issues with the Road PFTIR only became known while performing the initial bias checks (field hot cell check and FCCU test). These issues would not have been obvious during flare testing. Because they expose possible problems with PFTIR measurements, these bias checks should be a required part of the PFTIR test protocol.

After testing concluded, the spectra were analyzed more closely and a hardware problem with the Road PFTIR detector was discovered. The detector was sent to the manufacturer for repair. IMACC was unsuccessful in working around the problems with the spectra. Therefore, all data from the Road PFTIR was invalidated.

3.4.2 Run Lengths

During the Texas City test, each run was 10 minutes long. It was unknown whether the variation in minute-by-minute points would be more effectively averaged out with longer runs. Therefore, the Detroit test initially required 30 minute run lengths.

The 30 minute runs were analyzed to see if minute-by-minute combustion efficiency variability affected the run average. If the average combustion efficiency of three 10 minute sections were similar to the overall 30 minute run average, it indicated that longer run times would not improve the precision of the combustion efficiency results.

At the beginning of each day, the first run was performed for 30 minutes and PFTIR data was processed for preliminary combustion efficiency results. The run was split into three 10 minute sections. The average combustion efficiency of each section was compared to the average combustion efficiency of the entire 30 minute run. If the sections did not vary by more than 0.5% absolute combustion efficiency, the remainder of the runs for the day could be shorted to 20 minute run times.

After the Detroit test program was completed and PFTIR data was finalized, further analysis of run length variability was performed. Each run was split into 5, 10, and 15 minute sections. The average of each section was compared to the overall run combustion efficiency average. Results are shown in Figures 3.4-1 through 3.4-11. Only the LTS runs were analyzed for 15 minute sections because they were the only test series to have 30 minute run lengths for all runs.

From the graphs, it appears that 5 minute sections have significantly more variability than 10 minute sections. Also, as combustion efficiency begins to decline in the later runs for Test Series A, B, and C, the individual sections appear to become more variable. From the LTS runs, the change in variability between the 10 minute sections and the 15 minute sections is minimal. Combustion efficiency variability does not seem to decrease above 10 minutes. Therefore, the analysis indicates that runs over 10 to 15 minutes in length do not improve test precision.

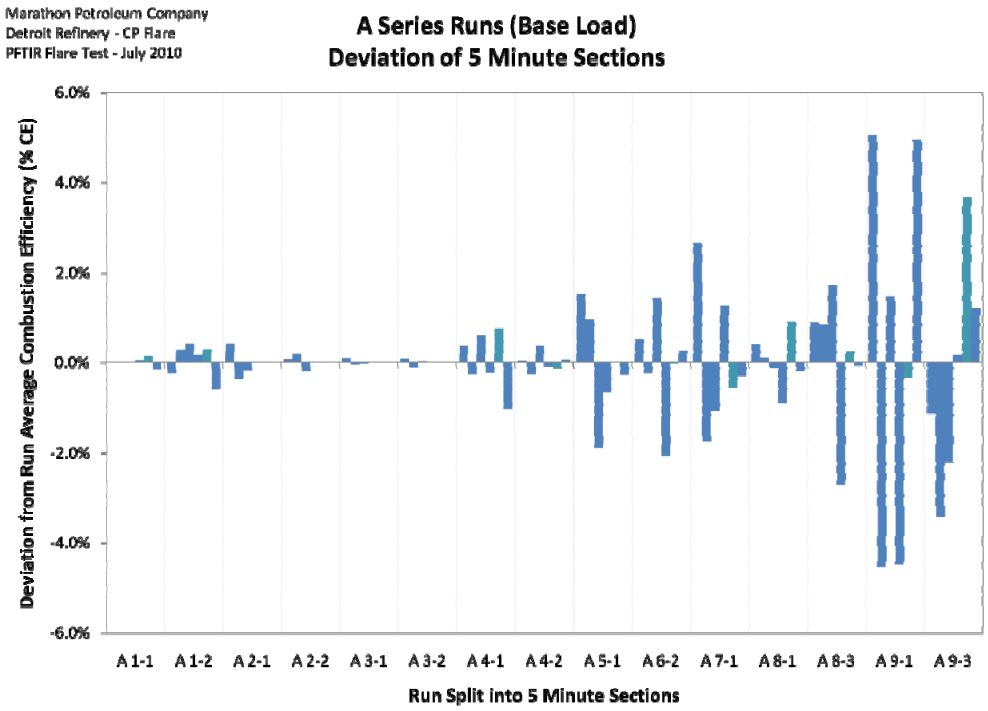

Figure 3.4-1: Test Series A – Deviation of 5 Minutes Sections

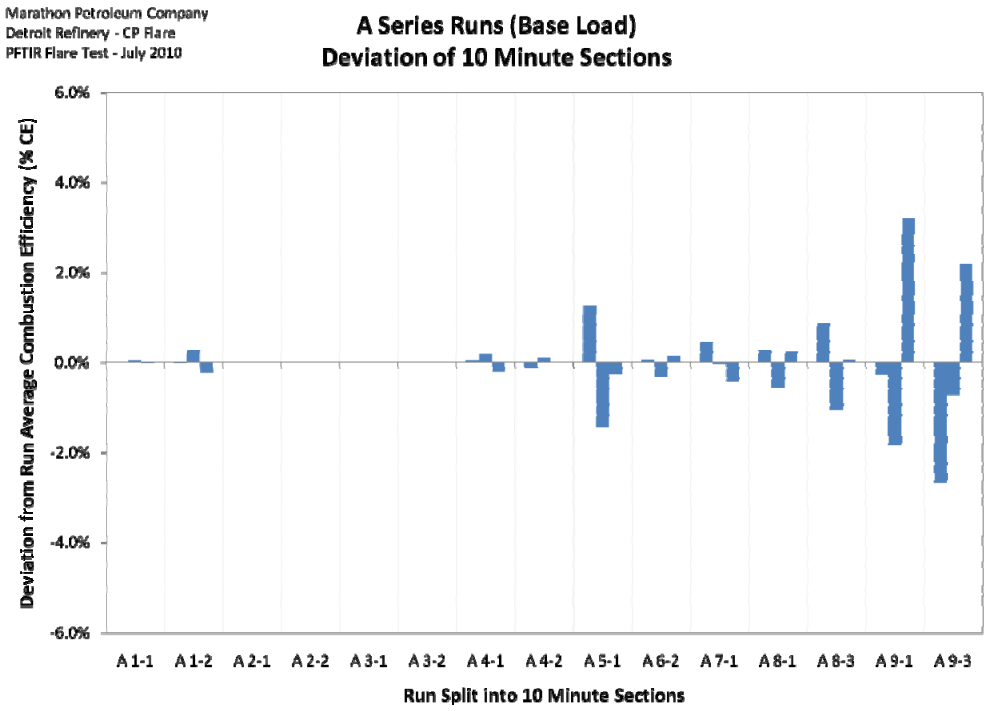

Figure 3.4-2: Test Series A – Deviation of 10 Minutes Sections

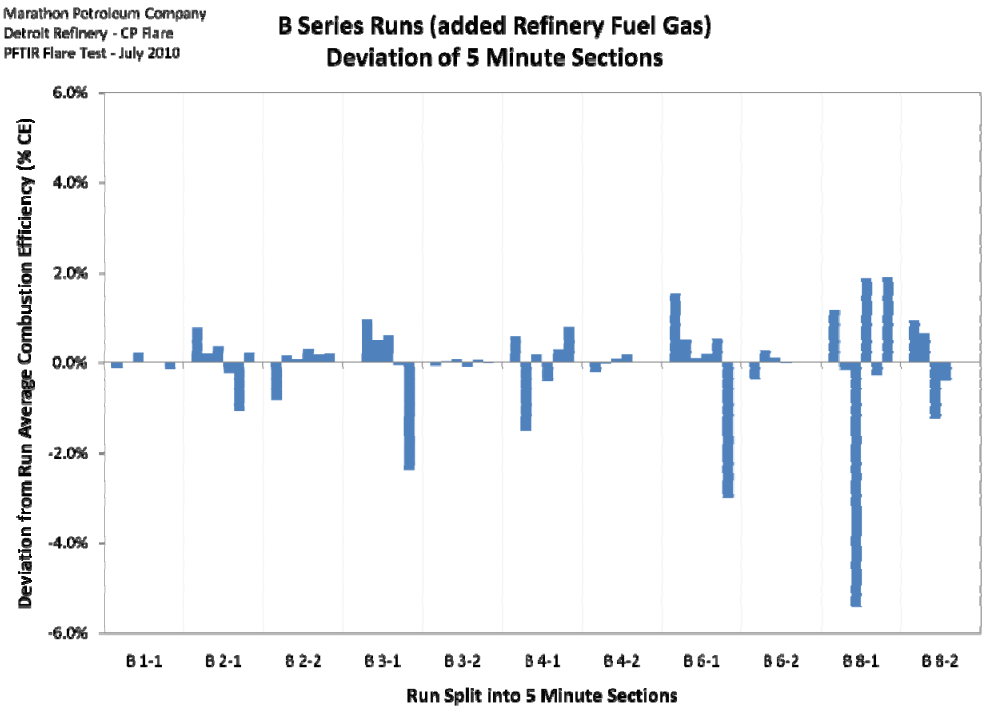

Figure 3.4-3: Test Series B – Deviation of 5 Minutes Sections

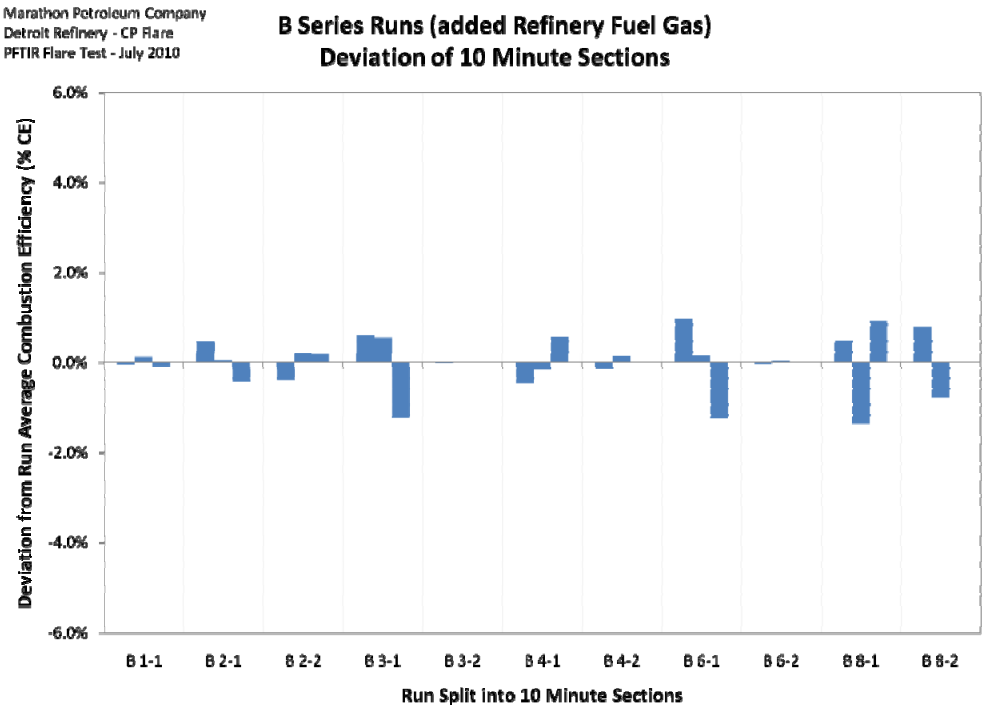

Figure 3.4-4: Test Series B – Deviation of 10 Minutes Sections

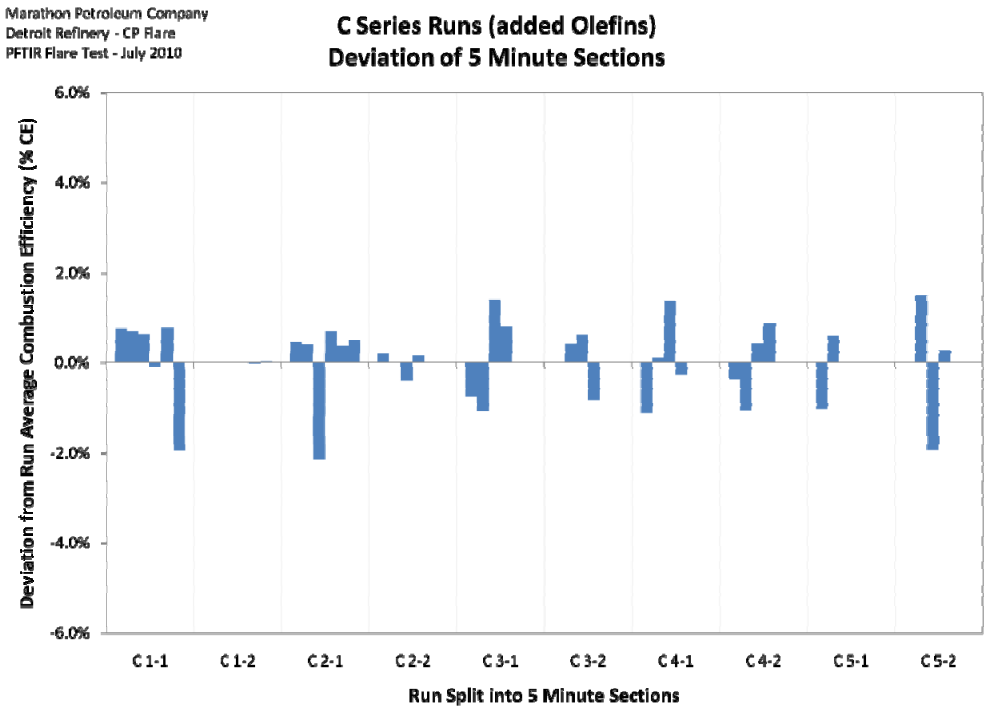

Figure 3.4-5: Test Series C – Deviation of 5 Minutes Sections

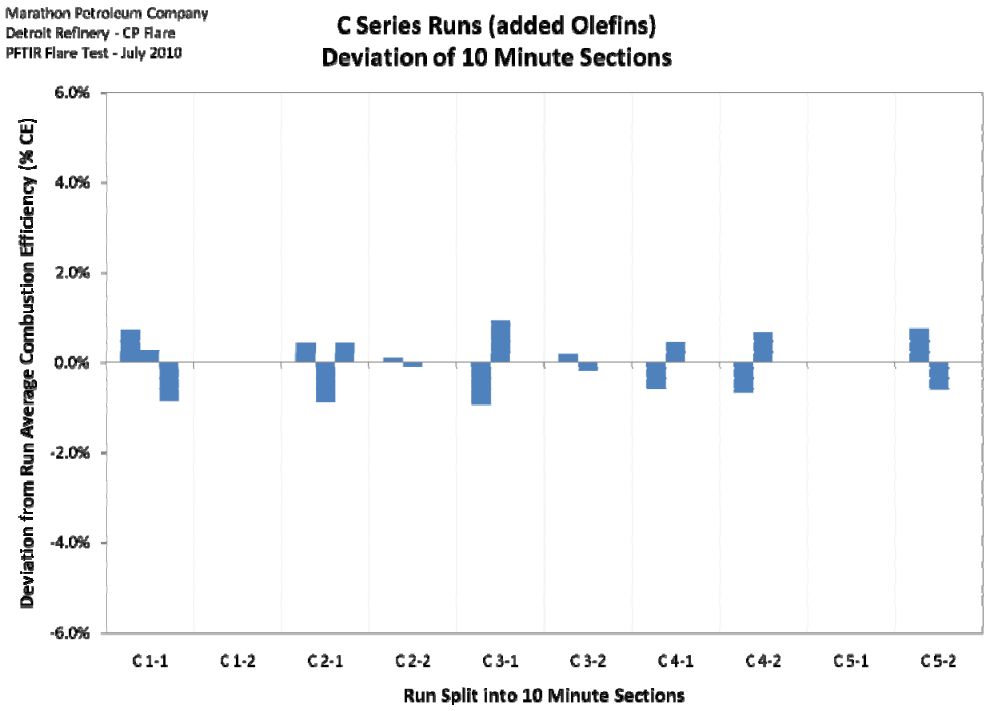

Figure 3.4-6: Test Series C – Deviation of 10 Minutes Sections

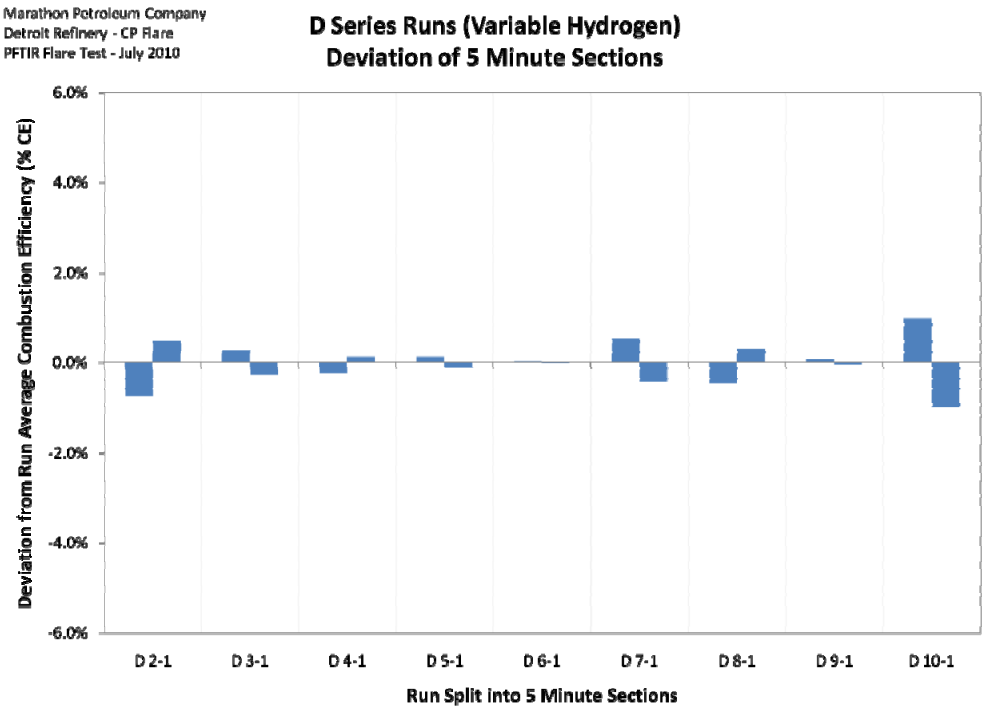

Figure 3.4-7: Test Series D – Deviation of 5 Minutes Sections

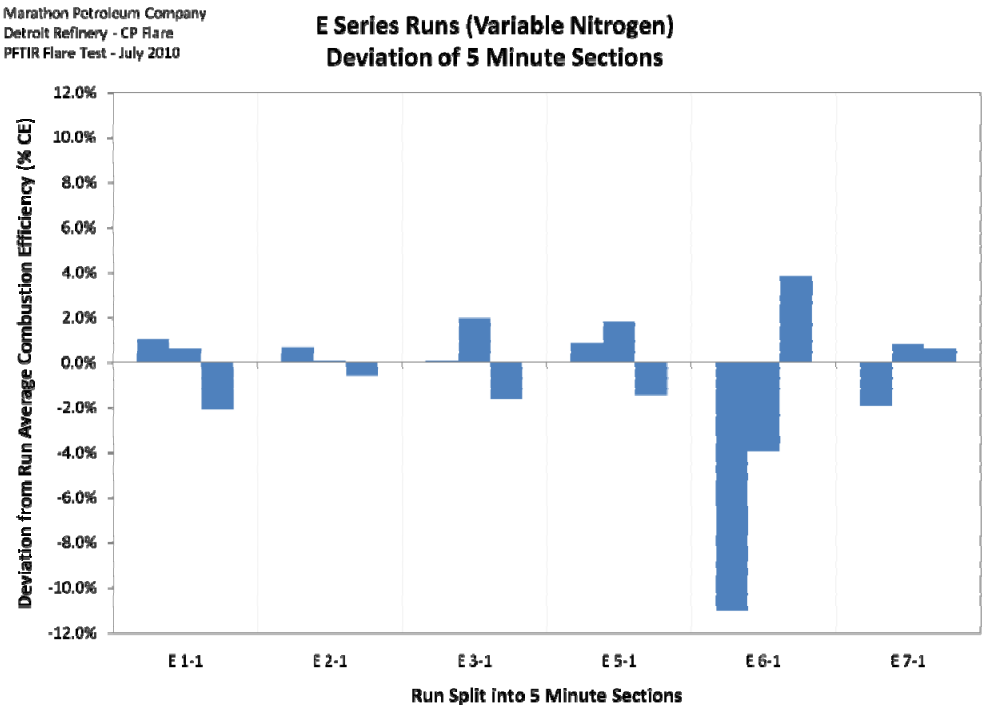

Figure 3.4-8: Test Series E – Deviation of 5 Minutes Sections

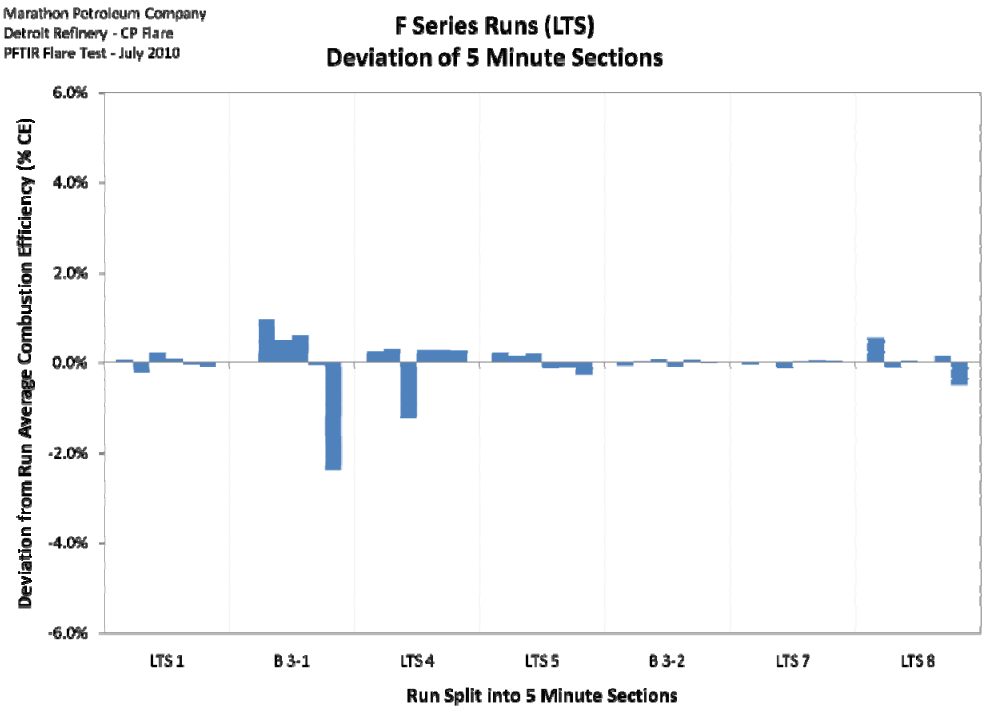

Figure 3.4-9: Test Series F (LTS) – Deviation of 5 Minutes Sections

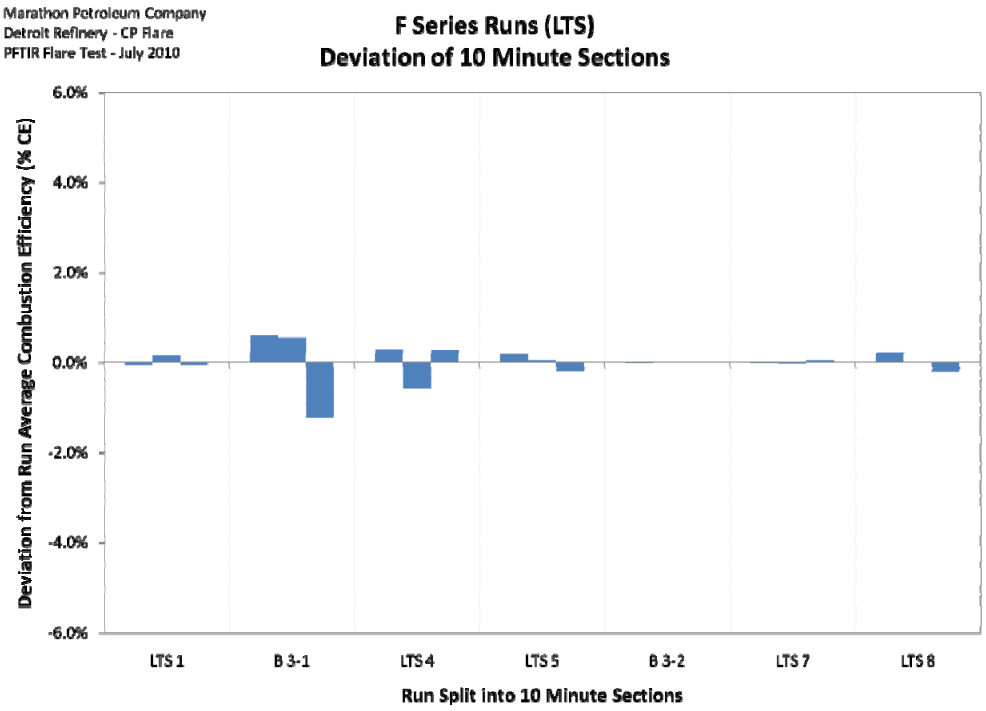

Figure 3.4-10: Test Series F (LTS) – Deviation of 10 Minutes Sections

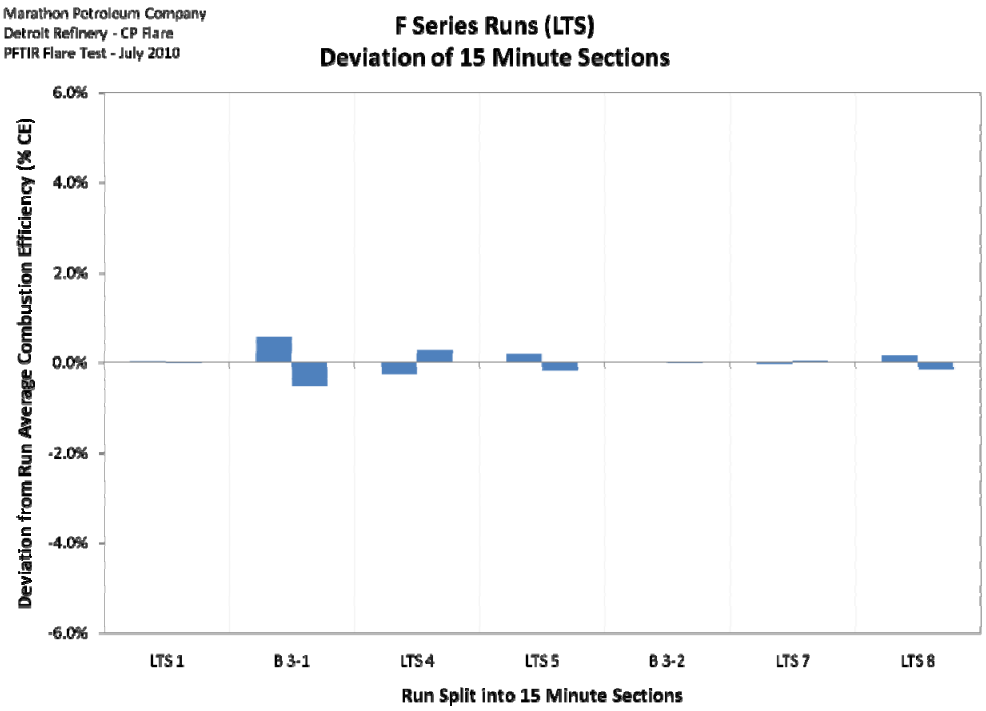

Figure 3.4-11: Test Series F (LTS) – Deviation of 15 Minutes Sections

3.4.3 PFTIR Detectors

The PFTIRs at the Detroit test used a dual-color detector that had both indium antimonide (InSb) and mercury cadmium telluride (HgCdTe or MCT) detectors combined. The PFTIR used at Texas City was equipped only with an MCT detector. The new dual-color detector provided a larger detection range (600-3500 wavenumbers) because it combined the InSb detection region (1800-3500 wavenumbers) with the MCT detection region (600-2400 wavenumbers).

Each detector has specific advantages. Speciation of hydrocarbons is possible in the MCT range. A total hydrocarbon measurement and a more defined region for the CO_2 band near 2000 wavenumbers are possible in the InSb range. Figure 3.4-12 shows an example spectrum with InSb and MCT regions noted.

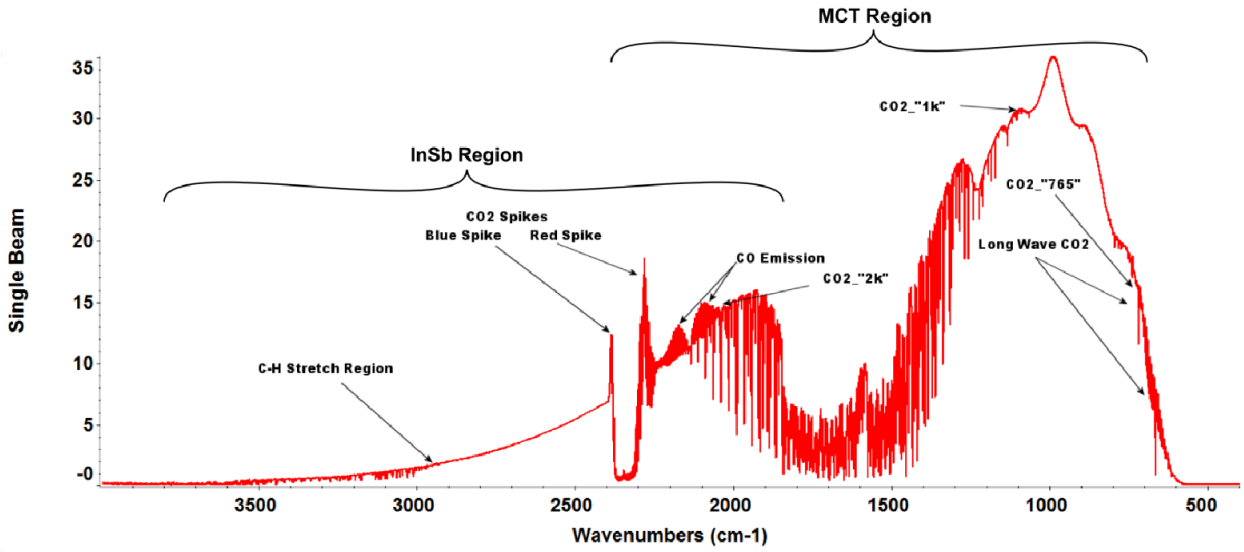

Figure 3.4-12: Example Spectrum with InSb and MCT detectors.

3.4.3.1 Spectral Regions for CO_2

Another benefit of having a dual-color detector is that CO_2 can be measured in multiple regions (765, 1000, or 2000 wavenumbers). The 1000 band has significant water interference, so it cannot be used for most CO_2 measurements. The 765 band is measured only by the MCT detector. The 2000 band is measured by the InSb detector and more weakly by the MCT detector. To determine which band would be used to measure CO_2 for this project, both the 765 and 2000 CO_2 detection bands were analyzed for CO_2 concentration using data from the FCCU test (see Section 3.5.3.2). Figure 3.4-13 compares the CO_2 readings for the 765 and 2000 bands using the Lot PFTIR against the CEMS CO_2 values. The 765 band showed significant scatter and bias, but the 2000 band was stable and closer to the CEMS values. Thus, the 2000 wavenumber CO_2 detection region was used for the entire Detroit test program. This differs from the Texas City test, where the 765 region was used. The 765 region was used at Texas City because the PFTIR only had a MCT detector at the time, so the 2000 region was too weak to measure and the 1000 region was very unstable.

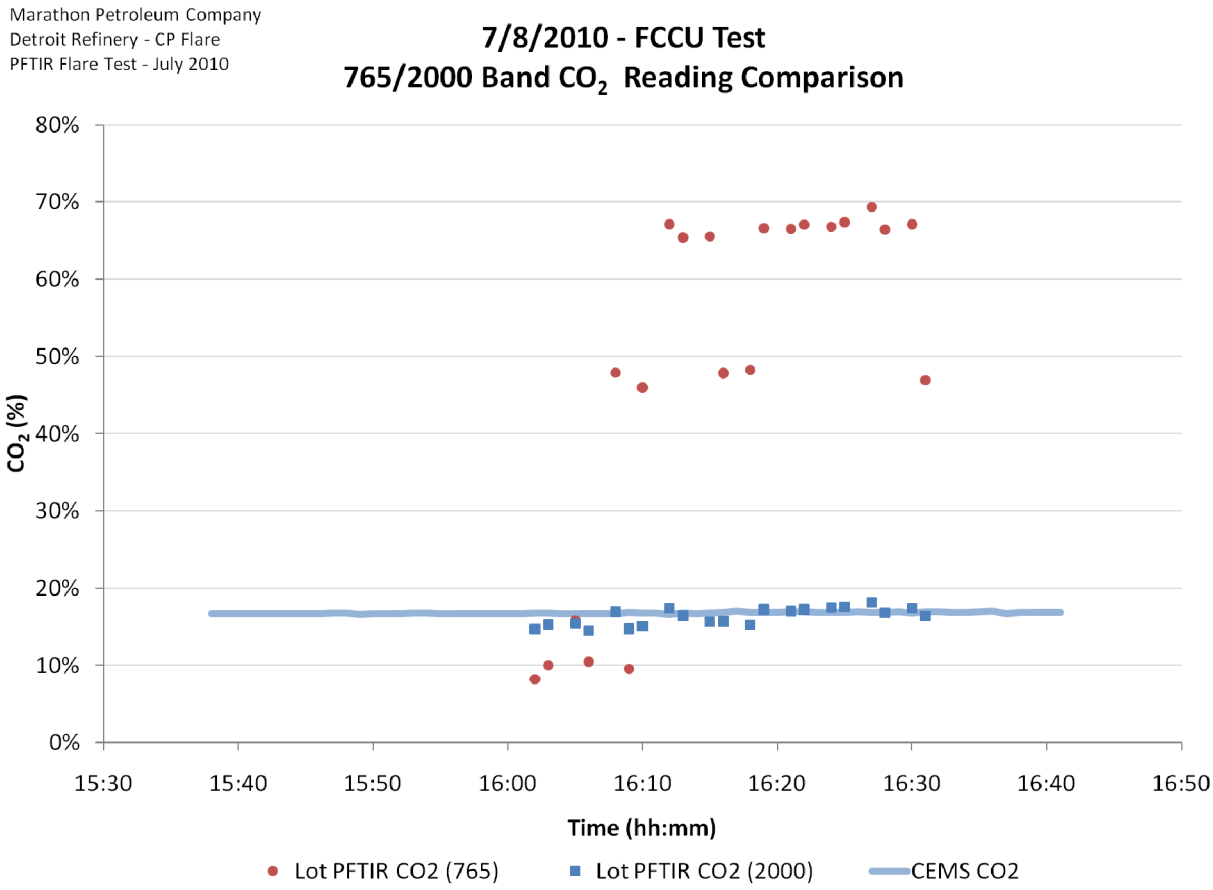

Figure 3.4-13: 765/2000 Band CO_2 Readings for Lot PFTIR in FCCU Test

3.4.4 PFTIR Aiming

Proper aiming of the PFTIR is critical to acquisition of valid data. Ideally, the PFTIR should be aimed near the centerline of the flare plume about one flame length away from the flare tip. At this distance, all thermal destruction reactions have reached completion. However, the plume is a moving target. Therefore, in an attempt to maintain an optimal view, the PFTIR operator must continually adjust the aiming position of the PFTIR. This task becomes increasingly difficult when the wind is shifting, causing the plume to move in different directions. Aiming is poor and readings are invalid when the flare plume is blowing directly away from the PFTIR at more than 5 mph (see Section 3.4.5).

Because two PFTIRs were used at perpendicular locations at the Detroit test, at least one PFTIR always had a good view of the flare plume. Aiming videos were monitored during the test program to ensure that acceptable aiming was maintained. Even though both PFTIRs could collect data simultaneously, only one PFTIR instrument at a time was used. When plume alignment or aiming became poor, the data collection instrument was switched. This enabled a run to continue through a wind shift.

PFTIR aiming for the Detroit test was improved over the previous Texas City test. Each PFTIR was equipped with joystick controlled motorized mounts. This enabled the PFTIR operator to watch and control the PFTIR aiming position from inside the PFTIR trailer while also watching live spectral feedback from the PFTIR software. At the Texas City test, aiming was controlled by manually cranking the two PFTIR mounts under the instrument. Also, the aiming camera video quality for the Detroit test was improved over that in the Texas City test.

3.4.5 Wind Effects

During the Detroit CP flare test program, wind speed and direction were recorded on a minute-by-minute basis from a meteorological station located at the MPC Detroit refinery on the 9th floor of the CCR structure. The run averages for wind direction and speed are shown on the summary data tables in Section 5.1.

The flare elevation (125 ft above grade) is higher than the meteorological elevation (105 ft above grade). Therefore, the true wind conditions at the flare tip may be different than the wind conditions recorded in the process data.

Wind speed and direction play an important role in the quality of data collected by the PFTIR method. The alignment of the flare plume with the PFTIR must be optimal to have the best chance of obtaining a representative sample. The best opportunity for the PFTIR to obtain a representative sample of the flare plume is when:

1. The flame is buoyant and plume is rising directly above the flame, or

2. The flame is “bent over” by the wind and the plume is roughly perpendicular to the PFTIR field of view. Figure 3.4-14 shows a perpendicular view from a PFTIR location.

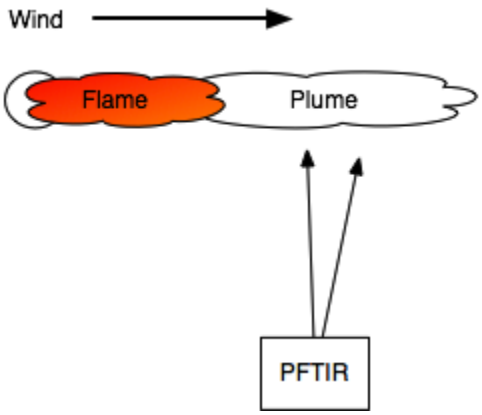

Figure 3.4-14: Example of Good Plume Alignment with PFTIR

The worst alignment occurs when the flame and plume are bent by the wind and blowing directly away from the PFTIR. Figure 3.4-15 shows an example of poor PFTIR alignment. When this occurs, the flare structure, tip, and flame block the view of the plume from the PFTIR, making it difficult to obtain a representative sample of the plume.

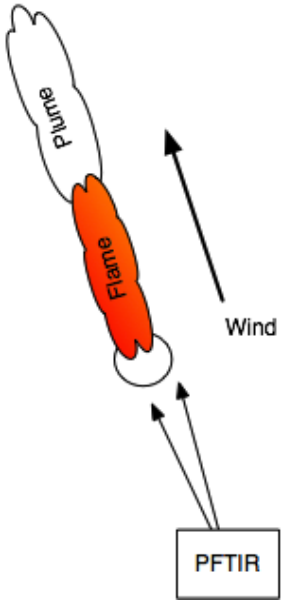

Figure 3.4-15: Example of Poor Plume Alignment with PFTIR

This effect can be seen visually on the PFTIR aiming camera. Figure 3.4-16 and 3.4-17 show example images of good plume alignment and poor plume alignment, respectively. The crosshair on the images shows the PFTIR field aiming point. Data collected from a poorly aligned plume will result in invalid data.

Figure 3.4-16: Aiming Camera with Good Plume Alignment

Figure 3.4-17: Aiming Camera with Poor Plume Alignment

To avoid the problem of poor plume alignment, two PFTIRs were placed at perpendicular locations so at least one PFTIR had good plume alignment regardless of wind direction. At each PFTIR location, an acceptable wind direction window was established to prevent collecting poorly aligned plume data. For winds greater than 5 mph, a window of ±30° directly opposite the PFTIR was considered poor alignment and the PFTIR could not collect a representative sample when the flare plume was in that window. Figure 3.4-18 shows the poor alignment window for both PFTIR locations. This poor plume alignment window is similar to the wind flagging algorithm used for data analysis in the Texas City flare test report.

This window does not consider a plume blowing towards the PFTIR location as poor alignment. This differs from the original Detroit test plan, which calls for a ±30° poor alignment window both away and toward the PFTIR locations. The logic behind restricting the plume blowing towards the PFTIR location was a concern that the PFTIR could not aim at a high enough angle to view a good cross-section of the plume when it is blowing toward the instrument. However, during the Detroit test program, the PFTIR operator was able to accomplish this, so the restriction was removed.

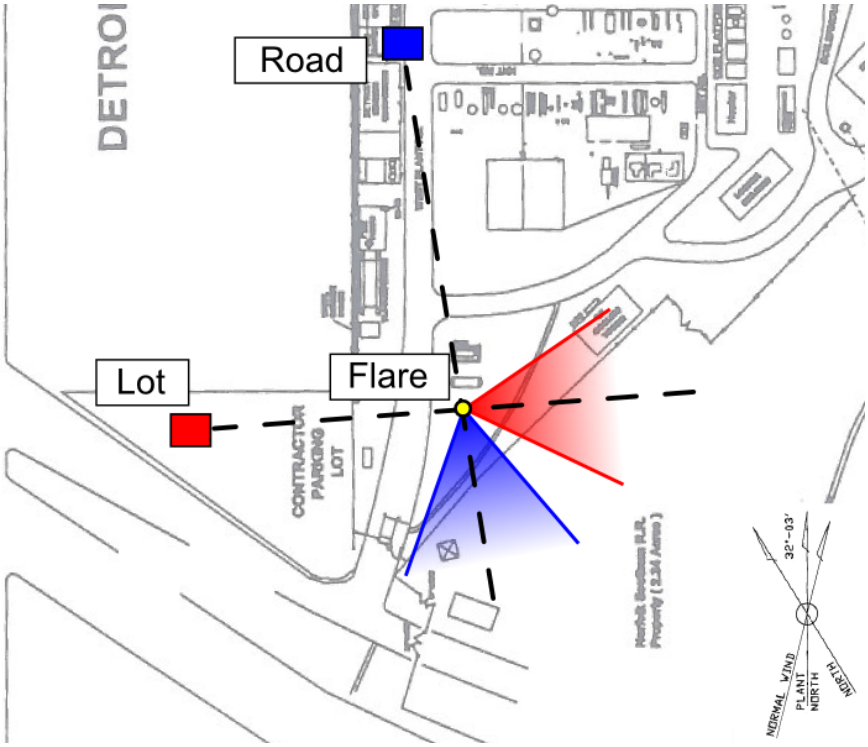

Figure 3.4-18: Poor Alignment Windows for PFTIR Locations

The lot location PFTIR was used as the primary data collection instrument unless the wind bent the flare plume into the poor alignment window, in which case the road location PFTIR was used to collect data. Figures 3.4-19 through 3.4-27 show the wind directions for each day of the test program.

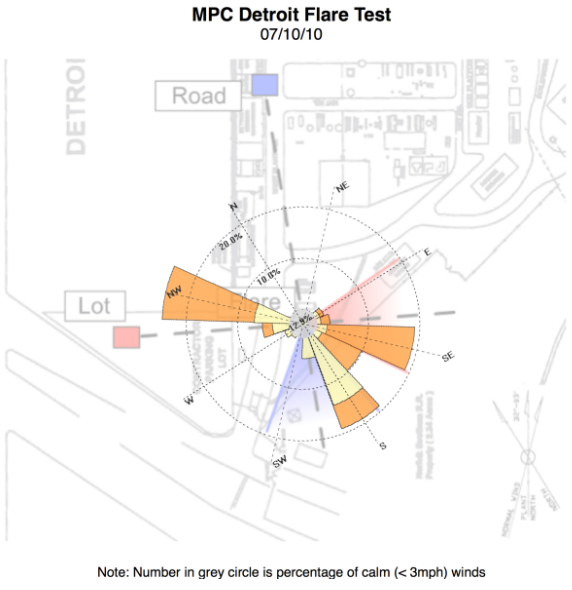

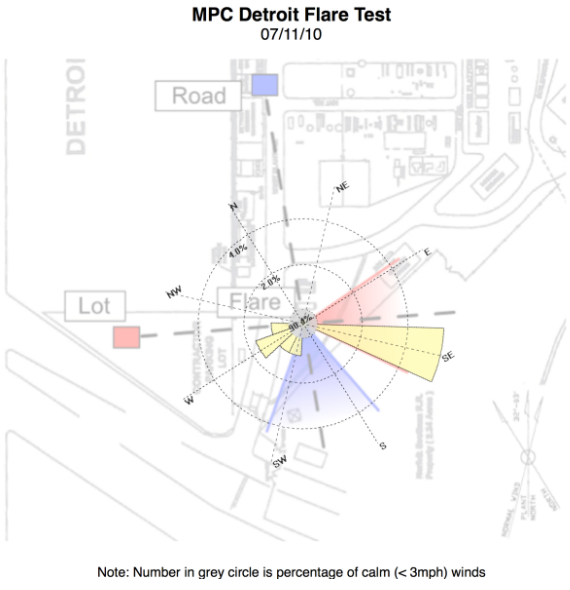

Figure 3.4-19: Wind Rose for 7/10/10

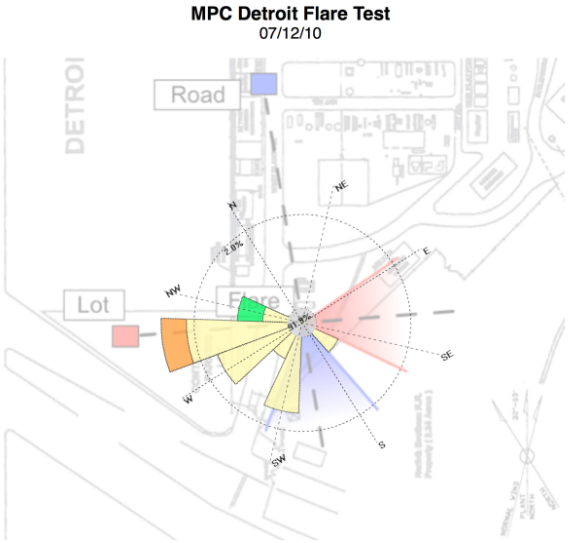

Note: Number in grey circle is percentage of calm (< 3mph) winds

Figure 3.4-21: Wind Rose for 7/12/10

Figure 3.4-20: Wind Rose for 7/11/10

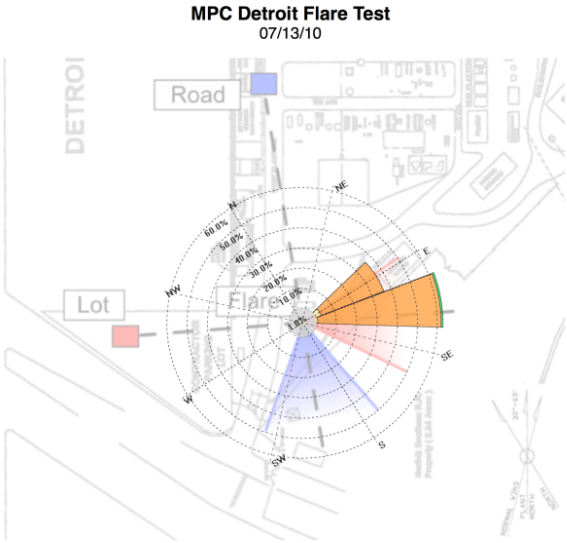

Note: Number in grey circle is percentage of calm (< 3mph) winds

Figure 3.4-22: Wind Rose for 7/13/10

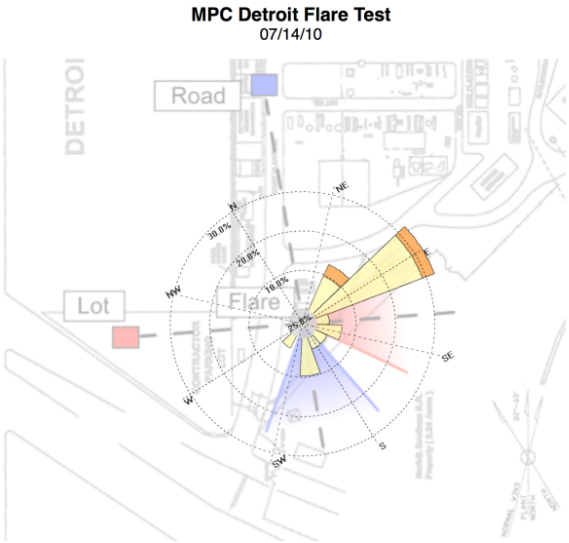

Note: Number in grey circle is percentage of calm (< 3mph) winds

Figure 3.4-23: Wind Rose for 7/14/10

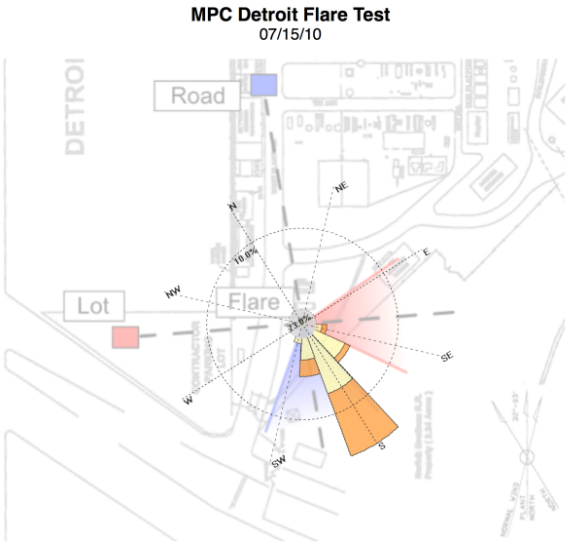

Note: Number in grey circle is percentage of calm (< 3mph) winds

Figure 3.4-24: Wind Rose for 7/15/10

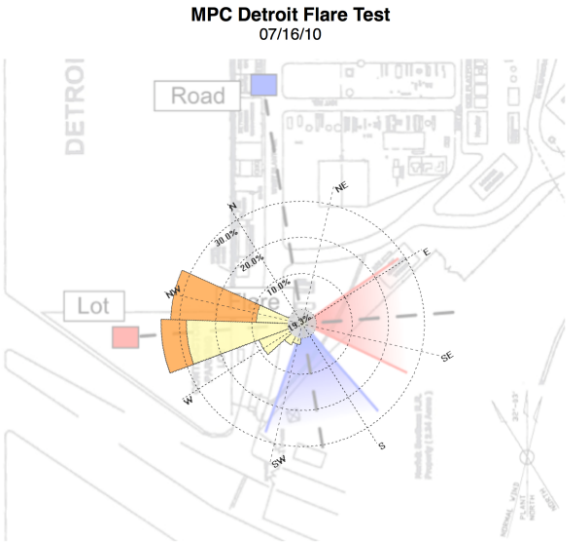

Note: Number in grey circle is percentage of calm (< 3mph) winds

Figure 3.4-25: Wind Rose for 7/16/10

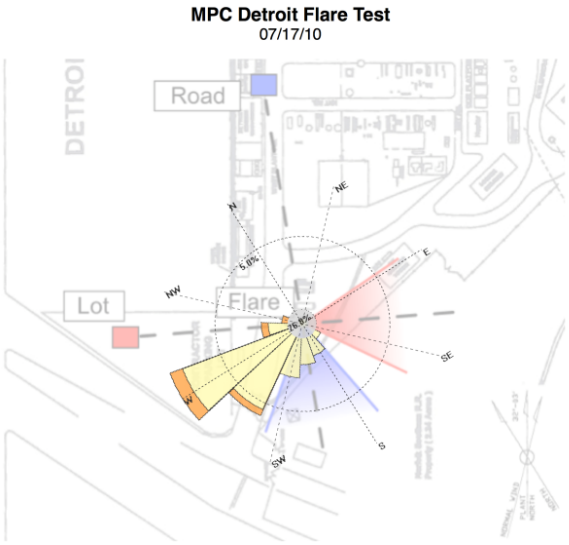

Note: Number in grey circle is percentage of calm (< 3mph) winds

Figure 3.4-26: Wind Rose for 7/17/10

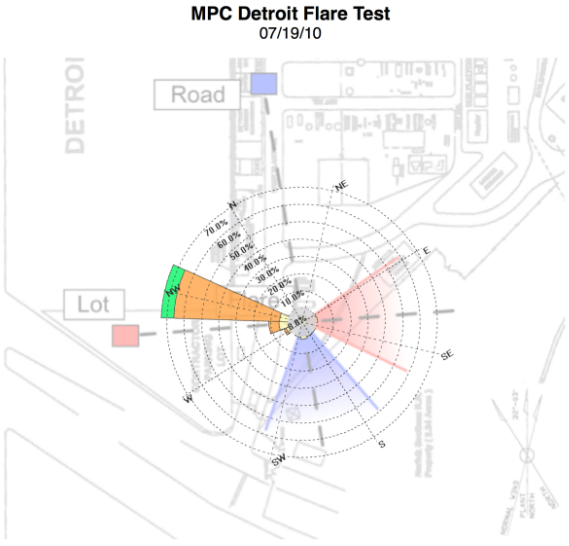

Note: Number in grey circle is percentage of calm (< 3mph) winds

Figure 3.4-27: Wind Rose for 7/19/10

3.4.5.1 Momentum Flux Ratio

Momentum flux ratio (MFR) is a ratio of the momentum of the flare exit gas to the momentum of the wind (see Equation 3.4-1). An MFR above 1.0 indicates that the wind momentum is less than the flare exit gas momentum. Under these conditions, the flare combustion zone is less likely to be influenced by the wind. An MFR below 1.0 indicates that the wind momentum is greater than the flare exit gas momentum. Under these conditions, the flare combustion zone may be bent or pushed more to one side of the flare tip. A more detailed analysis and description of momentum flux ratio is found in the MPC white paper on momentum flux ratio.[6]

$$MFR = \frac{\rho_{czg} \cdot {v_{czg}}^2}{\rho_{air} \cdot {v_{wind}}^2} \qquad \text{Equation 3.4-1}$$

Where:

$$MFR = momentum\ flux\ ratio\ (unitless)$$
$$\rho_{czg} = combustion\ zone\ gas\ density\ \left(\frac{lb}{ft^3}\right)$$
$$\rho_{air} = ambient\ air\ density\ \left(\frac{lb}{ft^3}\right)$$
$$v_{czg} = combustion\ zone\ gas\ velocity\ \left(\frac{ft}{hr}\right)$$
$$v_{air} = wind\ velocity\ \left(\frac{ft}{hr}\right)$$

Depending on how much the combustion zone is pushed to one side of the flare tip, some of the ring steam upwind of the combustion zone might not be injected into the combustion zone. This non-mixing ring steam does not interact with the combustion zone gases and should be removed from the combustion zone gas net heating value calculation.

During the Detroit test program, the wind was mostly calm or light. Only 8 out of 64 valid runs had MFR values below 1.0. Only 3 runs with MFR values below 1.0 were in test series A, B, and C. The other 5 runs were in test series D and E, which were special test conditions that could not be used for MFR analysis. This sample size (3 runs) for windy conditions is too small to perform an MFR analysis on the Detroit flare.

[6] *Steam Contribution to Combustion Zone Gas in Variable Wind Conditions*, Marathon Petroleum Company, LLC, Texas City Refinery, June, 2010

3.5 Overall Test Variability

When assessing overall data uncertainty for this project, uncertainty related to precision (repeatability) issues must be distinguished from uncertainty related to bias ("closeness to truth") issues. This test program was designed to generate data to evaluate both precision and bias of test results.

3.5.1 Data Filtering

The raw FTIR data (one minute averages) are reported from the analytical software with a 2-sigma (2σ) error calculated from the fit of the reference spectra to the sample spectra. Any individual measurement that was less than 2 times this error (i.e., 4σ) was not used in calculating combustion efficiency.

3.5.2 Precision

3.5.2.1 Long Term Stability (Test Series F)

To assess long term data precision, one run was conducted each day during the test program under the same operating conditions – Condition B with an S/VG ratio of 1.0. This test series is referred to as the Long Term Stability (LTS) test. A total of eight 30-minute valid LTS replicates were conducted. This includes the two scheduled Condition B tests with 1.0 S/VG. These data are used to estimate the test method repeatability over a range of meteorological conditions and other long term factors. Complete details of the LTS test are further discussed in Section 5.7.

Figure 3.5-1 shows the combustion efficiency results from the LTS runs using a box and whiskers chart. Each box shows the boundaries of the 25th and 75th percentiles and contains, therefore, 50% of the data for that run. The line in the middle of the box indicates the median value of the data. The average is shown by a short black line. The "whiskers" at the top and bottom of the box show the range of the data. A blue line connects the average of each data set.

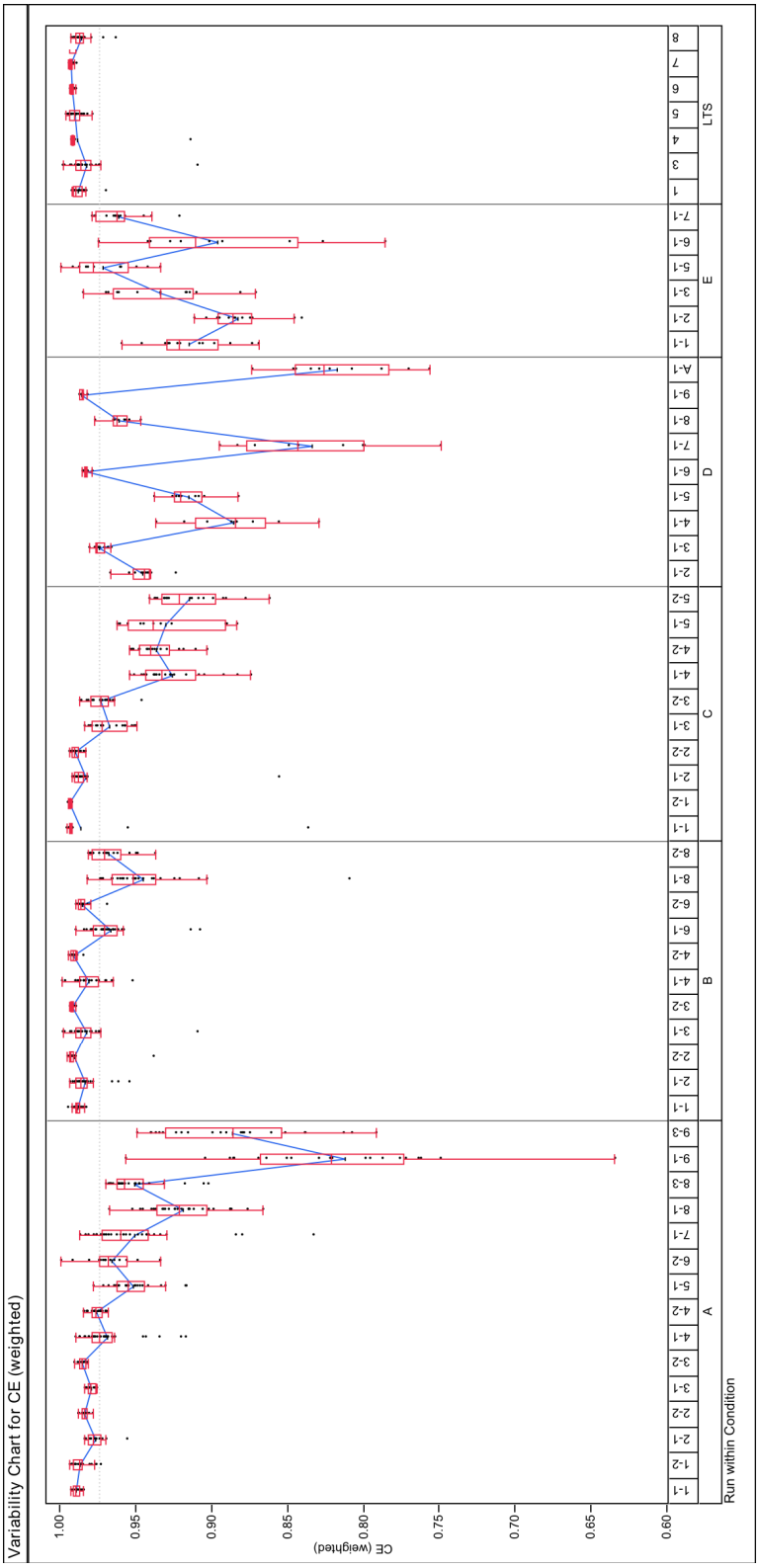

Figure 3.5-1: CE for Test Series F (LTS)

Table 3.5-1 shows a confidence interval (CI) determination for the combustion efficiency data from each of the seven LTS runs. The upper and lower confidence bounds under are also calculated with two confidence intervals. For both 99% CI and 95% CI, the confidence interval is determined for all seven LTS runs. Additionally, confidence intervals are determined assuming fewer runs (five runs and three runs). Three runs are typical for air emissions testing on stacks.

	99% CI			95% CI		
	All Runs	5 Runs	3 Runs	All Runs	5 Runs	3 Runs
Avg	98.9%	98.9%	98.9%	98.9%	98.9%	98.9%
SD	0.004	0.004	0.004	0.004	0.004	0.004
RSD	0.4%	0.4%	0.4%	0.4%	0.4%	0.4%
N	7	5	3	7	5	3
SE	0.001	0.002	0.002	0.001	0.002	0.002
% Prob	0.99	0.99	0.99	0.95	0.95	0.95
TINV	3.71	4.60	9.92	2.45	2.78	4.30
Factor	0.5%	0.8%	2.2%	0.4%	0.5%	1.0%
LCL	98.3%	98.1%	96.7%	98.5%	98.4%	97.9%
AVG	98.9%	98.9%	98.9%	98.9%	98.9%	98.9%
UCL	99.4%	99.7%	100.0%	99.2%	99.4%	99.8%

Table 3.5-1: Confidence Interval Analysis of LTS Runs

The data in each row of Table 3.5-1 are as follows:

Avg	=	Average combustion efficiency (CE)
SD	=	Sample standard deviation of the CE
RSD	=	Relative standard deviation (SD/Avg) of the CE
N	=	Number of data points for each data set (8, 5, or 3)
% Prob	=	The chosen probability level to determine the confidence interval(99% or 95%)
TINV	=	The coverage factor for the confidence interval calculated from the Student's t-distribution
Factor	=	The calculated confidence limit based on the criteria above (this is added to and subtracted from the average to arrive at the confidence interval)
LCL	=	The lower confidence limit (Avg – Factor)
UCL	=	The upper confidence limit (Avg + Factor)

The confidence intervals in Table 3.5-1 are calculated from the average run combustion efficiency. Individual runs will have greater variation (see Section 3.4.2). This confidence interval analysis shows that the measured combustion efficiency under identical process conditions may vary for a flare by about ±0.5%. This interval has decreased from the Texas City test, which was about ±1.5%. We believe this decrease is due to several factors. The most significant change is replacing crank aiming with joystick aiming. Other changes include the use of the two-color detector and improvements in the analysis software algorithms. It should be noted however, that this analysis does not include an important factor – the PFTIR operator – since the same operator was used for all tests.

3.5.2.2 Replicate Analysis

Because only two replicates were performed for runs in test series A, B, and C, statistical sanalysis of replicate precision is limited. Table 3.5-2 shows the absolute variation in combustion efficiency between all replicates. In each test series, the combustion efficiency variation between replicates widens at higher S/VG and as combustion efficiency declines. This could be because the flare flame becomes less stable at lower combustion efficiencies.

Replicate Analysis						
Replicate 1			Replicate 2			
Run	S/VG	CE	Run	S/VG	CE	**ΔCE**
A1-1	1.2	99.0%	A1-2	1.2	98.8%	0.2%
A2-1	1.5	97.7%	A2-2	1.6	98.5%	0.7%
A3-1	1.8	98.0%	A3-2	1.8	98.6%	0.6%
A4-1	2.1	96.9%	A4-2	2.0	97.7%	0.7%
A6-1	2.4	N/A	A6-2	2.4	96.7%	N/A
A7-1	3.0	92.0%	A8-3	2.9	95.2%	3.2%
A9-1	4.0	81.3%	A9-3	4.1	88.7%	7.4%
B1-1	0.6	98.9%	B1-2	0.6	N/A	N/A
B2-1	0.8	98.4%	B2-2	0.8	99.1%	0.7%
B3-1	1.0	98.3%	B3-2	1.1	99.3%	0.9%
B4-1	1.2	98.2%	B4-2	1.2	99.2%	1.0%
B6-1	1.7	96.7%	B6-2	1.6	98.6%	1.9%
B8-1	2.1	94.6%	B8-2	2.1	96.9%	2.3%
C1-1	0.8	98.7%	C1-2	0.7	99.4%	0.7%
C2-1	1.2	98.4%	C2-2	1.1	99.1%	0.7%
C3-1	1.6	96.8%	C3-2	1.5	97.4%	0.6%
C4-1	2.0	92.7%	C4-2	1.9	93.7%	1.1%
C5-1	2.2	93.1%	C5-2	2.3	91.5%	1.6%

Table 3.5-2: Replicate Combustion Efficiency Differences

In general, variability tends to increase in direct proportion to S/VG ratio. The largest variation between replicates in the program occurs in test series A at high S/VG. This test series had the lowest vent gas exit velocity, so a higher S/VG might impact the flame stability more than it does during test series with higher vent gas exit velocity.

3.5.3 Bias

3.5.3.1 Lab Hot Cell Calibrations

Before commencement of the test program, each PFTIR was calibrated using a "hot cell." The hot cell allows measurement of NIST traceable quantities of gas by the PFTIR at temperatures expected in the flare plume. These calibrations challenge the PFTIR with known concentrations of carbon dioxide, carbon monoxide, methane, and other gases expected to be found in the plume. Using a mass flow controller, the gases are flowed through a heated cell of known length. This hot cell was placed at the focal point of the collimator and measured at short range with the PFTIR. The PFTIR readings are compared to the known concentrations of the gases and path length of cell. A calculated calibration factor can then be determined and applied to the data. Using that calibration factor, the PFTIR software would correct any field reading against a known concentration. Figure 3.5-2 shows the hot cell at the back of the collimator.

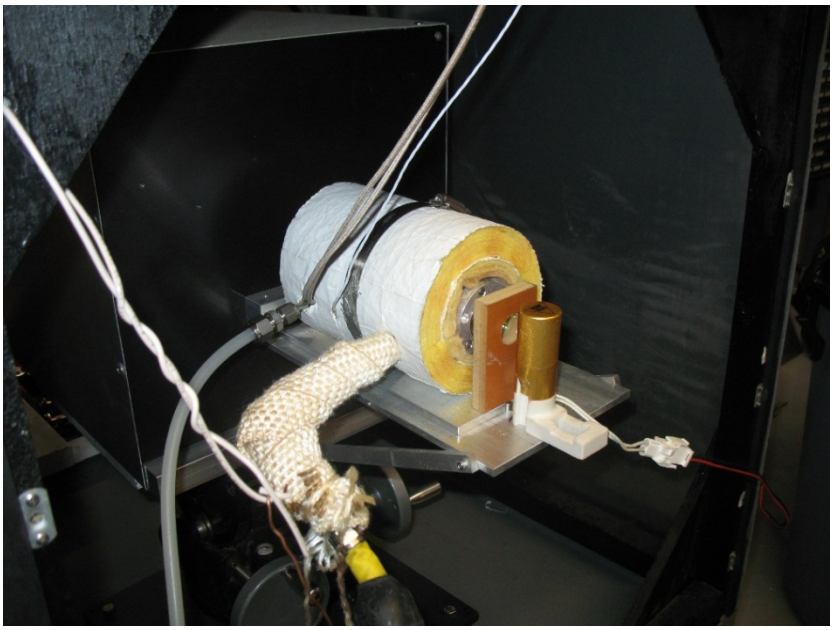

Figure 3.5-2: Picture of Hot Cell in Collimator

The PFTIR used at the lot location was calibrated once and verified twice before shipping to the MPC Detroit refinery. However, the PFTIR used at the road location was calibrated once with no verification before shipping to the MPC Detroit refinery. This may be why the hardware problem with the Road PFTIR was not discovered earlier.

3.5.3.2 Blind Test of PFTIR vs. CEMS

Due to the nature of this open-path technique, bias assessments are difficult to perform in the field. However, the Detroit refinery has a Fluid Catalytic Cracking Unit (FCCU) stack with a continuous emission monitoring system (CEMS) which measures concentrations of carbon dioxide and carbon monoxide. This stack provided a means of comparing the PFTIRs to a known source.

For this test, both PFTIRs were placed side-by-side at the road location and pointed at the FCCU stack. Data were collected data for approximately 30 minutes. To maintain a blind audit, the CEMS readings for the FCCU stack were not retrieved until after the readings from both PFTIRs were analyzed. Additionally, a temperature reading further upstream from the FCCU stack was retrieved and used to compare to the PFTIR temperature reading. The temperature drop from the upstream temperature probe to the stack outlet was estimated from a previous particulate source test report that had measured the stack temperature near the CEMS location. The estimated temperature drop was approximately 30°F.

Figure 3.5-3 shows CO_2 and CO readings of the lot PFTIR and compares them to the CEMS readings. This PFTIR (serial number "H") was mounted inside a trailer and moved to the lot location after the FCCU test. Figure 3.5-4 shows the temperature readings of the same PFTIR and compares them to the estimated stack temperature based on the upstream temperature probe.

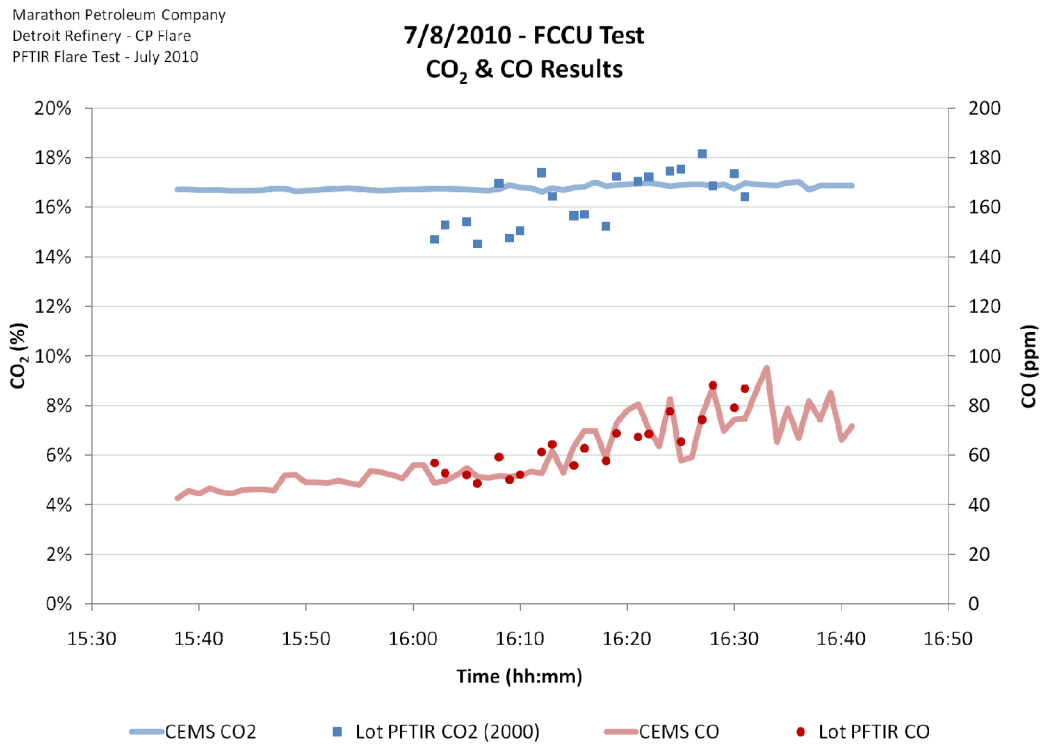

Figure 3.5-3: CO_2 and CO for Lot PFTIR in FCCU Test

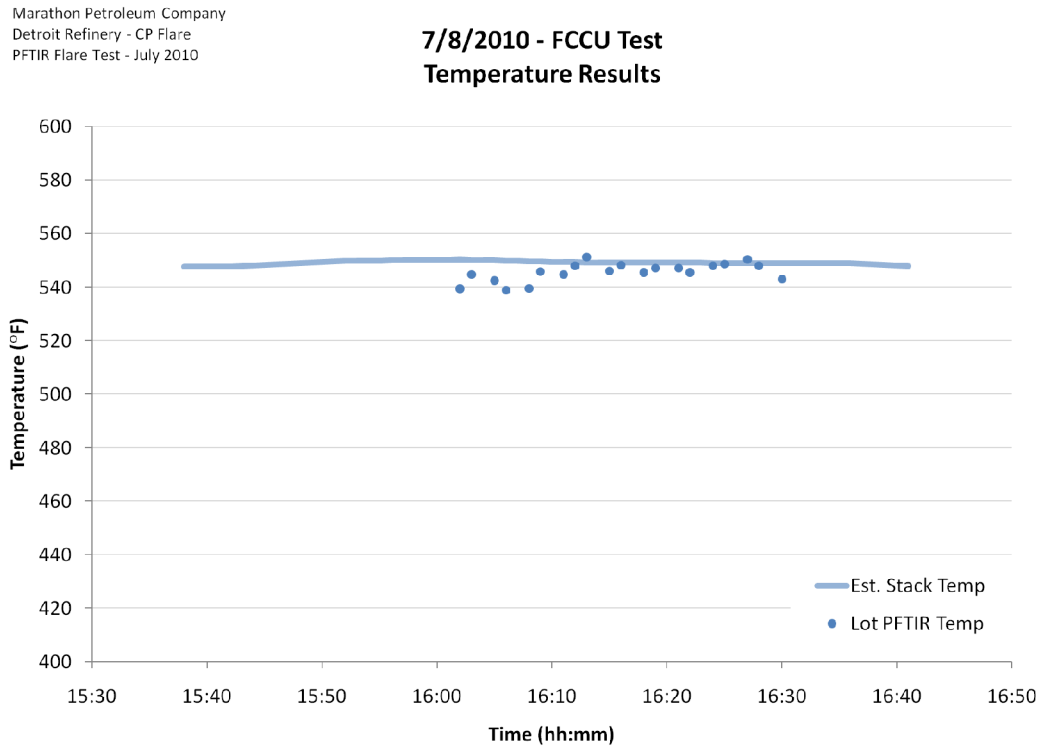

Figure 3.5-4: Temperature for Lot PFTIR in FCCU Test

In addition to graphical comparison to the plant CEMS, a modified relative accuracy (RA) test was performed on the PFTIR measurements. Table 3.5-3 shows the relative accuracy calculations for the FCCU Test. The calculations performed for the FCCU Test were the same as a Relative Accuracy Test Audit (RATA). Unlike a normal RATA, however, the plant CEMS is assumed to be the reference method and the PFTIR measurements are compared to the CEMS measurements (see Appendix A.1). The 30 minute FCCU Test was split into three 10 minute sections. Relative accuracy was calculated for each 10 minute section and for the overall 30 minute test. From Table 3.5-3, the relative accuracy of the PFTIR remains below the 40 CFR 75 10% for the full run and even for the 10 minute sections remains below the 40 CFR 60 20% limit.

	CEMS CO_2	PFTIR CO_2	RA	CEMS CO	PFTIR CO	RA
Time	%	%	%	ppm	ppm	%
16:01-16:09	16.8%	15.3%	**14.5%**	51.3	53.3	**14.2%**
16:10-16:19	16.8%	16.1%	**9.5%**	61.7	60.5	**10.5%**
16:20-16:31	16.9%	17.3%	**4.8%**	75.6	76.0	**9.2%**
Overall (16:01-16:31)	16.8%	16.4%	**5.9%**	64.1	63.8	**4.9%**

Table 3.5-3: Relative Accuracy for Lot PFTIR in FCCU Test

Unlike the Lot PFTIR, the PFTIR that was mounted on the tripod and was used at the road location (serial number "A") did not report values that were close to the plant readings in this blind test. This initially indicated a calibration issue with the road PFTIR, which was unable to be resolved after the conclusion of the test. Because the FCCU Tests were inconclusive for the road PFTIR, all data collected from this unit was invalidated and not reported.

3.5.3.3 Field Hot Cell Checks

In addition to the FCCU Test, a hot cell unit was brought into the field. The hot cell and collimator were setup at the base of the flare. A field hot cell check was performed on each PFTIR from each location to the base of the flare (full calibration distance). Two mixtures of CO_2 and CO were flowed through the hot cell, and five data points were collected by each PFTIR. The field hot cell checks were performed on the final day of testing during demobilization. The checks were performed only to determine if the hot cell equipment worked at long distances and was not used for calibration or analysis of the flare test results. This was not a blind test for the PFTIR operator or IMACC.

Table 3.5-4 shows the results from the field hot cell for the Lot PFTIR located at the lot location. The 30ppm CO check showed a >10% positive bias. IMACC explained that this was due to the low concentration of the check, which was on the edge of the detection limit for radiance at such a long range and short cell pathlength. These low radiance readings were not believed to have a substantial impact on combustion efficiency measurements because the plume radiance was significantly higher.

Field Hot Cell Check - Lot PFTIR

Time	Mixer CO_2	PFTIR CO_2	% Error	Mixer CO	PFTIR CO	% Error
07/20/2010 09:40	12.9%	13.0%	0.5%	29.9	35.7	19.4%
07/20/2010 09:41	12.9%	13.1%	1.3%	29.9	37.8	26.4%
07/20/2010 09:42	12.9%	13.1%	1.3%	29.9	33.3	11.3%
07/20/2010 09:43	12.9%	13.2%	2.1%	29.9	34.1	14.0%
07/20/2010 09:44	12.9%	13.3%	2.8%	29.9	34.1	14.0%
07/20/2010 09:51	8.3%	8.4%	1.4%	197.2	202.0	2.4%
07/20/2010 09:52	8.3%	8.3%	0.8%	197.2	201.6	2.2%
07/20/2010 09:53	8.3%	8.4%	1.8%	197.2	205.3	4.1%
07/20/2010 09:54	8.3%	8.5%	2.5%	197.2	208.3	5.6%
07/20/2010 09:55	8.3%	8.4%	1.5%	197.2	203.9	3.4%

Table 3.5-4: Lot PFTIR Field Hot Cell Check Results

The road PFTIR field hot cell results are not reported due to the previously mentioned channeling issue, which caused variability in the field hot cell results. Because the field hot cell check for the road PFTIR was inconclusive, all data collected from this unit was invalidated and not reported.

3.5.4 Dilution Assumption

Because the flare plume is continually moving during the test, it is impossible to collect all spectra at exactly the same point in the plume. As the gases in the plume move further from the combustion zone, they are increasingly diluted by ambient air. This means that the absolute concentration of the plume components will vary based solely on where in the plume the PFTIR is aimed and collecting data.

Since the calculation of combustion efficiency is based on the ratio of CO_2 to total carbon in the plume (i.e. the sum of CO_2, CO, and THC), it is the ratios of the components that matter rather than their absolute concentration. Therefore, even though absolute concentrations vary at different measurement points due to dilution, the ratios should be the same since, in theory, all plume components are diluted equally at any given sample point.

The data collected during this test, however, show differing degrees of variation in the CO_2 to CO ratio at different data points collected under the same conditions. For example Figure 3.5-5 shows the ratio variability during the LTS series runs. The CO_2 to CO ratio measured by the PFTIR varies from 200 to 2,500 between runs. This variability is similar to that observed in the Texas City test.

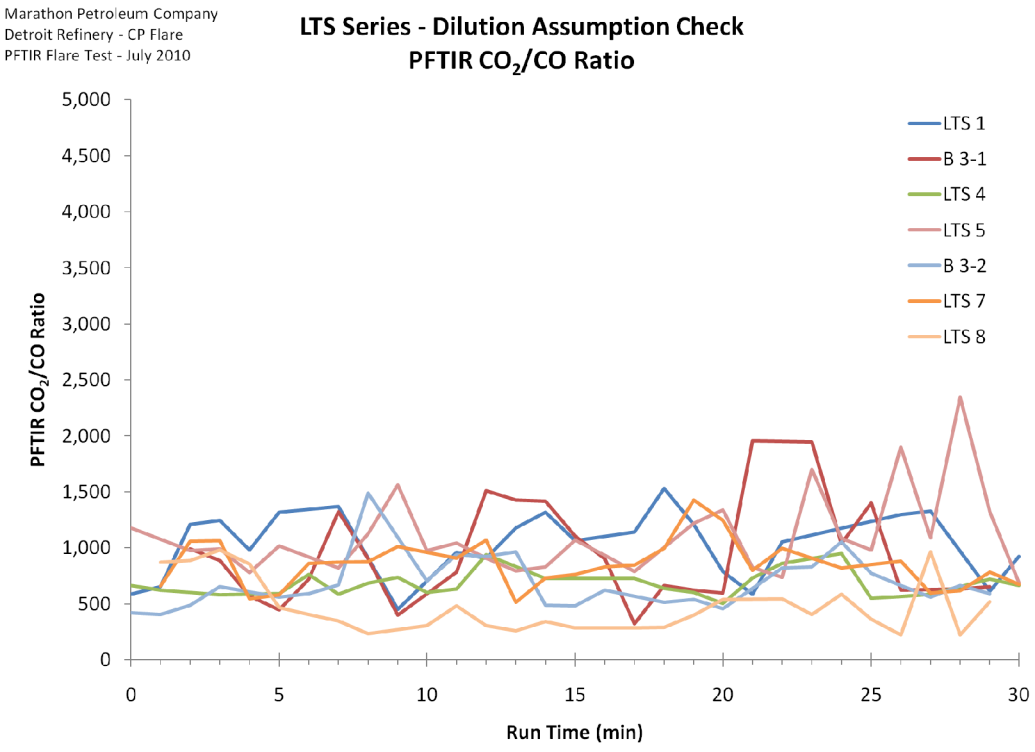

Figure 3.5-5: LTS Series – Dilution Assumption Check

3.5.5 PFTIR Calibration

Several calibrations were performed throughout the Detroit test program to account for the effects of sky background and atmospheric radiance and transmittance. Three radiant sources with various characteristics were placed at the focal point of a collimator at roughly the same distance from the PFTIR as the flare.. Precise alignment of the PFTIR with the collimator was critical during these calibrations. Since the calibrations were performed at grade with line-of-sight requirements, road traffic had to be either stopped or the calibrations paused while car and foot traffic passed. The sky background calibrations were performed as needed during testing. More detailed descriptions and calculations are found in Section 4.5 and Appendix A.2. Calibration files are found in Appendix A.8.

3.5.5.1 Black Body Calibration

To calibrate the PFTIR signal in absolute units of radiance, a black body with an IR source of known spectral radiance was used. A NIST-traceable commercial black body calibrator was placed in the collimator at the base of the flare, which produced a known IR spectrum as predicted by the Planck function. This calibration was done at least once each day.

3.5.5.2 IR Source Calibration

To determine the atmospheric transmission loss between the flare plume and the PFTIR, an infrared (IR) source was placed in the collimator at the base of the flare. It created a strong IR signal that the PFTIR could detect to determine atmospheric transmission. This calibration was done at the beginning and end of each day.

3.5.5.3 Cold Source Calibration

To determine the atmospheric radiance being generated by the air between the flare plume and the PFTIR and from the PFTIR instrument itself, a cold source of liquid nitrogen in a windowed cup was placed in the collimator at the base of the flare. It zeroed any radiance except for that created by the atmosphere and the PFTIR. This calibration was done at the beginning and end of each day.

3.5.5.4 Sky Background Calibration

Background radiance calibrations were conducted as needed during the Detroit test program. When the background was changing behind the flare plume, such as when clouds were passing, the PFTIRs would take backgrounds more often. It was not uncommon to take a background every 10 minutes during a run. During the background calibration, the PFTIR would swing off the flare plume and collect a reading for approximately one minute, then swing back to the flare plume and continue collecting data. Background times are included in the PFTIR raw data in Appendix A.8.

3.6 Conclusions

The performance test of the CP flare at MPC's Detroit refinery provided additional information to both the operation and performance of a petroleum refinery flare and also of the PFTIR instrument and method of measuring combustion efficiency.

Overall Observations

- A flare can be operated with greater than 300 BTU/scf vent gas net heating value and with acceptable exit gas velocities and still be over-steamed.
- Combustion efficiency becomes less stable and generally begins to decline once the flame transitions from a clean, visible flame to one that is invisible. However, depending on the vent gas composition, not all transparent flames have poor combustion efficiency.
- The data collected at Detroit shows significant correlation with the Texas City data despite the fact that the flare tips are different sizes, different designs, and from different manufacturers.
- Combustion efficiency declines with increased steam to vent gas ratios during normal stand-by and higher flow operations.
- Combustion efficiency does not decline as rapidly with increased steam to vent gas ratios when the vent gas contains significant amounts of hydrogen. The rate of decline is inversely proportional to the amount of hydrogen in the vent gas.
- Combustion efficiency declines when the vent gas contains significant amounts of nitrogen, even at low steam to vent gas ratios. Nitrogen dilution has the same effect on combustion efficiency as steam dilution.
- The combustion zone gas net heating value (CZG NHV) accounts for steam and inert impacts on flare performance.
- The PFTIR approach has improved in precision since the Texas City flare performance test in 2009.
- Although bias tests were performed using the FCCU stack and field hot cell checks, the PFTIR method has not been blind-validated for testing the flare plume itself. Therefore, there is no assessment of bias ("closeness to truth") against established extractive sampling techniques for flare testing pending the release of the TCEQ/UT study.
- PFTIR bias checks like the FCCU test are critical in identifying detection problems with each PFTIR instrument. Each PFTIR instrument is unique and should be checked for bias in the field.
- Provided both PFTIRs are functioning properly, locating the PFTIRs at perpendicular ground locations provides excellent coverage of the flare plume, even when the wind was shifting.
- Run lengths longer than 10-15 minutes provide no improvement in data precision.

4.0 PFTIR Testing Method and Procedure

4.1 Description and Principles of Passive FTIR

The instrument used to determine gas composition of the flare plume is the Passive Fourier Transform Infrared (PFTIR) analyzer. PFTIR analysis operates on the principle of spectral analysis of thermal radiation emitted by hot gases. Passive means that no "active" infrared light source is used. Instead, the hot gases of the flare are the infrared source. The spectrometer is a receiver only. This approach is possible because the infrared emission spectra of hot gases have the same patterns or "fingerprints" as their absorption spectra do. Consequently, observing a flare with an infrared instrument allows for identification and quantification of species through emission spectroscopy just as with absorption spectroscopy.

For this test program, the PFTIR operation and data analysis was overseen by Dr. Robert Spellicy of Industrial Monitor and Control Corporation (IMACC). This instrument and the analytical software were developed by IMACC.

Two PFTIRs were used for the Detroit flare test. One PFTIR was located north-northeast of the flare on the main Complex 3 & 4 road. This location was referred to as the Road Location. The other PFTIR was located west-northwest of the flare in a contractor parking lot. This location was referred to as the Lot Location. See Section 4.2 for a description of the PFTIR siting and plot plan showing the instrument and flare locations.

In order to collect valid data on flare plume composition, the PFTIR must be aimed at the flare plume approximately one flame length from the flame tip. To accomplish this, an infrared (IR) camera was mounted on each PFTIR body. The IR image of the flare plume was viewed on a monitor by the PFTIR operator. The aiming of the instrument was accomplished by joysticks that controlled stepper motors on each PFTIR mounting head. The Road PFTIR was mounted on a tripod and the Lot PFTIR was mounted inside a trailer. Both were controlled from a control room inside the trailer at the Lot Location. Various wires were run between the two locations to provide communication to the Road PFTIR and equipment.

In the previous Texas City test, PFTIR aiming was controlled by hand cranks. The joystick/motor aiming control during the Detroit test significantly improved aiming quality. Flamelets breaking off the main flame could be avoided more easily with the joystick control than with the hand crank control.

4.2 PFTIR Siting Configuration

Figure 4.2-1 shows the location of the location of the main flare, Road, and Lot sites. The Road Location consisted of a scaffold shelter that housed the Road PFTIR (serial number 'A'), computer equipment, and several cameras (see Section 2.6 for camera information). The Lot Location consisted of an IMACC trailer that housed the Lot PFTIR (serial number 'H'), the PFTIR aiming station, PFTIR data processing computers, and several cameras.

At the base of the flare, an elevated scaffold platform housed the collimator that was used for daily calibrations of each PFTIR. The main control room for the Detroit flare test was located

inside the Complex 3 & 4 control room building in the second floor conference room. Two computer displays showed process data from the plant and video camera feeds from each PFTIR location.

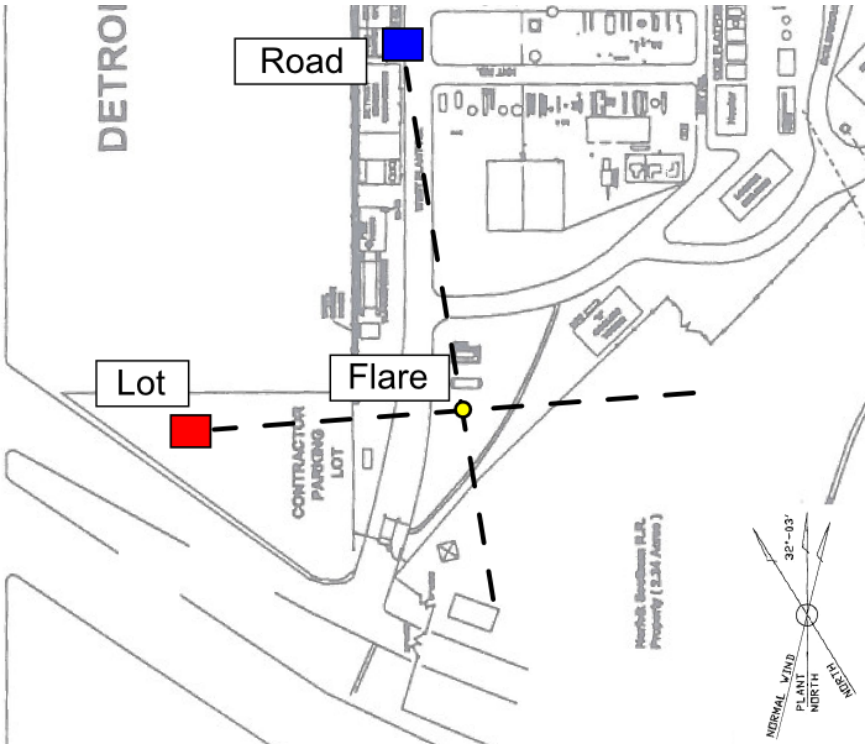

Figure 4.2-1: Map of PFTIR Locations

Figure 4.2-2: Picture of Road Location

Figure 4.2-3: View from the Road Location

Figure 4.2-4: Picture of Lot Location

Figure 4.2-5: View from the Lot Location

Figure 4.2-6: Picture of Aiming Control Station

Figure 4.2-7: Picture of Collimator at the Flare Base

Figure 4.2-8: Picture of the Flare Test Control Room

4.3 Background

To monitor elevated flares, standard "active" IR spectroscopy could be used. However, it is difficult from a practical standpoint to pass a beam of IR light through an elevated flare plume and then capture the transmitted light. A flare plume is constantly moving and would require that the IR light beam constantly move to remain inside the flare plume.

Therefore, for this project, a "passive" approach is used that does not require an independent IR light source. Instead, the IR radiation produced by the hot gases of the flare plume is used. With this approach, the spectrometer becomes a passive receiver of IR radiation. This approach is possible because the IR radiation emitted by hot gas, its "radiance spectrum," has the same patterns or "fingerprints" as its absorption spectrum. Spectroscopic techniques developed by Dr. Robert Spellicy, convert this radiance spectrum into an absorption spectrum at which point it can be analyzed with the same techniques used in standard active IR spectroscopy. This technique is referred to as PFTIR. Figure 4.3-1 shows a schematic of a PFTIR measuring a flare plume.

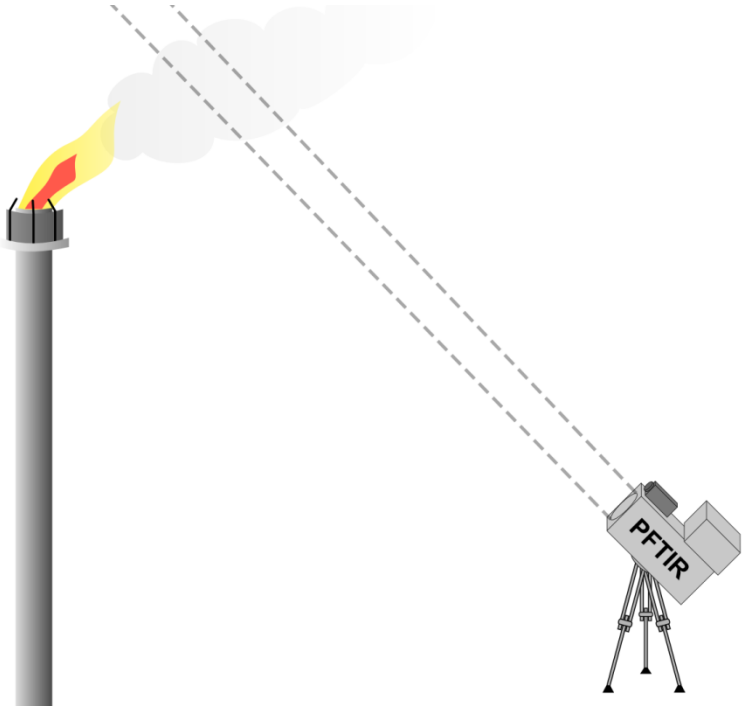

Figure 4.3-1: Schematic of PFTIR Measuring a Flare Plume

There is one main difference between these two approaches: the radiance spectrum from hot gases is proportional to the concentration of the gas (as it is absorption), but it also affected by gas temperature. In standard absorption FTIR, the temperature of the gas is known and controlled. With PFTIR measurements on a flare plume, the temperature is unknown. Therefore, when conducting PFTIR measurements, the temperature of the flare plume must be determined. Details of how this temperature determination is made are found in Appendix A.2.

Consequently, unlike absorption spectroscopy, the PFTIR signal must be calibrated in absolute units of radiance. This requires that the instrument be calibrated utilizing an IR source of known

spectral radiance. This calibration is accomplished with a commercial black body calibrator. This calibrator produces a known IR distribution as predicted by the Planck function. Details of the calibration are found in Appendix A.2.

Calibrations were performed each day at the beginning and end of testing. Calibration results are found in Appendix A.8.

4.4 PFTIR Operation

The two PFTIR instruments were located at the Road and Lot Locations. The Road PFTIR was housed inside a scaffold shelter. The Lot PFTIR was housed inside an IMACC trailer. Calibrations for each PFTIR were performed at the beginning and end of each day. On one day, July 13th, an incoming storm prevented calibrations at the end of the day. Results of these daily calibrations are found in Appendix A.8.

The calibration of this equipment required three different calibration sources: a cold source, IR source, and black body source. A more detailed description of the calibration procedure is found in Appendix A.2. Calibration sources in a collimator were located on an elevated scaffold platform adjacent to the base of the flare. The location was chosen so the distance between the PFTIR and the calibration equipment was approximately the same as the ground distance between the PFTIRs and the flare. The platform was elevated to achieve line-of-sight clearance to each PFTIR location.

After calibration was completed the equipment was ready to start testing. A sky background was taken to be used in later analysis to subtract background radiance. A new sky background would be taken approximately every 10 minute or as sky conditions changed during testing. In PFTIR testing, it is important to adjust collected spectra with representative sky backgrounds.

During test runs during the Detroit test, one or both PFTIRs would be aimed at the flare plume and collect spectral data in minute averages. The Road PFTIR showed inconclusive FCCU Test and field hot cell test results, so it was only used when the Lot PFTIR did not have an acceptable view of the flare plume. When both PFTIRs were collecting spectra, the location with the best view of the flare would be used for combustion efficiency analysis. However, all Road PFTIR data was not reported because channeling issues in the detector cause variable readings for the FCCU Test and field hot cell checks that could not be resolved. Only the Lot PFTIR data was used for combustion efficiency analysis.

Wind did not play as big a role in the Detroit flare test as it did in the Texas City test. The wind speed was significantly lower, which resulted in a more upright and thicker plume. Aiming problems were significantly improved by replacing the Texas City hand cranks with joystick/motor controls on the PFTIR mounting heads. Also, an experienced PFTIR aiming operator was controlling the joystick for each PFTIR location. Video review was unnecessary because the aiming operator successfully kept each PFTIR properly aimed during runs.

4.5 PFTIR Data Reduction

Once collected, the raw PFTIR data must be processed to yield the individual flare component concentrations. This data processing was performed by Dr. Robert Spellicy from IMACC. Data were compiled at approximately one minute intervals. Each one minute point consists of approximately 40 individual measurements averaged into a single spectrum.

As shown in Figure 4.5-1, the total radiance measured by the PFTIR consists of:

1. The background radiance altered by its transmission through the flare plume and the atmosphere between the plum and the PFTIR instrument.

2. The flare radiance altered by its transmission the atmosphere between the plume and the PFTIR instrument.

3. The atmospheric radiance of the air between the flare plume and the PFTIR instrument.

4. The radiance from the PFTIR instrument itself.

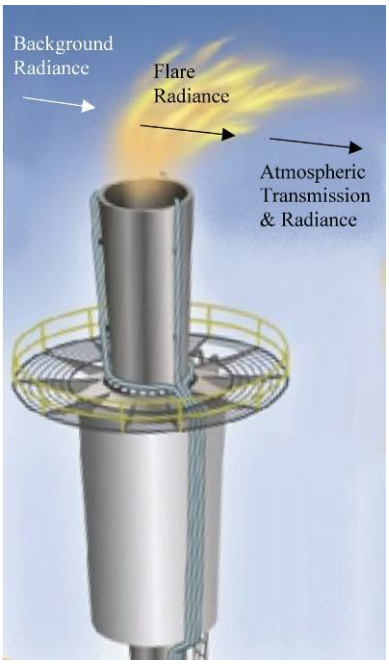

Figure 4.5-1: Contributions to Total Radiance

For this test program, everything except the flare transmission is considered interference. In equation form, the measured plume radiance can be represented by:

$$N_{total} = N_{bkg} * \tau_{flr} * \tau_{atm} + N_{flr} * \tau_{atm} + N_{atm} + N_f \qquad \text{Equation 4.5-1}$$

Where:

N_{total} = total radiance (radiance observed by the PFTIR)
N_{bkg} = background sky radiance
τ_{flr} = flare transmissivity
τ_{atm} = atmospheric transmissivity
N_{flr} = flare plume radiance
N_{atm} = atmospheric radiance
N_f = radiance of the FTIR instrument itself

In the broadest sense, the data analysis procedure has four major components:

1. Convert the raw interferogram to a single-beam spectrum using a Fourier Transform process.

2. Isolate the flare transmissivity from the other interferences listed above.

3. Convert the isolated flare transmissivity spectrum to an absorbance spectrum so it can be further analyzed with standard spectroscopic techniques.

4. Determine the concentrations of individual components of the flare plume from the absorbance spectrum.

Each of these steps is discussed briefly below. A more detailed treatment is found in Appendix A.2.

Step 1 – Convert the raw interferogram to a radiance spectrum
The raw data from the PFTIR are in the form of an interferogram, which is radiance as a function of FTIR scan position. The Fourier Transform (FT) process converts this data into a radiance spectrum, which is radiance as a function of wavelength or, in this case, wavenumber. The result is what is referred to as a "single beam" radiance spectrum. These single beam spectra have been supplied on the data hard drives that accompany this report. The FT process is a standard spectroscopic procedure and is not discussed in detail in this report.

Step 2 – Isolate the flare transmission spectrum
Once the radiance spectrum has been generated, the flare transmission must be isolated from all the interferants that the PFTIR also "sees". In order to accomplish this, each term in Equation 4.5-1 above must be determined. This is done as follows:

Background radiance (N_{bkg}) – As described in Section 3.4.5, at least once each day, the PFTIR was aimed at an unobstructed part of the sky. Since the background radiance is affected by conditions such as sun position and cloud cover, this procedure was repeated whenever a significant change in background was observed.

Flare transmissivity (τ_{flr}) – This is the value we are looking for and is the result when all competing factors are removed. It actually appears two places: 1) in transmitting the sky background through the flare to the PFTIR and 2) in the radiance term for the flare itself. So the flare transmission must be extracted from the complex mixture of signals received by the PFTIR. This task is accomplished by the IMACC software.

Atmospheric transmissivity (τ_{atm}) – This value is determined by aiming the PFTIR at an IR source and taking the ratio of the value obtained (minus the atmospheric radiance) to a "synthetic background" spectrum. This synthetic background (referred to as I_0) represents the shape of the radiance spectrum that would be generated by the PFTIR in the absence of all gases. For this project the IR source was a SiC source operated at a temperature of 1250 K. This is a standard source used in most active FTIR systems. This source has sufficient signal throughout the infrared to allow for a transmission spectrum to be determined over the range of wavenumbers needed.

Flare plume radiance (N_{flr}) – Plume radiance is (1 – plume transmission) times the Planck function (evaluated at the temperature of the plume). The radiance is what is measured by the PFTIR but it is mixed in with other signals and so must be corrected with respect to this interference.

Atmospheric radiance (N_{atm}) – This value is determined by aiming the PFTIR at very cold source in the calibration telescope located at the same distance from the PFTIR as the flare. Any radiance observed will then be due to the intervening atmosphere plus any radiance from the PFTIR instrument itself. This measured value is referred to as M_n. For this project, the cold source was a windowed cup filled with liquid nitrogen where the level of the liquid nitrogen was just below the collimator inlet.

PFTIR radiance (N_f) – PFTIR radiance is the emissions of the instrument itself. It is measured together with atmospheric radiance and is part of the M_n measurement.

Once these values are known, they are applied to the total radiance spectrum by IMACC proprietary software to isolate the flare transmission spectrum. For a more detailed description of this process, see Appendix A.2.

Step 3 – Convert the transmission spectrum to an absorption spectrum
Once the flare transmission spectrum has been isolated, it must be converted to an absorbance spectrum so that standard spectroscopic techniques can be used for further analysis. Transmission and absorbance are related by the Beer-Lambert law through the following equation.

$$\tau_{plume} = e^{-K(\upsilon)*c*l} \qquad \text{Equation 4.5-2}$$

Essentially, absorbance is the negative log of transmission, thus:

$$\text{Absorbance}(\upsilon) = (0.434)K(\upsilon) * c * l \qquad \text{Equation 4.5-3}$$

See Appendix A.2 for further detail. This conversion is a standard spectroscopic procedure.

Step 4 – Determine the concentrations of individual components in the flare plume
Once the absorbance spectrum has been generated, there are several analytical techniques that may be used to estimate individual component concentrations. For this project, a modified Classical Least Squares (CLS) analysis was used. IMACC proprietary software was used for this step of the data analysis. The modifications to standard CLS include algorithms for linearizing the absorbance for each analyte with concentration, corrections for spectral baseline shifts, corrections for any spectral line shifts observed, and algorithms for dynamic reference spectra selection based upon observed concentrations of each compound.

The CLS technique compares measured spectra to combinations reference spectra of known concentration and interfering compounds and matches the absorbance of the data and the references to determine gas concentration. This process is performed for all components present to account for all spectral features present.

After fitting, CLS also determines the difference or residual between the measured and scaled references. The fitting process minimizes the residuals in each analysis region. The software used for this project uses dynamic reference selection to select reference spectra based upon measured gas concentrations. In most cases, this means different reference spectra will be chosen for each analyte in the measured spectrum. This process will be repeated up to four times to optimize all spectra compared to the measured data.

A flow chart of the PFTIR data analysis process is shown in Figure 4.5-2.

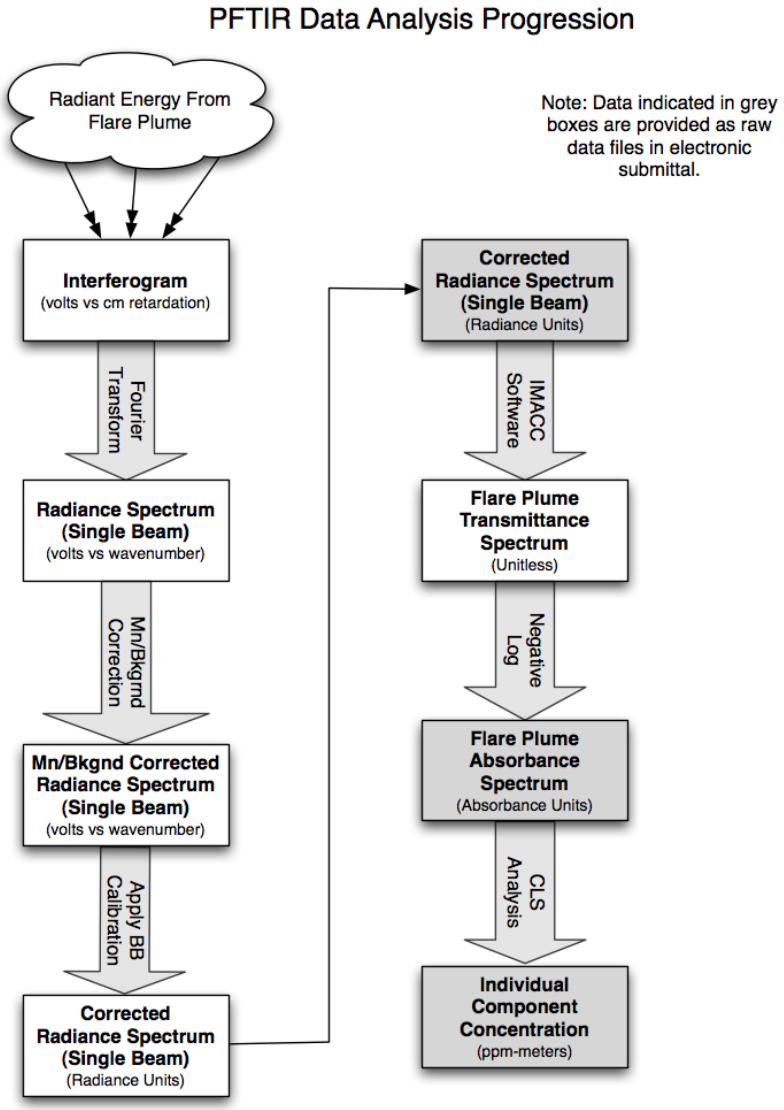

Figure 4.5-2: PFTIR Data Analysis Progression

5.0 Data Tables

Due to the large quantity of data collected for this project, three levels of data reduction are provided. Section 5.1 is the most concise summary providing run averages for a few key parameters at each test condition. Sections 5.2 through 5.7 provide more details on the individual test series, show a large number of test parameters, and provide wind information. Appendices A.5 through A.9 contain raw run data collected during the test program and any additional calibration or support data.

5.1 Data Summary Tables

The following data table includes summary data for each run. Column headings for this table are described below:

Condition: The designation for each test condition described in Section 2.4.2.
Run: The run number indicating the test and replicate. For example, Run 3-2 indicates Test 3, Replicate 2. A test is a given S/VG set point.
Start Time: The date and time each run began.
End Time: The date and time each run ended.
Visual Rating: The visual rating given to each run based on Table 3.2-1.
Std Flare Gas Flow: The average vent gas flow in standard cubic feet per hour.
Flare Gas Flow: The average vent gas flow in pounds per hour.
Flare Tip Velocity: The average velocity that the vent gas is exiting the tip in feet per second.
Flare Gas NHV: The average net heating value of the vent gas in BTU per standard cubic foot.
Steam Flow: The average steam flow to the flare tip in pounds per hour. This is the sum of the center steam flow (constant at 250 lb/hr) and ring steam flow.
Hydrogen: The average mole percent hydrogen in the vent gas.
Nitrogen: The average mole percent nitrogen in the vent gas.
THC: The average mole percent of total hydrocarbons in the vent gas.
MWvg: The average molecular weight of the vent gas in pounds per pound-mole.
Wind Direction: The average wind direction during the run in degrees.
Wind Speed: The average wind speed during the run in miles per hour.
Momentum Flux Ratio: The average momentum flux ratio during the run.
S/VG: The average steam to vent gas ratio during the run.
S/S521: The average steam to API 521 steam ratio during the run
CZG NHV: The average combustion zone gas net heating value in BTU per standard cubic foot.
S/HC: The average steam to hydrocarbon ratio during the run.
CE (weighted): The average weighted combustion efficiency for the run.

Test Conditions					Process Data				GC Data				Weather		Calculations				
Condition --	Run --	Start Time --	End Time --	Visual Rating --	Std Flare Gas Flow scf/hr	Flare Gas Flow lb/hr	Flare Tip Velocity ft/s	Flare Gas NHV BTU/scf	Steam Flow lb/hr	Hydrogen mol %	Nitrogen mol %	THC mol %	MWvg (GC calc) lb/lbmol	Wind Direction degrees	Wind Speed mph	Momentum Flux Ratio	S/VG (calc) --	S/SS21 (calc) --	CZG NHV BTU/scf	S/HC (calc) --	CE (weighted) %
A	1-1	07/10/2010 08:22:00	07/10/2010 08:52:00	5	10177	591	2.11	914	642	21.2	14.8	65.3	21.15	307	5.1	0.43	1.18	2.82	393	2.34	99.0%
A	1-2	07/11/2010 08:36:00	07/11/2010 09:06:00	4.5	9804	550	2.05	911	640	20.1	14.9	66.2	21.17	136	2.4	2.39	1.18	2.83	393	2.32	98.8%
A	2-1	07/11/2010 09:20:00	07/11/2010 09:35:00	2	9915	559	2.03	951	827	20.2	14.7	66.4	21.88	186	1.2	9.57	1.48	3.52	350	2.87	97.7%
A	2-2	07/17/2010 13:30:00	07/17/2010 13:45:00	1	9766	478	1.96	870	772	26.2	13.5	61.9	19.72	207	3.3	1.10	1.62	3.97	329	3.41	98.5%
A	3-1	07/11/2010 09:44:00	07/11/2010 09:59:00	1	10071	546	2.03	928	971	20.4	14.9	66.0	21.50	175	1.4	9.06	1.78	4.25	309	3.50	98.0%
A	3-2	07/17/2010 13:48:00	07/17/2010 14:03:00	1	9787	487	1.96	849	894	25.9	14.1	61.6	19.49	221	3.6	1.52	1.84	4.53	292	3.94	98.6%
A	4-1	07/10/2010 09:40:00	07/10/2010 09:55:00	1.5	10648	655	2.18	932	1350	17.3	21.5	62.6	23.53	297	4.7	1.85	2.12	4.90	258	4.78	96.9%
A	4-2	07/11/2010 10:17:00	07/11/2010 10:47:00	1	9726	528	2.00	907	1073	20.7	14.8	65.7	21.02	179	1.6	8.17	2.04	4.90	279	4.05	97.7%
A	5-1	07/10/2010 10:03:33	07/10/2010 10:18:27	1	11917	684	2.41	824	1496	16.9	27.5	57.0	23.13	265	5.8	1.86	2.20	5.11	228	5.99	95.2%
A	6-2	07/11/2010 10:52:00	07/11/2010 11:22:00	1	9957	537	2.03	909	1294	20.3	14.8	66.2	21.06	205	2.1	6.94	2.41	5.79	247	4.74	96.7%
A	7-1	07/10/2010 16:27:00	07/10/2010 16:57:00	1.5	9831	513	1.95	885	1319	21.7	15.3	64.3	20.74	147	6.7	0.67	2.61	6.30	232	5.37	95.2%
A	8-1	07/10/2010 17:11:00	07/10/2010 17:41:00	1.5	9519	529	1.93	912	1573	20.4	16.1	64.8	21.52	168	4.4	2.29	2.98	7.11	207	6.09	92.0%
A	8-3	07/19/2010 14:34:00	07/19/2010 15:04:00	1	9191	565	1.92	972	1623	18.9	15.6	66.8	22.57	311	6.7	0.88	2.88	6.75	213	5.56	95.2%
A	9-1	07/10/2010 18:01:00	07/10/2010 18:31:00	1	9365	504	1.90	908	2025	20.4	14.8	66.0	21.10	178	4.2	4.97	4.02	9.66	166	7.95	81.3%
A	9-3	07/19/2010 15:11:00	07/19/2010 15:41:00	1	9432	545	1.89	999	2209	18.3	15.2	67.9	22.99	309	6.7	2.13	4.06	9.45	169	7.62	88.7%
B	1-1	07/12/2010 08:55:00	07/12/2010 09:25:00	5	27254	1511	5.41	1037	903	30.4	9.2	61.9	21.70	186	1.5	15.34	0.60	1.43	606	1.15	98.9%
B	2-1	07/12/2010 09:37:00	07/12/2010 10:07:00	4	28249	1533	5.40	1056	1201	28.6	9.4	63.4	22.16	185	1.7	17.26	0.79	1.86	543	1.48	98.4%
B	2-2	07/16/2010 10:30:00	07/16/2010 11:00:00	4	27475	1505	5.39	1046	1259	23.2	9.3	68.9	22.04	292	4.6	2.31	0.85	2.02	524	1.47	99.1%
B	3-1	07/12/2010 10:24:00	07/12/2010 10:54:00	3	26929	1546	5.34	1110	1567	27.3	9.4	64.8	23.26	221	2.1	27.11	1.05	2.43	493	1.91	98.3%
B	3-2	07/16/2010 11:13:00	07/16/2010 11:43:00	3	29069	1549	5.59	1036	1638	24.5	9.1	67.8	21.77	285	4.7	4.10	1.06	2.52	462	1.85	99.3%
B	4-1	07/12/2010 11:12:00	07/12/2010 11:42:00	2	27926	1564	5.45	1075	1798	28.3	9.3	63.8	22.52	174	1.5	38.71	1.16	2.73	447	2.15	98.2%
B	4-2	07/16/2010 11:51:00	07/16/2010 12:11:00	2	27806	1509	5.34	1042	1867	25.2	9.4	66.9	21.94	215	2.4	17.76	1.25	2.96	418	2.22	99.2%
B	6-1	07/12/2010 13:22:00	07/12/2010 13:52:00	1.5	27261	1530	5.37	1073	2497	28.1	9.4	64.0	22.50	198	2.0	32.58	1.65	3.86	360	3.05	96.7%
B	6-2	07/17/2010 12:21:00	07/17/2010 12:41:00	1.5	27545	1568	5.43	1093	2540	25.7	9.2	66.6	22.88	171	2.5	20.40	1.62	3.78	366	2.86	98.6%
B	8-1	07/12/2010 14:36:00	07/12/2010 15:06:00	1.5	29858	1577	5.85	1019	3303	35.1	8.2	58.3	20.95	213	2.5	38.48	2.11	5.07	300	4.29	94.6%
B	8-2	07/17/2010 12:48:00	07/17/2010 13:08:00	1	27945	1587	5.49	1082	3301	25.6	9.1	66.8	22.62	209	3.3	23.76	2.09	4.89	305	3.66	96.9%
C	1-1	07/15/2010 08:38:00	07/15/2010 09:08:00	5.5	19916	1647	3.77	1683	1219	8.0	6.2	87.5	34.04	171	1.5	20.58	0.74	1.47	709	0.90	98.7%
C	1-2	07/17/2010 08:39:00	07/17/2010 09:09:00	5	21360	1714	3.91	1717	1264	7.9	5.7	88.2	34.57	225	2.2	10.84	0.74	1.46	722	0.89	99.4%
C	2-1	07/15/2010 09:19:00	07/15/2010 09:49:00	4	18742	1577	3.67	1636	1917	8.3	6.6	86.8	33.21	165	1.6	36.13	1.23	2.49	568	1.55	98.4%
C	2-2	07/17/2010 09:18:00	07/17/2010 09:38:00	4	22065	1674	3.88	1643	1923	8.4	6.3	87.0	33.27	202	2.0	22.42	1.18	2.39	530	1.50	99.1%
C	3-1	07/15/2010 10:36:49	07/15/2010 10:47:11	3	21005	1699	3.86	1650	2641	9.2	6.0	86.5	33.30	167	2.5	30.84	1.57	3.15	423	1.94	96.8%
C	3-2	07/17/2010 09:46:00	07/17/2010 10:06:00	3	21412	1728	3.99	1682	2597	7.7	5.9	88.1	33.94	212	2.1	30.58	1.51	3.00	447	1.82	97.4%
C	4-1	07/15/2010 13:12:00	07/15/2010 13:32:00	2	20440	1643	3.79	1697	3256	7.3	5.7	88.7	34.19	171	2.4	29.82	1.98	3.93	365	2.37	92.7%
C	4-2	07/17/2010 10:12:00	07/17/2010 10:32:00	3	20960	1718	3.97	1676	3269	7.9	5.9	88.0	33.80	224	2.3	34.97	1.91	3.81	373	2.31	93.7%
C	5-1	07/15/2010 14:36:40	07/15/2010 14:36:20	2	21564	1741	3.99	1683	3912	8.4	5.7	87.7	33.85	187	3.6	25.80	2.25	4.48	326	2.73	93.1%
C	5-2	07/17/2010 10:36:00	07/17/2010 10:56:00	2	20270	1630	3.79	1642	3751	8.4	6.3	87.1	33.25	183	2.2	47.30	2.30	4.62	319	2.85	91.5%
D	2-1	07/13/2010 10:27:00	07/13/2010 10:37:00	1	16514	895	4.65	750	2461	54.8	8.0	39.0	15.31	98	5.4	3.02	2.75	7.28	232	5.16	94.6%
D	3-1	07/13/2010 10:43:00	07/13/2010 10:53:00	1	16627	863	4.40	755	1687	52.2	8.2	41.4	15.47	97	5.4	1.68	1.94	5.14	287	6.26	97.5%
D	4-1	07/13/2010 13:26:00	07/13/2010 13:36:00	1	24148	1012	4.88	799	4432	50.5	7.1	44.2	16.03	104	6.3	6.15	4.65	12.16	163	13.14	88.6%
D	5-1	07/13/2010 13:43:00	07/13/2010 13:53:00	1	20512	871	4.14	789	3542	51.6	6.9	43.3	15.74	106	6.8	3.41	4.25	11.16	169	12.29	91.6%
D	6-1	07/13/2010 14:07:00	07/13/2010 14:17:00	1	26423	1135	5.14	794	1959	52.6	6.5	42.7	15.73	99	6.5	1.76	1.79	4.71	300	5.22	98.4%
D	7-1	07/13/2010 15:05:00	07/13/2010 15:15:00	1	20743	880	3.57	879	3933	40.5	8.9	52.3	18.33	109	8.0	2.90	4.61	11.58	157	10.94	83.5%
D	8-1	07/13/2010 15:25:00	07/13/2010 15:35:00	1	21115	931	4.17	853	2756	43.8	8.2	49.6	17.60	114	7.4	1.94	3.02	7.69	225	7.61	96.2%
D	9-1	07/13/2010 15:41:00	07/13/2010 15:51:00	2	22771	1044	4.71	849	1742	44.8	8.0	48.9	17.39	113	8.1	0.86	1.74	4.43	327	4.40	98.6%
D	10-1	07/13/2010 17:02:00	07/13/2010 17:12:00	1	15661	889	3.43	955	3883	33.8	9.4	58.4	20.10	103	8.8	2.29	4.42	10.77	164	9.22	81.8%
E	1-1	07/19/2010 09:30:00	07/19/2010 10:05:00	1	23702	1411	4.60	390	923	7.2	67.2	27.6	26.21	319	9.9	0.33	0.65	1.45	213	8.42	91.6%
E	2-1	07/19/2010 10:29:00	07/19/2010 10:44:00	1	24642	1466	4.81	337	914	7.0	70.1	24.8	25.95	297	7.2	0.69	0.62	1.39	189	10.15	88.3%
E	3-1	07/19/2010 11:49:26	07/19/2010 11:57:34	1	21324	1237	4.14	411	803	8.6	62.8	30.3	25.29	309	6.6	0.68	0.69	1.57	219	7.67	93.5%
E	5-1	07/19/2010 12:50:00	07/19/2010 13:05:00	1	19012	1098	3.69	426	648	9.2	60.8	31.7	25.01	312	8.0	0.27	0.59	1.33	247	5.87	97.2%
E	6-1	07/19/2010 13:12:45	07/19/2010 13:20:15	1	19211	1109	3.73	428	1068	9.3	60.7	31.8	25.00	280	5.9	1.24	0.96	2.18	196	9.48	89.7%
E	7-1	07/19/2010 13:47:00	07/19/2010 14:02:00	1	17046	982	3.34	477	947	10.0	56.1	35.6	24.65	157	3.3	2.75	0.96	2.19	219	7.55	96.2%
LTS	1	07/10/2010 19:20:00	07/10/2010 19:50:00	4	24999	1513	4.79	1155	1495	16.9	10.9	73.4	24.82	182	3.6	4.87	0.99	2.25	497	1.59	98.9%
LTS	4	07/14/2010 08:36:00	07/14/2010 09:06:00	3	24324	1519	4.89	1166	1583	17.4	10.5	73.5	24.86	126	3.5	5.65	1.05	2.38	489	1.67	98.9%
LTS	5	07/15/2010 16:41:00	07/15/2010 17:11:00	5	26575	1572	5.02	1186	1607	18.2	9.3	73.9	24.89	181	4.6	3.94	1.02	2.32	503	1.60	99.1%
LTS	7	07/17/2010 11:38:00	07/17/2010 12:08:00	4	28988	1607	5.44	1167	1581	22.2	9.2	70.1	24.41	223	2.9	9.06	1.01	2.31	521	1.69	99.3%
LTS	8	07/19/2010 16:14:00	07/19/2010 16:44:00	4	26167	1493	4.99	1124	1609	15.7	9.6	76.1	23.79	304	6.0	3.32	1.08	2.48	475	1.65	98.7%

5.2 Test Series A

The purpose of test series A is to simulate the base load with typical flow conditions for the flare. This test represents day-to-day operation.

5.2.1 Process Conditions

Figures 5.2-1 and 5.2-2 show process conditions for test series A.

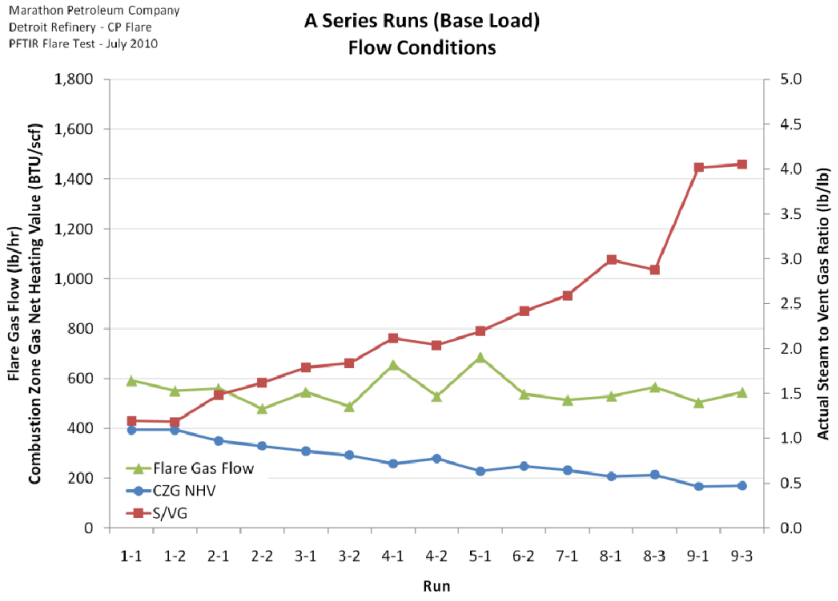

Figure 5.2-1: Vent Gas Flow Rate, CZG NHV, and S/VG for Test Series A

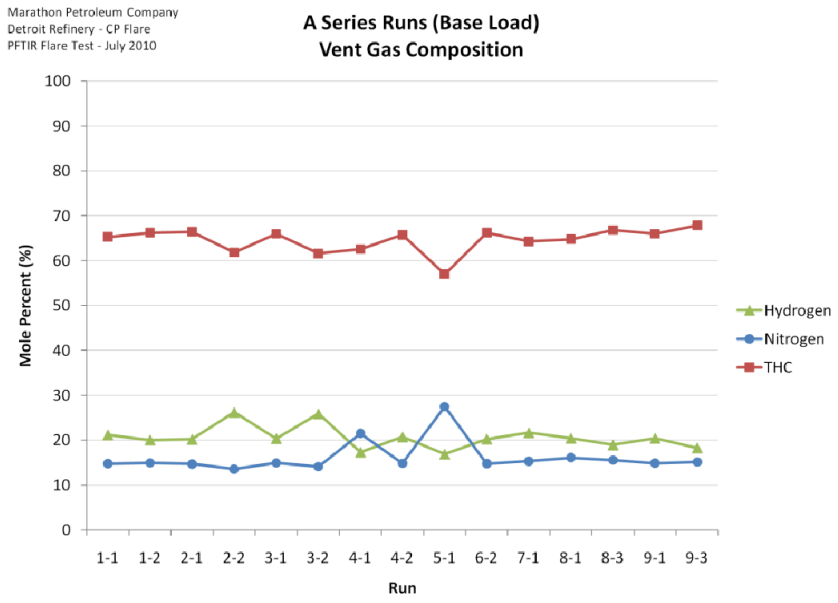

Figure 5.2-1: Vent Gas Composition for Test Series A

5.2.2 Wind Conditions

Figure 5.2-3 shows wind direction and speed during this test series A. Table 5.2-1 details which PFTIR was used for each run.

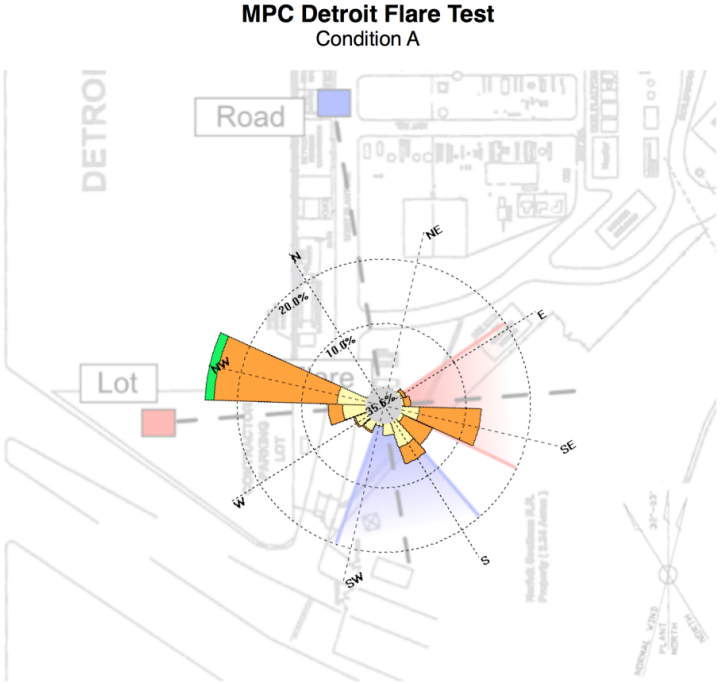

Note: Number in grey circle is percentage of calm (< 3mph) winds

Figure 5.2-3: Wind Speed and Direction for Test Series A

Run	PFTIR Used
1-1	Lot
1-2	Lot
2-1	Lot
2-2	Lot
3-1	Lot
3-2	Lot
4-1	Lot
4-2	Lot
5-1	Lot
6-1	Road (Invalid Run)
6-2	Lot
7-1	Lot
8-1	Lot
8-2	Lot (Invalid Run)
8-3	Lot
9-1	Lot
9-2	Lot (Invalid Run)
9-3	Lot

Table 5.2-1: PFTIR Times for Test Series A

5.3 Test Series B

The purpose of test series B is to demonstrate flare performance with a higher flow rate of hydrocarbons by adding refinery fuel gas (RFG) having a low S/VG for smokeless operation.

5.3.1 Process Conditions

Figures 5.3-1 and 5.3-2 show process conditions for test series B.

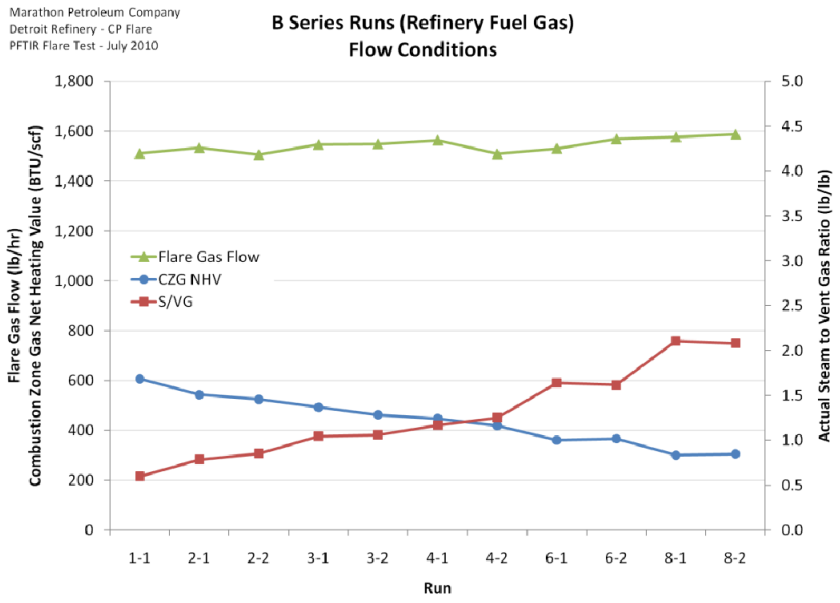

Figure 5.3-1: Vent Gas Flow Rate, CZG NHV, and S/VG for Test Series B

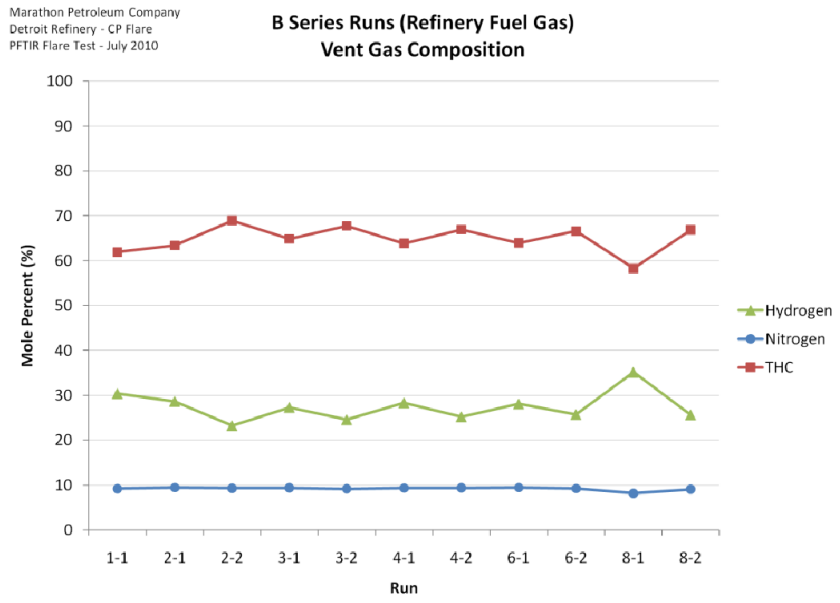

Figure 5.3-1: Vent Gas Composition for Test Series B

5.3.2 Wind Conditions

Figure 5.3-3 shows wind direction and speed during this test series B. Table 5.3-1 details which PFTIR was used for each run.

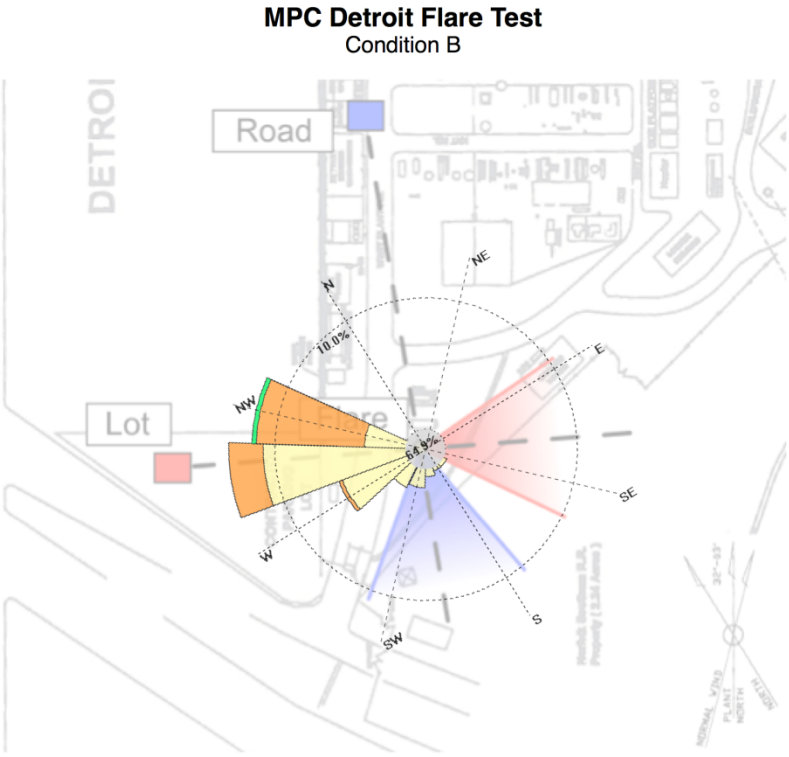

Figure 5.3-3: Wind Speed and Direction for Test Series B

Run	PFTIR Used
1-1	Lot
1-2	Road (Invalid Run)
2-1	Lot
2-2	Lot
3-1	Lot
3-2	Lot
4-1	Lot
4-2	Lot
6-1	Lot
6-2	Lot
8-1	Lot
8-2	Lot

Table 5.3-1: PFTIR Times for Test Series B

5.4 Test Series C

The purpose of test series C is to demonstrate flare performance at flow rates similar to test series B with addition of a 95% propylene / 5% propane mix that would require a higher S/VG for smokeless operation than the refinery fuel gas added in test series B.

5.4.1 Process Conditions

Figures 5.4-1 and 5.4-2 show process conditions for test series C.

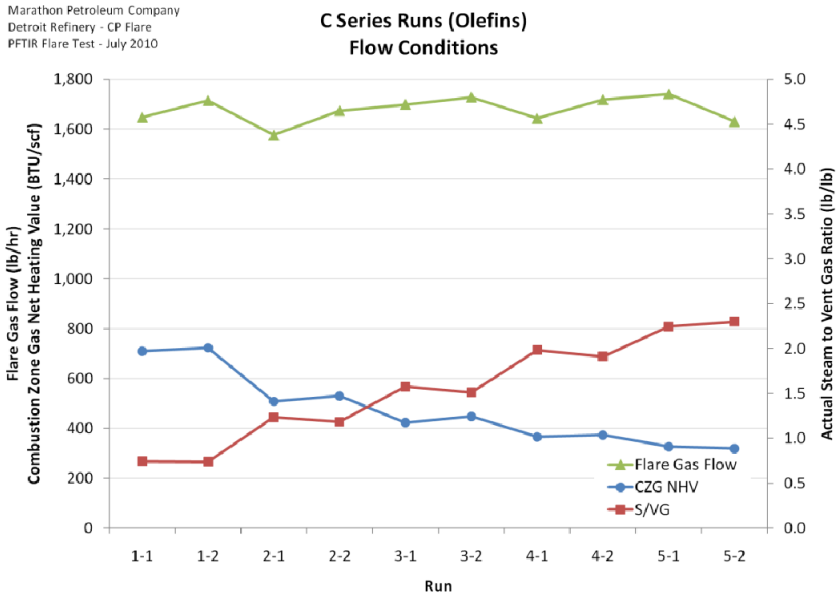

Figure 5.4-1: Vent Gas Flow Rate, CZG NHV, and S/VG for Test Series C

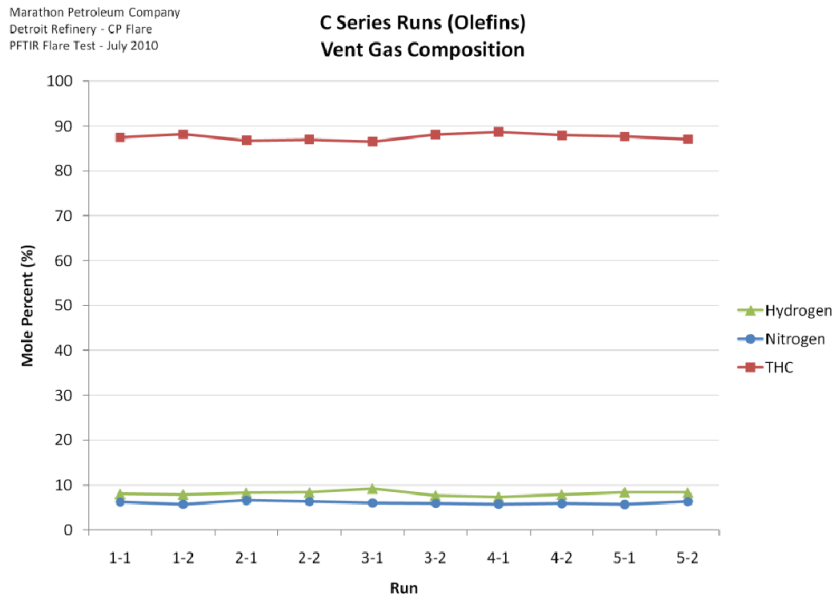

Figure 5.4-1: Vent Gas Composition for Test Series C

5.4.2 Wind Conditions

Figure 5.4-3 shows wind direction and speed during this test series C. Table 5.4-1 details which PFTIR was used for each run.

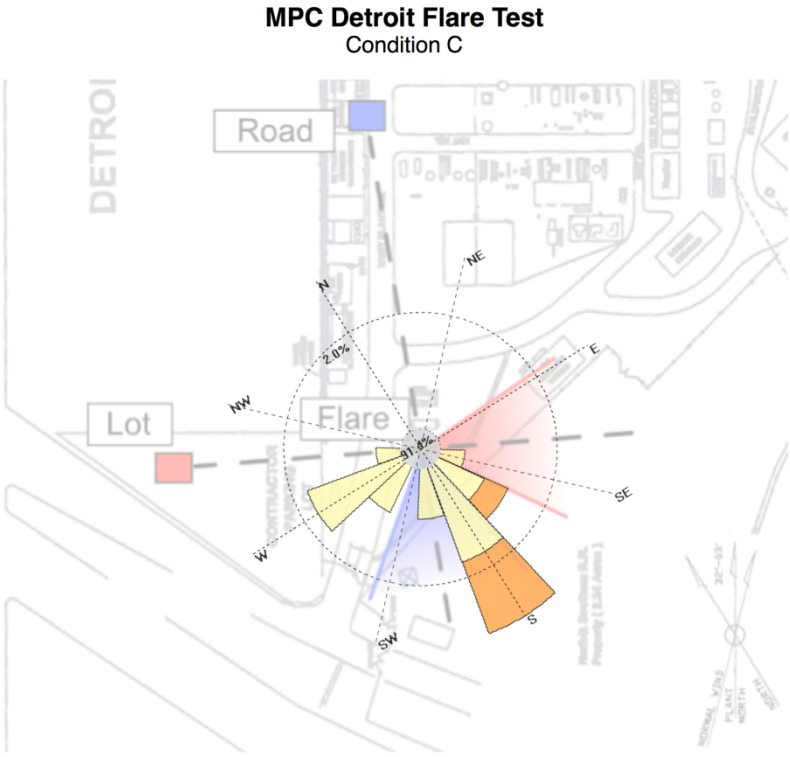

Figure 5.4-3: Wind Speed and Direction for Test Series C

Run	PFTIR Used
1-1	Lot
1-2	Lot
2-1	Lot
2-2	Lot
3-1	Lot
3-2	Lot
4-1	Lot
4-2	Lot
5-1	Lot
5-2	Lot

Table 5.4-1: PFTIR Times for Test Series C

5.5 Test Series D

The purpose of test series D is to demonstrate flare performance when operating at higher levels of hydrogen than typically found in the base load. Hydrogen has been shown to have exceptional combustion characteristics but has low volumetric heat content (270 BTU/scf). The hydrogen source for this test will be the Reformer at a purity of approximately 85 – 90%. NOTE: The base load contains nominal amounts of hydrogen from 20% to 30%.

5.5.1 Process Conditions

Figures 5.5-1 and 5.5-2 show process conditions for test series D.

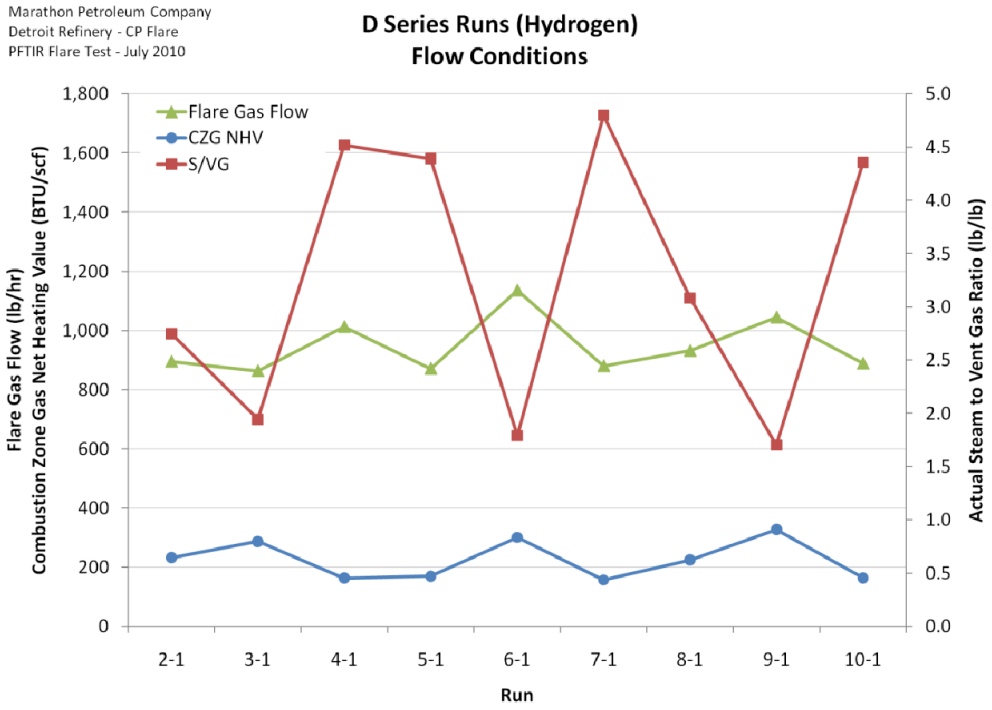

Figure 5.5-1: Vent Gas Flow Rate, CZG NHV, and S/VG for Test Series D

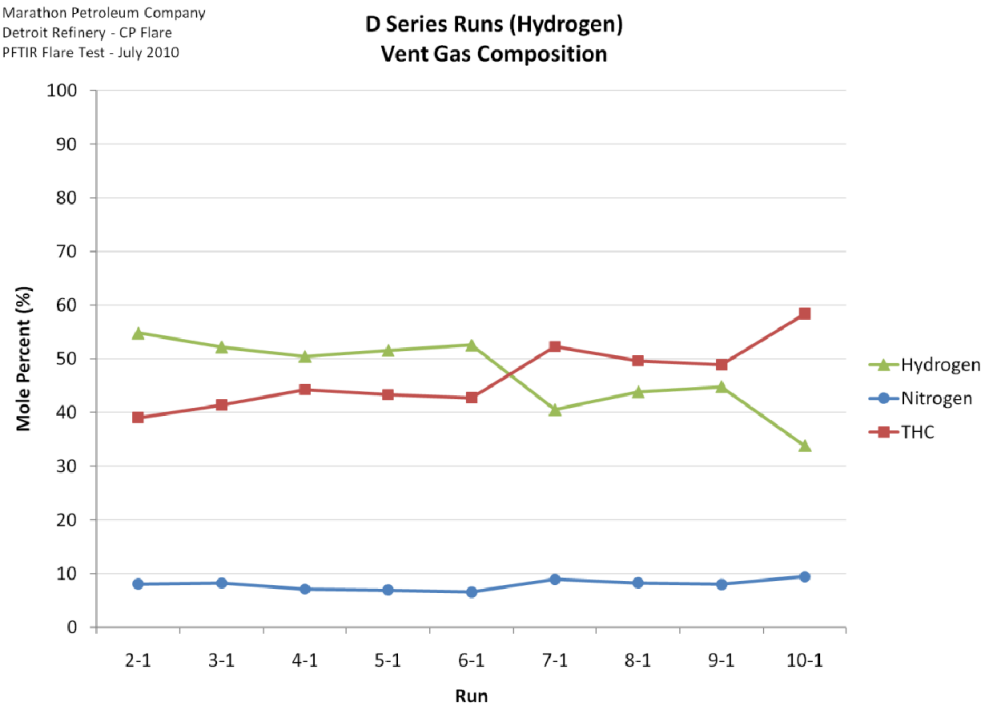

Figure 5.5-1: Vent Gas Composition for Test Series D

5.5.2 Wind Conditions

Figure 5.5-3 shows wind direction and speed during this test series D. Table 5.5-1 details which PFTIR was used for each run.

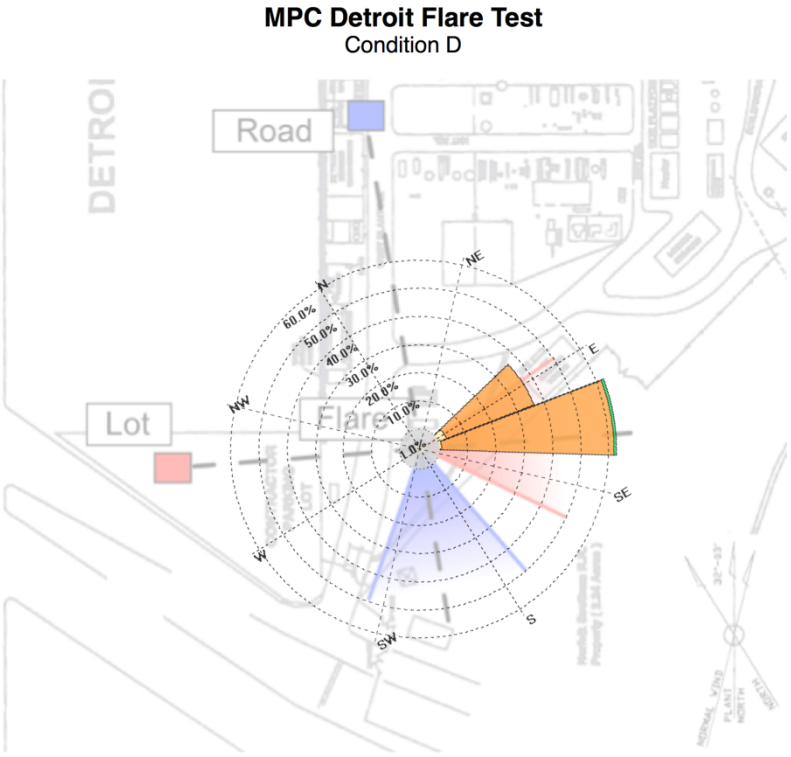

Note: Number in grey circle is percentage of calm (< 3mph) winds

Figure 5.5-3: Wind Speed and Direction for Test Series D

Run	PFTIR Used
1-1	Lot (Invalid Run)
2-1	Lot
3-1	Lot
4-1	Lot
5-1	Lot
6-1	Lot
7-1	Lot
8-1	Lot
9-1	Lot
10-1	Lot

Table 5.5-1: PFTIR Times for Test Series D

5.6 Test Series E

The purpose of test series E is to demonstrate performance at a set steam rate with varying nitrogen content. This test will demonstrate the effect of the hydrogen benefit on a low BTU gas. NOTE: this test was changed at the request of the Administrator to study the effect of nitrogen rich vent gas streams on combustion efficiency.

5.6.1 Process Conditions

Figures 5.6-1 and 5.6-2 show process conditions for test series E.

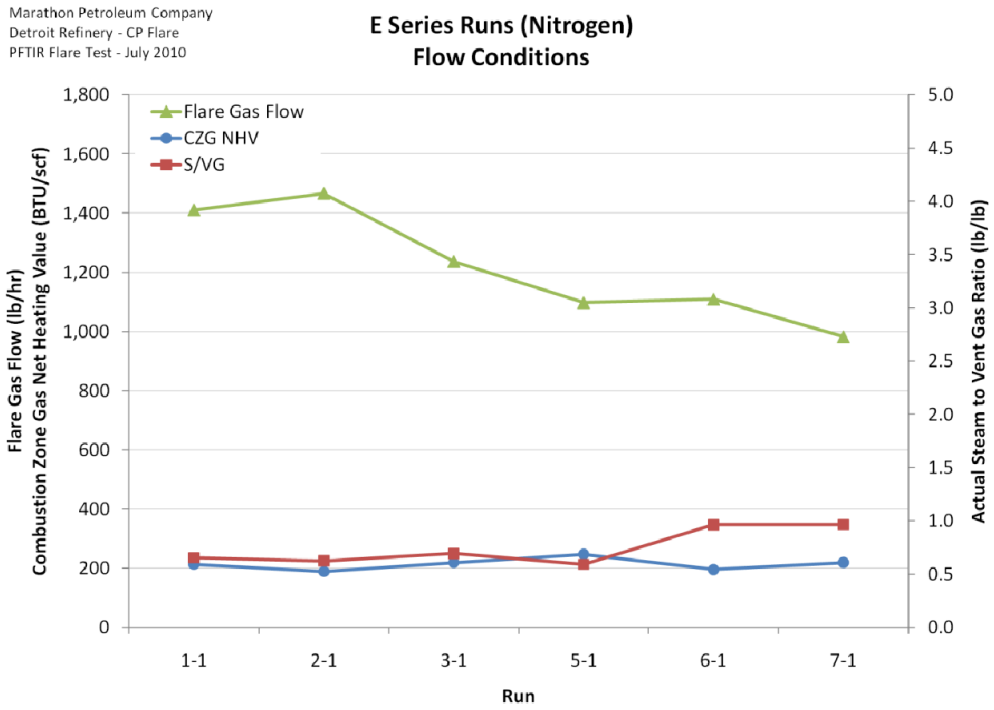

Figure 5.6-1: Vent Gas Flow Rate, CZG NHV, and S/VG for Test Series E

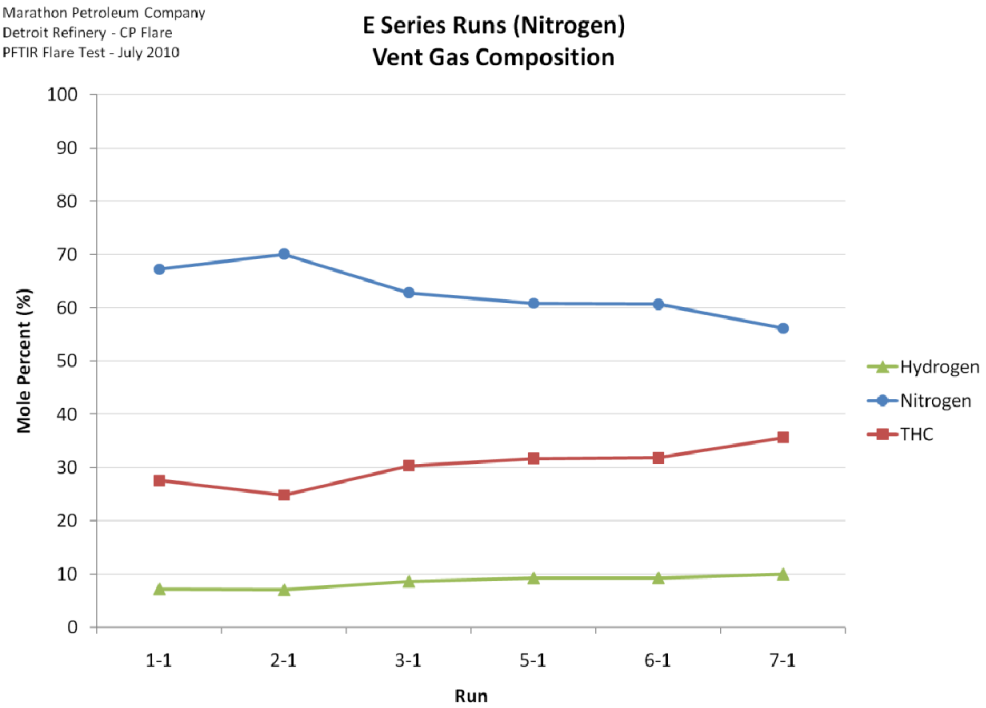

Figure 5.6-1: Vent Gas Composition for Test Series E

5.6.2 Wind Conditions

Figure 5.6-3 shows wind direction and speed during this test series E. Table 5.6-1 details which PFTIR was used for each run.

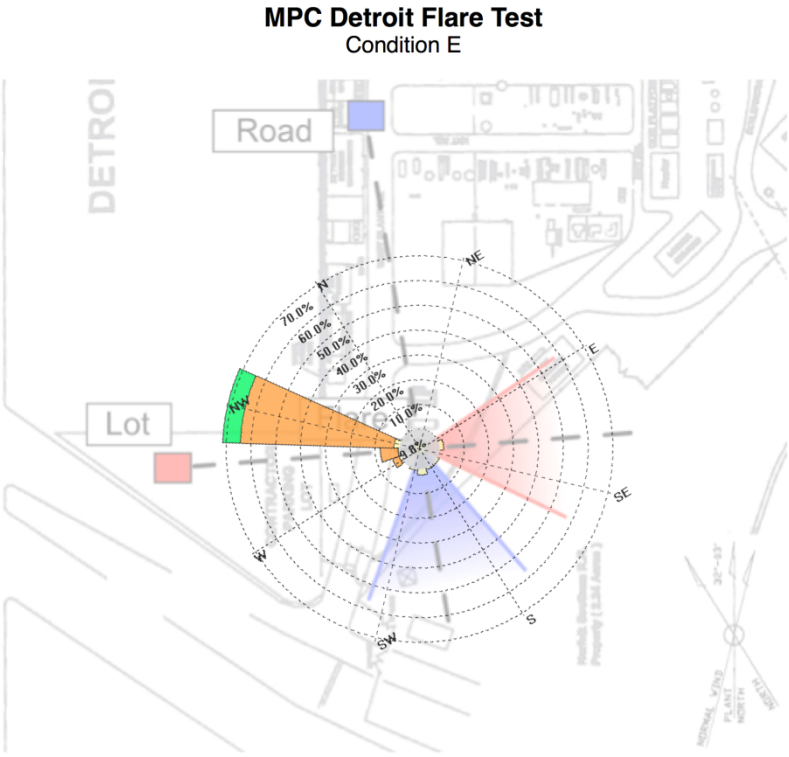

Note: Number in grey circle is percentage of calm (< 3mph) winds

Figure 5.6-3: Wind Speed and Direction for Test Series E

Run	PFTIR Used
1-1	Lot
2-1	Lot
3-1	Lot
4-1	Road (Invalid Run)
5-1	Lot
6-1	Lot
7-1	Lot

Table 5.6-1: PFTIR Times for Test Series E

5.7 Test Series F (Long Term Stability)

Test series F is the Long Term Stability (LTS) test. The purpose of this test is to demonstrate the repeatability of PFTIR measurements over an extended period. This test may also provide information on the effects of uncontrolled variables such as wind on the overall test result. The LTS tests will be conducted under test series B conditions at an S/VG of 1.0. Every effort will be made to ensure the controllable variables are held as constant as possible from run to run.

5.7.1 Process Conditions

Figures 5.7-1 and 5.7-2 show process conditions for test series F.

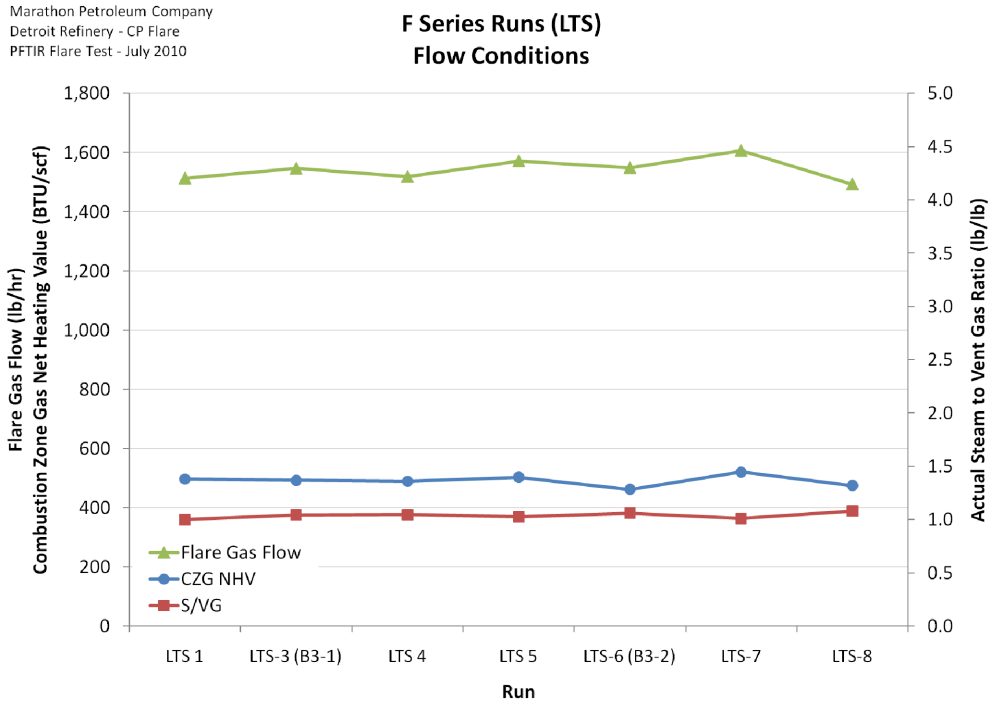

Figure 5.7-1: Vent Gas Flow Rate, CZG NHV, and S/VG for Test Series F

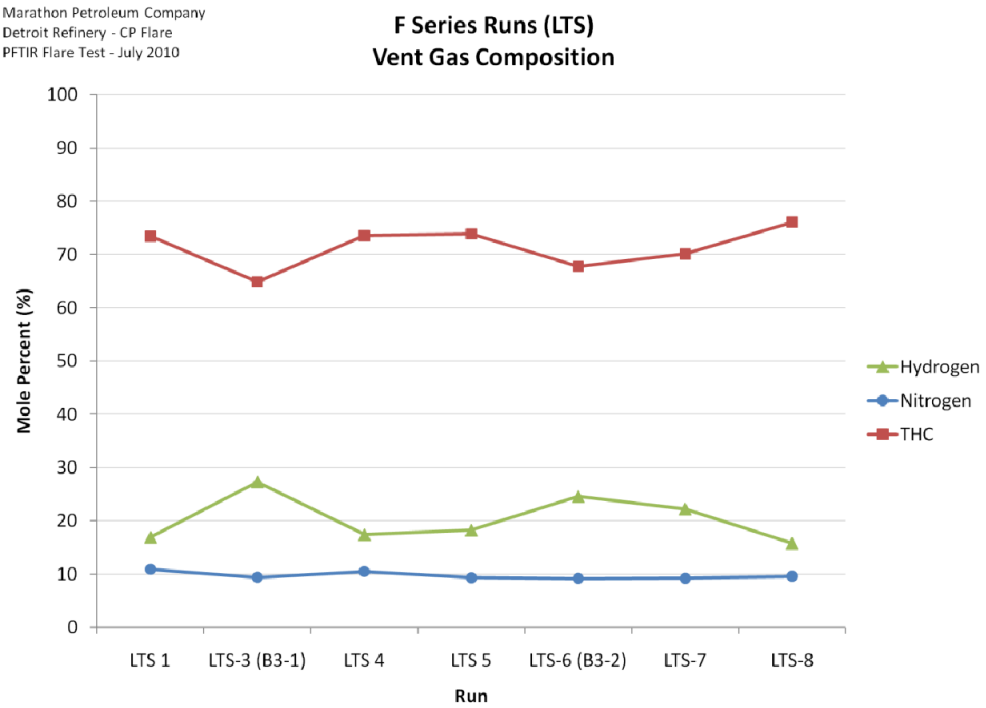

Figure 5.7-1: Vent Gas Composition for Test Series F

5.7.2 Wind Conditions

Figure 5.7-3 shows wind direction and speed during this test series F. Table 5.7-1 details which PFTIR was used for each run.

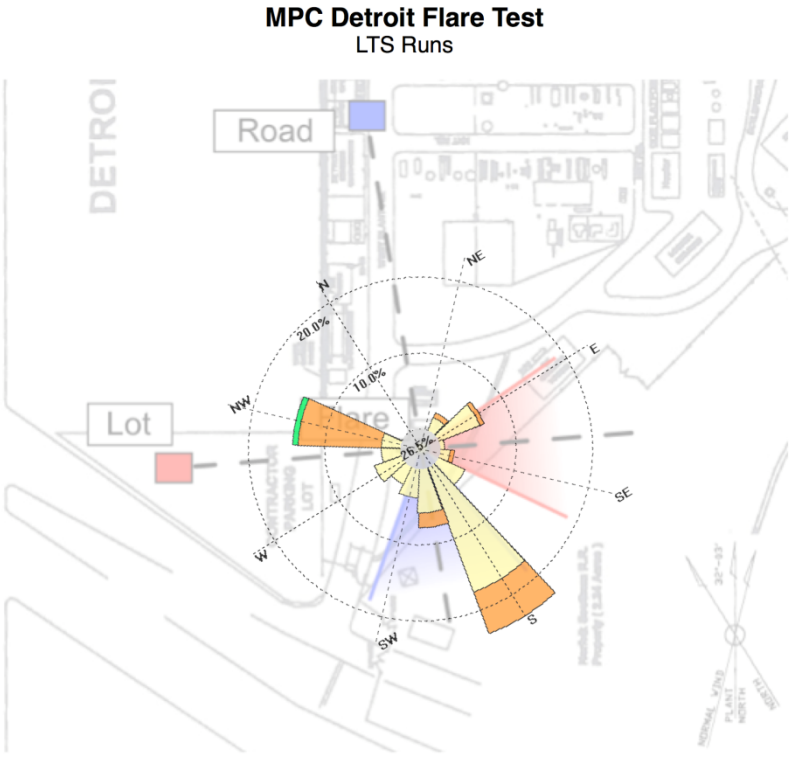

Note: Number in grey circle is percentage of calm (< 3mph) winds

Figure 5.7-3: Wind Speed and Direction for Test Series F

Run	PFTIR Used
LTS-1	Lot
LTS-2	Road (Invalid Run)
LTS-3 (B3-1)	Lot
LTS-4	Lot
LTS-5	Lot
LTS-6 (B3-2)	Lot
LTS-7	Lot
LTS-8	Lot

Table 5.7-1: PFTIR Times for Test Series F

6.0 Appendix

A.1 Calculations

The following calculations are used this report. In addition to the calculations listed below, many of the calculations used in reducing the PFTIR data are provided in Appendix A.2.

A.1.1 Mass Flow - Hydrocarbons

The flare vent header Gas Chromatograph (GC) measures the following hydrocarbons on a 15-minute cycle.

i	Measured Component	MW (lb/lb-mol)	NHV (BTU/scf)	Range	GC Units
1	Methane	16.04	896.2	0 - 100	Mole %
2	Ethane	30.07	1595.3	0 - 100	Mole %
3	Ethylene	28.05	1477.4	0 - 100	Mole %
4	Acetylene	26.04	1403.8	0 - 100	Mole %
5	Propane	44.1	2281.4	0 - 100	Mole %
6	Propylene	42.08	2150.6	0 - 100	Mole %
7	Iso-Butane	58.12	2957.0	0 - 100	Mole %
8	Normal Butane	58.12	2967.5	0 - 100	Mole %
9	i-Butene, Butene-1	56.11	2827.9	0 - 100	Mole %
10	Trans-Butene-2	56.11	2825.6	0 - 100	Mole %
11	Cis-Butene-2	56.11	2829.6	0 - 100	Mole %
12	1,3 Butadiene	54.09	2689.7	0 - 100	Mole %
13	Pentane-Plus (C5+)	72.15	3645.7	0 - 100	Mole %

Table A.1-1. List of hydrocarbons measured by Gas Chromatograph

The hydrocarbon mass flow rate is determined as follows:

$$HC = \sum_{i=1}^{13} \left(\frac{MW_i \cdot HC_{mol_i}}{386} \right) \cdot Q_{FM} \qquad \text{Equation A.1-1}$$

Where:

HC = hydrocarbon mass rate $\left({}^{\text{lb}}/_{\text{hr}}\right)$

MW_i = molecular weight of each compound i from Table A.1-1

Q_{FM} = vent gas flow from ultrasonic monitor $\left({}^{\text{scf}}/_{\text{hr}}\right)$

HC_{mol_i} = lb-mol of each compound i as a percentage of total mole % of vent gas

386 = molar volume of an ideal gas at 68°F and 1 atm $\left({}^{\text{scf}}/_{\text{lb-mol}}\right)$

A.1.2 Hydrocarbon Molecular Weight

The hydrocarbon molecular weight is calculated as:

$$MW_{hc} = \sum_{i=1}^{13} MW_i \cdot \left(\frac{HC_{mol_i}}{THC_{mol}}\right) \qquad \text{Equation A.1-2}$$

Where:

MW_{hc} = molecular weight of the hydrocarbon fraction of the vent gas $\left({}^{\text{lb}}/_{\text{lb-mol}}\right)$

MW_i = molecular weight of each compound i from Table A.1-1 $\left({}^{\text{lb}}/_{\text{lb-mol}}\right)$

HC_{mol_i} = mole percent of each compound i fraction from GC (%)

THC_{mol} = mole percent of total hydrocarbon fraction from GC (%)

A.1.3 Net Heating Value of Vent Gas

The Net Heating Value of the Vent Gas is calculated and reported from the GC at the conclusion of each analytical cycle (~15 minutes). The Net Heating Value is the Lower Heating Value or LHV defined as:

> *"Lower Heating Value" or "LHV" shall mean the theoretical total quantity of heat liberated by the complete combustion of a unit volume or weight of a fuel initially at 25° Centigrade and 760 mmHg, assuming that the produced water is vaporized and all combustion products remain at, or are returned to, 25° Centigrade; however, the standard for determining the volume corresponding to one mole is 20° Centigrade.*

The Combustion Zone Gas Net Heating Value combines the vent gas, pilot gas, and steam net heating values and is determined as follows:

$$CZG\ NHV = \frac{(Q_{VG} \cdot NHV_{VG}) + (Q_{PG} \cdot NHV_{PG}) + (Q_S \cdot NHV_S)}{(Q_{VG}) + (Q_{PG}) + (Q_S)} \qquad \text{Equation A.1-3}$$

Where:

$CZG\ NHV$ = combustion zone gas net heating value $\left({}^{\text{BTU}}/_{\text{scf}}\right)$

Q_{VG} = volumetric vent gas flow rate $\left({}^{\text{scf}}/_{\text{hr}}\right)$

NHV_{VG} = net heating value of vent gas from GC $\left({}^{\text{BTU}}/_{\text{scf}}\right)$

Q_{PG} = volumetric pilot gas flow rate $\left(\text{constant, } 135\ {}^{\text{scf}}/_{\text{hr}}\right)$

NHV_{PG} = net heating value of pilot gas $\left(\text{constant, } 914\ {}^{\text{BTU}}/_{\text{scf}}\right)$

Q_S = volumetric steam rate from ultrasonic flow meter $\left({}^{\text{scf}}/_{\text{hr}}\right)$

NHV_S = net heating value of steam $\left(\text{assumed to be zero, } 0\ {}^{\text{BTU}}/_{\text{scf}}\right)$

The volumetric vent gas flow rate is calculated as:

$$Q_{VG} = VG \cdot \frac{386}{MW_{VG}}$$ Equation A.1-4

Where:

Q_{VG} = volumetric vent gas flow rate $\left(\text{scf}/\text{hr}\right)$

VG = vent gas mass rate from ultrasonic flow meter $\left(\text{lb}/\text{hr}\right)$

MW_{VG} = molecular weight of vent gas from ultrasonic flow meter $\left(\text{lb}/\text{lb-mol}\right)$

386 = molar volume of an ideal gas at 68°F and 1 atm $\left(\text{scf}/\text{lb-mol}\right)$

A.1.4 Steam Ratios

Four steam ratios are included in this report. They are calculated as described below.

Actual Total Steam to API 521 Total Steam Ratio (S/S_{521})

The Actual Total Steam to API 521 Total Steam Ratio is calculated as follows:

$$\text{S/S}_{521} = \frac{S}{S_{521}}$$ Equation A.1-5

Where:

S/S_{521} = actual total steam to API 521 total steam ratio $\left(\text{lb}/\text{lb}\right)$

S = actual total steam mass rate from Equation A.1-6 $\left(\text{lb}/\text{hr}\right)$

S_{521} = API 521 total steam mass rate from Equation A.1-7 $\left(\text{lb}/\text{hr}\right)$

The actual total steam mass rate is calculated as:

$$S = Q_S \cdot \frac{MW_{H_2O}}{386}$$ Equation A.1-6

Where:

S = actual total steam mass rate $\left(\text{lb}/\text{hr}\right)$

Q_S = volumetric steam rate from ultrasonic flow meter $\left(\text{scf}/\text{hr}\right)$

MW_{H_2O} = molecular weight of steam $\left(\text{constant, } 18.02\ \text{lb}/\text{lb-mol}\right)$

386 = molar volume of an ideal gas at 68°F and 1 atm $\left(\text{scf}/\text{lb-mol}\right)$

The API 521 total steam mass rate is calculated as:

$$S_{521} = (0.0067 \cdot MW_{VG} + 0.275) \cdot VG \qquad \text{Equation A.1-7}$$

Where:

S_{521} = API 521 total steam mass rate $\left({}^{\text{lb}}/_{\text{hr}}\right)$

MW_{VG} = molecular weight of vent gas from ultrasonic meter $\left({}^{\text{lb}}/_{\text{lb-mol}}\right)$

VG = vent gas mass rate from ultrasonic flow meter $\left({}^{\text{lb}}/_{\text{hr}}\right)$

Note: The equation is derived from a regression on the compound-specific steam-to-gas-ratios (pounds of steam to pounds of gas) set forth in Table 11 of the American Petroleum Institute's *Recommended Practice 521* (Fifth Edition, May 2007).

Actual Total Steam to Vent Gas Ratio (S/VG)
The Actual Total Steam to Vent Gas Ratio is calculated as follows:

$$\text{S/VG} = \frac{S}{VG} \qquad \text{Equation A.1-8}$$

Where:

S/VG = actual total steam to vent gas ratio $\left({}^{\text{lb}}/_{\text{lb}}\right)$

S = actual total steam mass rate from Equation A.1-6 $\left({}^{\text{lb}}/_{\text{hr}}\right)$

VG = vent gas mass rate from ultrasonic flow meter $\left({}^{\text{lb}}/_{\text{hr}}\right)$

Actual Total Steam to Hydrocarbon Ratio (S/HC)
The Actual Total Steam to Hydrocarbon Ratio is calculated as follows:

$$\text{S/HC} = \frac{S}{HC} \qquad \text{Equation A.1-9}$$

Where:

S/HC = actual total steam to hydrocarbon ratio $\left({}^{\text{lb}}/_{\text{lb}}\right)$

S = actual total steam mass rate from Equation A.1-6 $\left({}^{\text{lb}}/_{\text{hr}}\right)$

HC = hydrocarbon mass rate from Equation A.1-1 $\left({}^{\text{lb}}/_{\text{hr}}\right)$

Volumetric Steam to Vent Gas Ratio (S/VG_{scf})
The Volumetric Steam to Vent Gas Ratio is calculated as follows:

$$S/VG_{scf} = \frac{Q_S}{Q_{VG}} \qquad \text{Equation A.1-10}$$

Where:

S/VG_{scf} = volumetric steam to vent gas ratio $\left({}^{scf}/_{scf}\right)$
Q_S = volumetric steam rate from ultrasonic flow meter $\left({}^{scf}/_{hr}\right)$
Q_{VG} = volumetric vent gas flow rate from Equation A.1-4 $\left({}^{scf}/_{hr}\right)$

A.1.5 Total Hydrocarbons from PFTIR

The total hydrocarbons calculation for hydrocarbons in the flare plume uses PFTIR measurements and is weighted as follows:

$$THC_w = C_{CH_4} + 2 \cdot C_{C_2H_4} + 3 \cdot C_{C_3H_6} + 4 \cdot \left(C_{But} + C_{1,3But}\right) + 5 \cdot C_{HC} \qquad \text{Equation A.1-11}$$

Where:

THC_w = weighted total hydrocarbons from PFTIR ($ppm{\cdot}m$)
C_{CH_4} = methane from PFTIR ($ppm{\cdot}m$)
$C_{C_2H_4}$ = ethylene from PFTIR ($ppm{\cdot}m$)
$C_{C_3H_6}$ = propylene from PFTIR ($ppm{\cdot}m$)
C_{But} = butane from PFTIR ($ppm{\cdot}m$)
$C_{1,3But}$ = 1,3 butadiene from PFTIR ($ppm{\cdot}m$)
C_{HC} = pentane and larger hydrocarbons from PFTIR ($ppm{\cdot}m$)
$2, 3, 4, 5$ = number of carbon atoms in each molecule

A.1.6 Flare Combustion Efficiency

"Flare Combustion Efficiency" means the actual efficiency of converting organic carbon compounds to carbon dioxide based on reading from the PFTIR. Flare combustion efficiency is calculated as follows:

$$CE = \frac{CO_2}{CO_2 + CO + THC_w} \qquad \text{Equation A.1-12}$$

Where:

CE = flare combustion efficiency (%)
THC_w = weighted total hydrocarbons from Equation A.1-11 ($ppm{\cdot}m$)
CO_2 = carbon dioxide from PFTIR ($ppm{\cdot}m$)
CO = carbon monoxide from PFTIR ($ppm{\cdot}m$)
THC_w = weighted total hydrocarbons from PFTIR ($ppm{\cdot}m$)

A.1.7 Momentum Flux Ratio

Momentum Flux Ratio (MFR) is defined as the ratio of the CZG momentum flux to the wind momentum flux. This ratio is shown by Equation A.1-13.

$$MFR = \frac{\rho_{czg} \cdot {v_{czg}}^2}{\rho_{air} \cdot {v_{wind}}^2} \qquad \text{Equation A.1-13}$$

The densities of the gases (ρi) are calculated by general Equation A.1-14.

$$\rho_i = \frac{MW_i \cdot P}{R \cdot T_{abs}} = \frac{MW_i \cdot 14.73}{10.73 \cdot (460 + T_i)} = \frac{1.373 \cdot MW_i}{460 + T_i} \qquad \text{Equation A.1-14}$$

From general Equation A.1-14, the densities of ambient air (ρ_{air}), vent gas (ρ_{vg}), and steam (ρ_{steam}) can be calculated, shown in Equations A.1-15, A.1-16, and A.1-17. The temperature for steam and ambient air is measured, and the temperatures for ambient air and vent gas are assumed to be equal.

$$\rho_{air} = \frac{1.373 \cdot MW_{air}}{460 + T_{air}} \qquad \text{Equation A.1-15}$$

$$\rho_{vg} = \frac{1.373 \cdot MW_{vg}}{460 + T_{air}} \qquad \text{Equation A.1-16}$$

$$\rho_{steam} = \frac{1.373 \cdot MW_{H_2O}}{460 + T_{steam}} \qquad \text{Equation A.1-17}$$

The density of the CZG (ρ_{czg}) is calculated by combining the mass flow rates of the vent gas and steam adjusted for the density of each component gas. This is shown by Equation A.1-18.

$$\rho_{czg} = \frac{\dot{m}_{vg} + \dot{m}_{steam}}{Q_{vg} + Q_{steam}} = \frac{\dot{m}_{vg} + \dot{m}_{steam}}{\frac{\dot{m}_{vg}}{\rho_{vg}} + \frac{\dot{m}_{steam}}{\rho_{steam}}} \qquad \text{Equation A.1-18}$$

The velocity of the CZG (v_{czg}) is calculated by Equation A.1-19.

$$v_{czg} = \frac{Q_{vg} + Q_{steam}}{A_{tip}} = \frac{\frac{\dot{m}_{vg}}{\rho_{vg}} + \frac{\dot{m}_{steam}}{\rho_{steam}}}{\pi \cdot \frac{{D_{tip}}^2}{4}} \qquad \text{Equation A.1-19}$$

For Equations A.1-14 through A.1-19, the MFR for each run is calculated by using measured averages for the run.

MFR constants:

$$D_{tip} = diameter\ of\ flare\ tip\ (1.333\ ft)$$

$$MW_{air} = molecular\ weight\ of\ air\ \left(28.96\frac{lb}{lbmol}\right)$$

$$MW_{H_2O} = molecular\ weight\ of\ water\ \left(18.02\frac{lb}{lbmol}\right)$$

$$P = absolute\ ambient\ pressure\ (14.73\ psia)$$

$$R = gas\ constant\ \left(10.73\frac{psi \cdot ft^3}{lbmol \cdot °R}\right)$$

MFR measured variables:

$$MW_{vg} = molecular\ weight\ of\ vent\ gas\ \left(\frac{lb}{lbmol}\right)$$

$$\dot{m}_{steam} = mass\ flow\ rate\ of\ steam\ \left(\frac{lb}{hr}\right)$$

$$v_{wind} = velocity\ of\ wind\ \left(\frac{ft}{hr}\right)$$

MFR calculated variables:

$$A_{tip} = area\ of\ flare\ tip\ (ft^2)$$

$$MFR = momentum\ flux\ ratio\ (unitless)$$

$$MW_i = molecular\ weight\ of\ component\ i\left(\frac{lb}{lbmol}\right)$$

$$\rho_{air} = density\ of\ air\ \left(\frac{lb}{ft^3}\right)$$

$$\rho_{czg} = density\ of\ combustion\ zone\ gas\ \left(\frac{lb}{ft^3}\right)$$

$$\rho_i = density\ of\ component\ i\ \left(\frac{lb}{ft^3}\right)$$

$$Q_{steam} = volumetric\ flow\ rate\ of\ steam\ \left(\frac{ft^3}{hr}\right)$$

$$Q_{vg} = volumetric\ flow\ rate\ of\ vent\ gas\ \left(\frac{ft^3}{hr}\right)$$

$$T_{abs} = absolute\ temperature\ (°R)$$

$$v_{czg} = velocity\ of\ combustion\ zone\ gas\ \left(\frac{ft}{hr}\right)$$

A.1.8 Modified RATA for FCCU Test

For the 30-minute FCCU Test, the PFTIR data was split into three 10-minute sections for analysis. Using a method similar to a Relative Accuracy Test Audit (RATA), the relative accuracy (RA) of each section was calculated as:

$$RA = \frac{\left|\frac{\sum_{i=1}^{n}\left(C_{CEMS_i} - C_{PFTIR_i}\right)}{n}\right| + |\mathrm{CC}|}{\frac{\sum_{i=1}^{n}\left(C_{CEMS_i}\right)}{n}} \qquad \text{Equation A.1-20}$$

Where:

RA = relative accuracy of the PFTIR to the CEMS (%)
C_{CEMS_i} = concentration measured by the CEMS (ppm or %)
C_{PFTIR_i} = concentration measured by the PFTIR (ppm or %)
CC = confidence coefficient (ppm or %)
n = number of data points taken by the PFTIR

The confidence coefficient is calculated as:

$$CC = \sigma \cdot \frac{t}{\sqrt{n}} \qquad \text{Equation A.1-21}$$

Where:

CC = confidence coefficient (ppm or %)
σ = standard deviation of the CEMS and PFTIR data (ppm or %)
t = confidence factor from Student's t-distribution table
n = number of data points taken by the PFTIR

The Student's t-distribution table is provided in Table A.1-2.

n	t-value (97.5%)
2	12.706
3	4.303
4	3.182
5	2.776
6	2.571
7	2.447
8	2.365
9	2.306
10	2.262
11	2.228
12	2.201
13	2.179
14	2.160
15	2.145
16	2.131
17	2.120
18	2.110
19	2.101
20	2.093
21	2.086
22	2.080
23	2.074

Table A.1-2: Student's t-distribution table for 97.5% confidence.

A.2 PFTIR Theory and Operation

A.2-1 PFTIR Analytical Method and Procedure

Gases have highly variable absorption with wavelength. It is this variation that produces the absorption patterns that allow for their identification in the infrared. If the transmission of a gas is given by $\tau(\nu, T)$ then $[1 - \tau(\nu, T)]$ is the amount of absorption. The radiation the gas emits at temperature T is then given by:

$$N(\nu, T) = [1 - \tau(\nu, T)] \cdot N_{bb}(\nu, T) \qquad (1)$$

For flare measurements, it is this signal that is being detected from the hot gases above the combustion zone.

However, there are also other contributions to the signal an analyzer "sees." As shown in Figure A.2-1, the background (typically the sky) has some emission, also defined by Equation (2) that when transmitted through the plume and the intervening atmosphere is seen by the analyzer. The plume emissions transmitted through this same atmospheric path provides the signal of interest. The intervening atmosphere itself has some emission as does the FTIR instrument itself. These are also seen by the analyzer.

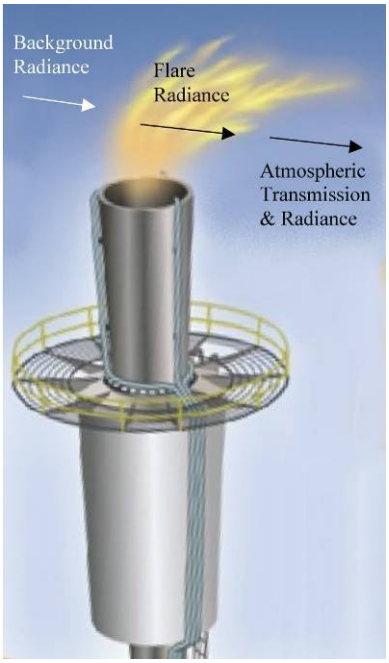

Figure A.2-1: Contributions to the measured flare radiance.

The total radiant signal received then consists of:

$$N_{total} = N_{bkg} \cdot \tau_{flr} \cdot \tau_{atm} + N_{flr} \cdot \tau_{atm} + N_{atm} + N_f \quad (2)$$

In Equation (2), the arguments (ν, T) have been dropped for clarity and the individual terms are:

N_{total} = total radiance
N_{bkg} = background sky radiance
τ_{flr} = flare transmissivity
τ_{atm} = atmospheric transmissivity
N_{atm} = atmospheric radiance
N_f = radiance of the FTIR instrument itself

The actual measurements performed by the PFTIR consist of the following:

M_{flr} = the measured plume radiance
M_b = the measured background radiance taken by moving the PFTIR off the flare to monitor the sky background.This is given by:
$M_b = N_{bkg} \cdot \tau_{atm} + N_{atm} + N_f$
M_n = a measurement made looking at the calibration source (see below) with a cold (liquid nitrogen) emitter in place of the normal (black body)
M_{bb} = a measurement made looking at the calibration source with a commercial black body emitter in the source
τ_{atm} = measured atmospheric path transmission

A.2-2 From Radiance to Transmission Spectra

Based on these measurements Equation (2) can be rearranged to give the plume transmission as:

$$\tau_{flr} = \frac{C \cdot \left(M_{flr} - M_n\right) - N_{BB}^{flr} \cdot \tau_{atm}}{C \cdot (M_b - M_n) - N_{BB}^{flr} \cdot \tau_{atm}} \quad (3)$$

In this equation, the superscript on the Planck function radiance (N_{BB}) denotes that this is the Planck function computed at the temperature of the flare. *C* is a calibration measurement made with a black body calibration source. This is the initial derivation that has had some proprietary modifications to improve stability and performance.

Atmospheric transmission τ_{atm} is also measured using the calibration source. In this case the black body is replaced by a standard infrared source and the measurement is made at a path length roughly equal to that of the slant-path from the PFTIR to the flare.

Atmospheric transmission is then given by:

$$\tau_{atm} = \frac{M_{IR} - M_n}{I_0} \qquad (4)$$

M_{IR} is the measured signal from the calibration source using the IR source and M_n is the measured cold source as defined earlier. The only term not defined is I_0. This is the so-called synthetic background. It is frequently used in open-path FTIR measurements to convert a measured spectrum to transmission. It represents the shape of the spectrum that the PFTIR would measure if no gases were present. It can be synthesized from the $(M_{IR} - M_n)$ measurement by doing a mathematical fit to points in the spectrum known to be free of molecular absorptions. An example is given in Figure A.2-2. In this figure, the bottom plot is the measured spectrum (here a relatively clean spectrum done in the laboratory), the middle plot the points chosen for fitting, and the top plot the mathematical fit to the chosen points. The top plot is the I_0 spectrum.

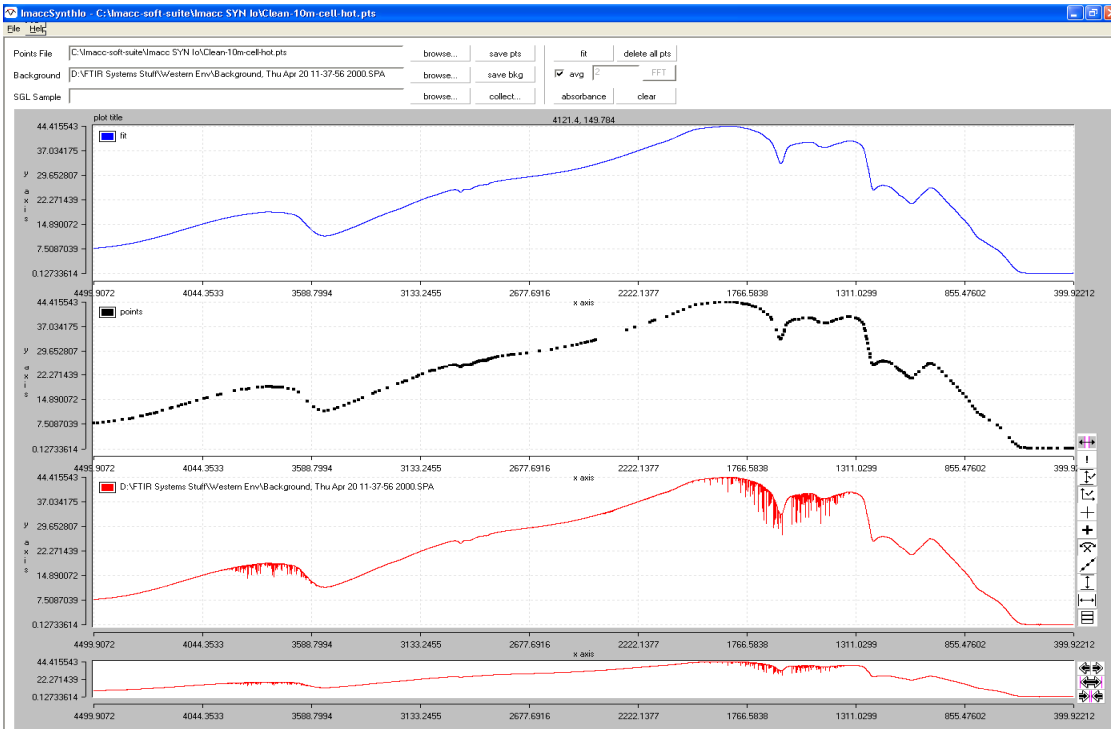

Figure A.2-2: Development of synthetic spectrum

A.2-3 Determination of Flare Temperature

With Equations (3) and (4), Equation (2) then contains only measured or computed terms. However, to compute the Planck function at the temperature of the flare, N_{BB}^{flr}, the flare gas temperature must be known. Fortunately, this can be measured using features in the PFTIR data itself. One convenient feature is the CO band near 2150 cm^{-1}. Figure A.2-3 shows this band at two different temperatures. The upper plot is at ambient temperature (300 K) and the bottom plot is at 550 K. The effect of increasing temperature is to expand the band shifting the peak position

away from band center while increasing the strength of the weaker lines farther from band center. This is a sensitive function of temperature, so the shape of the band essentially measures temperature.

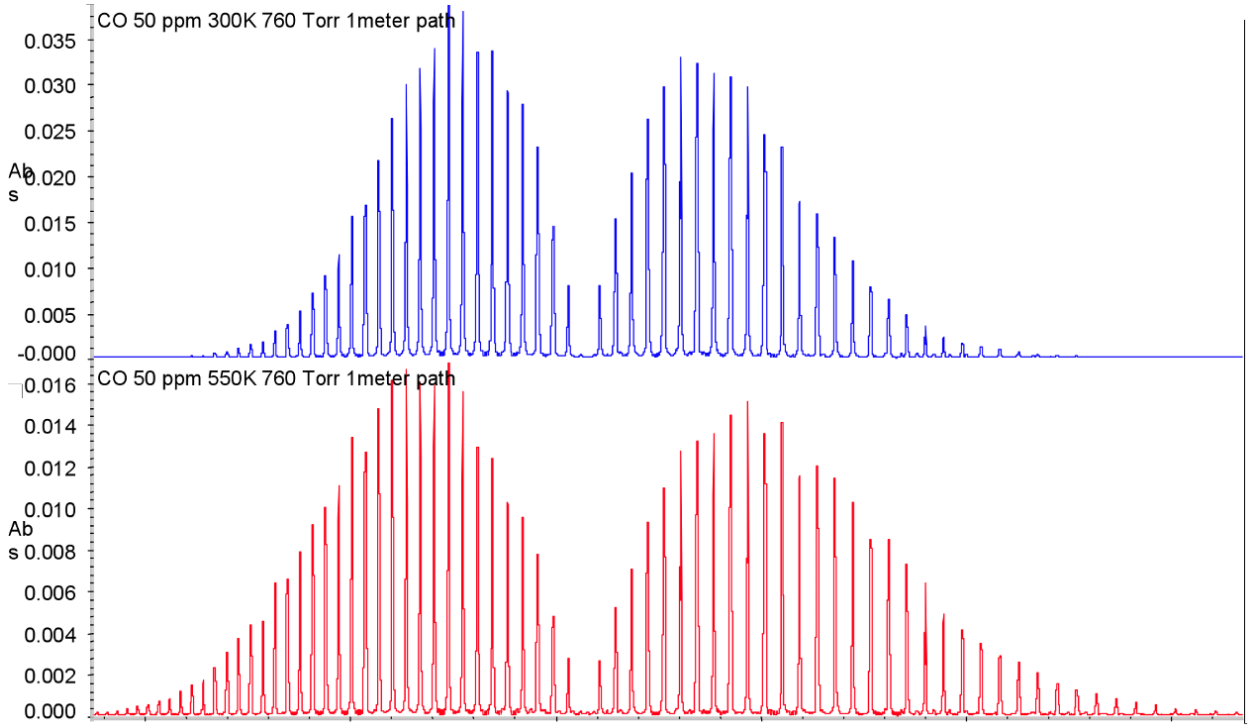

Figure A.2-3: Structure of the Fundamental CO Band at 300K (top) and 550K (bottom) showing alteration of band shape with temperature

The CO lines arise (in emission) from a transition of the molecule from a higher vibration/rotation state to a lower one. The transitions are dictated by quantum mechanics. However, the intensities of the individual lines are strongly influenced by the number of molecules in the initial state available to make the transition. This "population" of the initial states is dictated by the Boltzmann distribution which is given by:

$$N_{J"} = N_0 \cdot \frac{2 \cdot J" + 1}{Q} \cdot e^{\frac{-E"}{k \cdot T}} \qquad (5)$$

Here $N_{j"}$ is the number of molecules in the initial rotational state defined by the rotational quantum number $J"$. N_0 is the total number of molecules available, $E"$ the energy of the initial state, k Boltzmann's constant, T the absolute temperature, and Q a "partition sum." The partition sum is just the sum of the exponential term over all possible energy levels. If the log of the measured intensity of the CO lines is plotted against the initial state energy, the plot is linear and its slope is proportional to

$$\frac{hc}{kT} \qquad (6)$$

Where h is Planck's constant and c the speed of light.

Temperature can therefore be determined by measuring the slope of the plot. An example of this process is shown in Figure A.2-4. In this case the temperature was 225°C and the group of lines to the left in Figure A.2-4 was used. These are defined as the R-branch lines of the CO band.

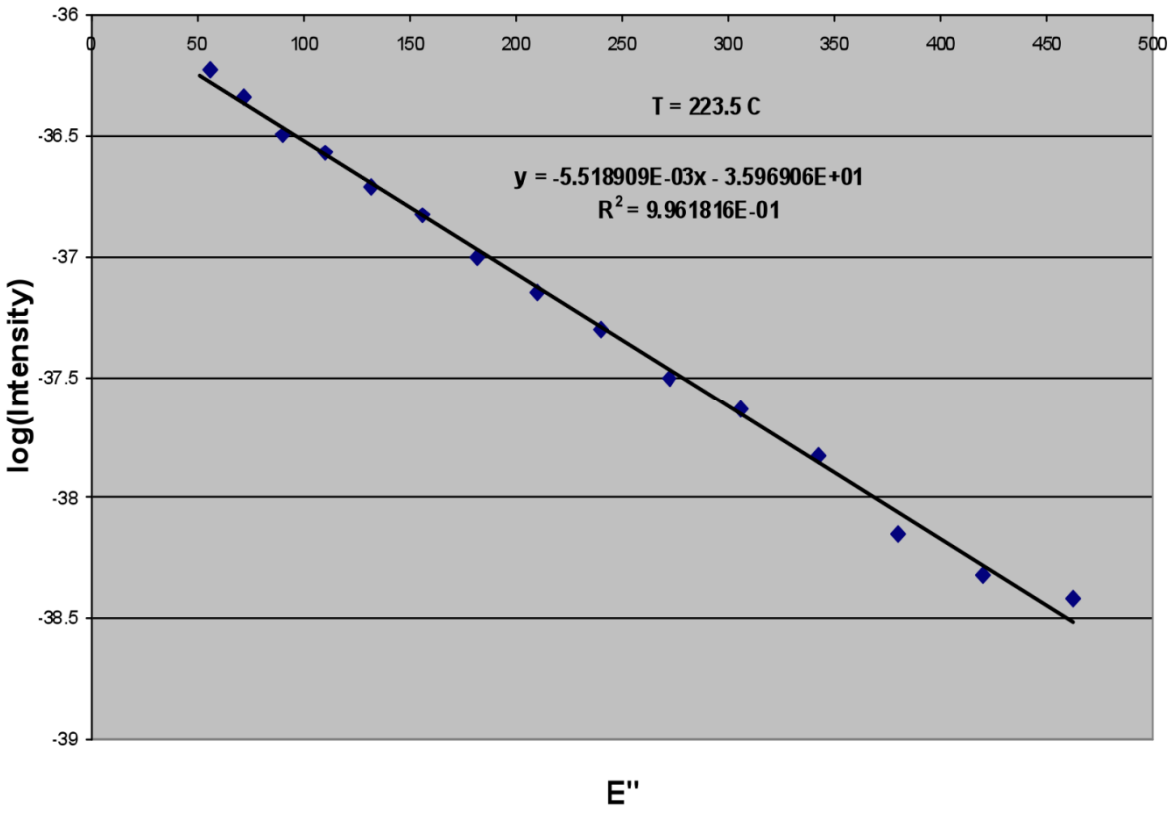

Figure A.2-4 Plot of the log of the measured intensity of the CO lines vs. initial state energy

Given temperature, all terms in Equation (3) can be determined. Equation (3) represents the transmission spectrum, just as would be observed if an active FTIR were used and an IR beam propagated through the plume. As a result, the same algorithms used in normal spectroscopy can be used to analyze this transmission spectrum.

A.2-4 From Transmission to Absorption Spectra

As in normal absorption spectroscopy, the transmission is exponential in gas concentration. That is transmission is given by:

$$\tau_{plume} = e^{-K(\nu)\cdot c\cdot l} \qquad (7)$$

Where $K(\nu)$ is the absorption coefficient for the spectral line, c the gas concentration, and l the path length in the gas. Effectively $K(\nu)$ is the reference standard in the FTIR for the gas being monitored. Taking the negative log of this equation gives what is called Absorbance. For historical reasons, log base 10 is used and thus gives:

$$Absorbance(\nu) = (0.434) \cdot K(\nu) \cdot c \cdot l \quad (8)$$

Where the constant 0.434 is the log base 10 of e. Absorbance is linear in concentration times path length and the absorbance spectrum is analyzed using standard Classical Least Squares (CLS) procedures to get the individual gas concentrations in the spectrum.

A.3 Vent Gas Composition

Marathon Petroleum Company
Detroit Refinery - CP Flare
PFTIR Flare Test - July 2010

Vent Gas
Component Distribution

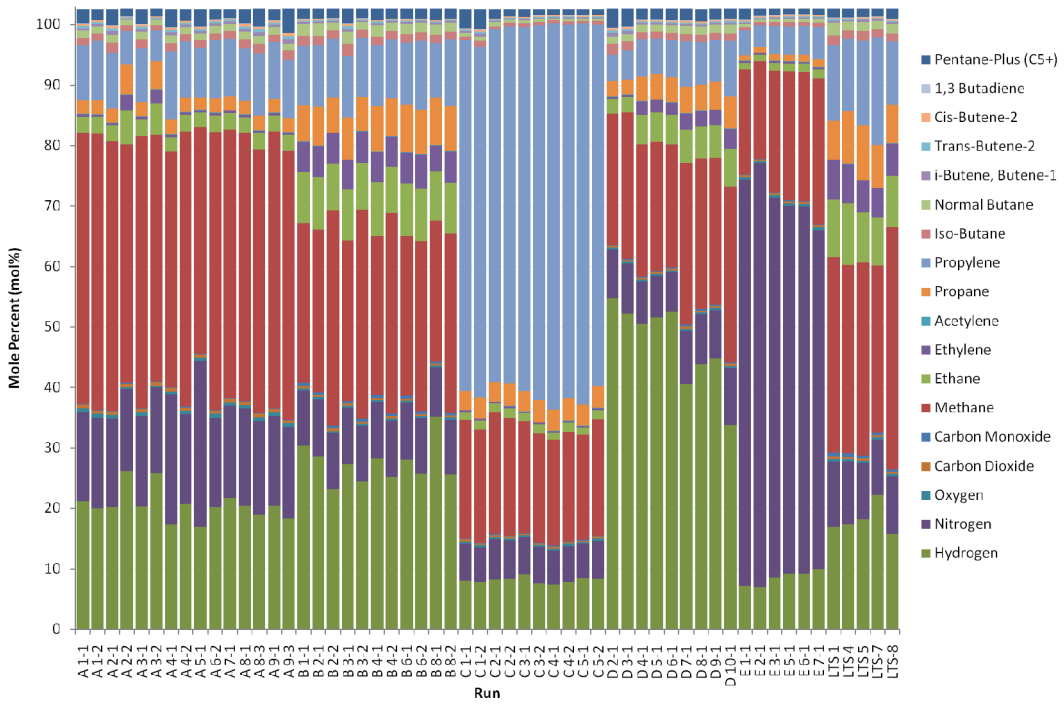

Marathon Petroleum Company
Detroit Refinery - CP Flare
PFTIR Flare Test - July 2010

Vent Gas Component
Net Heating Value Contribution

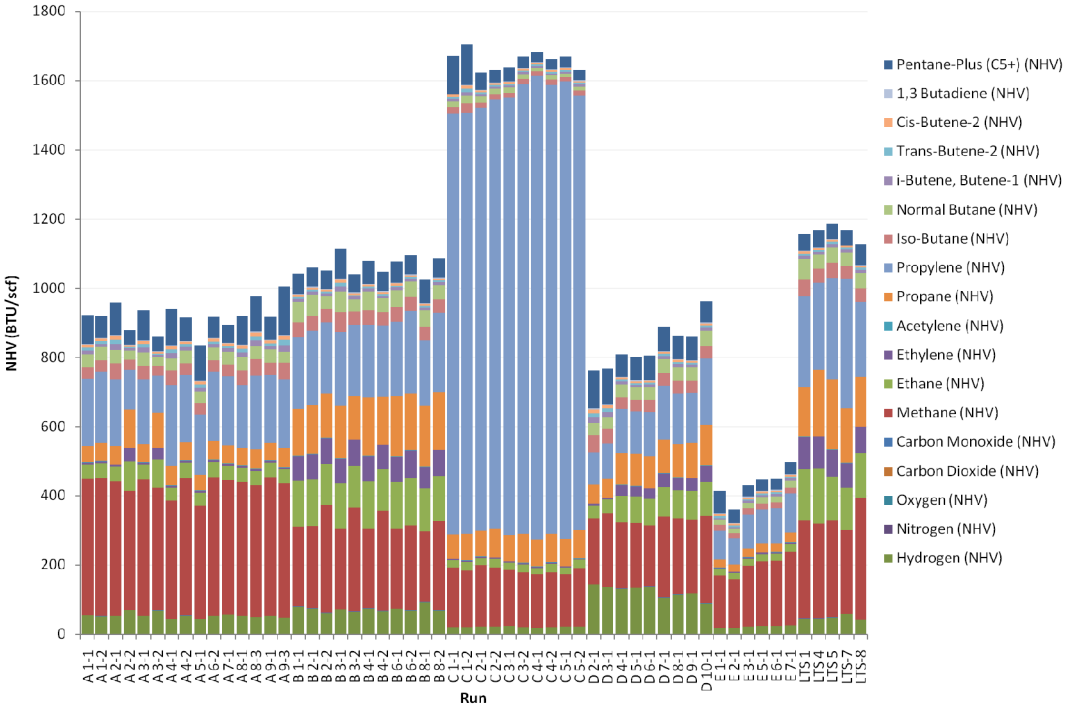

Condition	Run	Hydrogen (mol%)	Nitrogen (mol%)	Oxygen (mol%)	Carbon Dioxide (mol%)	Carbon Monoxide (mol%)	Methane (mol%)	Ethane (mol%)	Ethylene (mol%)	Acetylene (mol%)	Propane (mol%)	Propylene (mol%)	Iso-Butane (mol%)	Normal Butane (mol%)	i-Butene, Butene-1 (mol%)	Trans-Butene-2 (mol%)	Cis-Butene-2 (mol%)	1,3 Butadiene (mol%)	Pentane-Plus (C5+) (mol%)	Total (mol%)	Mol Wt (lb/lb-mol)
A	1-1	21	15	1	1	0	45	3	0	0	2	9	1	1	0	0	0	0	2	103	21.2
A	1-2	20	15	1	1	0	46	3	0	0	2	10	1	1	0	0	0	0	2	103	21.2
A	2-1	20	15	1	1	0	45	3	0	0	2	9	2	1	1	0	0	0	3	103	21.9
A	2-2	26	14	0	0	0	39	6	3	0	5	5	1	1	0	0	0	0	1	103	19.7
A	3-1	20	15	1	1	0	45	3	0	0	2	9	1	1	0	0	0	0	2	103	21.5
A	3-2	26	14	0	1	0	41	5	2	0	5	5	1	1	0	0	0	0	1	103	19.5
A	4-1	17	22	1	1	0	39	2	0	0	3	11	1	1	1	0	0	0	3	103	23.5
A	4-2	21	15	1	1	0	45	3	0	0	2	9	1	1	0	0	0	0	2	103	21.0
A	5-1	17	28	1	0	0	38	2	0	0	2	8	1	1	0	0	0	0	3	103	23.1
A	6-2	20	15	1	1	0	46	3	0	0	2	10	1	1	0	0	0	0	2	103	21.1
A	7-1	22	15	1	1	0	44	3	0	0	2	10	1	1	0	0	0	0	1	103	20.7
A	8-1	20	16	1	1	0	44	3	0	0	2	9	1	1	1	0	0	0	2	103	21.5
A	8-3	19	16	1	1	0	44	3	0	0	3	10	2	1	1	0	0	0	3	103	22.6
A	9-1	20	15	1	1	0	46	3	0	0	2	9	1	1	0	0	0	0	2	103	21.1
A	9-3	18	15	1	1	0	44	3	0	0	2	9	2	1	1	1	0	0	4	103	23.0
B	1-1	30	9	0	0	0	26	9	5	0	6	10	2	2	0	0	0	0	2	103	21.7
B	2-1	29	9	0	0	1	27	9	5	0	6	10	2	2	0	0	0	0	2	103	22.2
B	2-2	23	9	0	0	0	36	8	5	0	6	10	1	1	0	0	0	0	2	103	22.0
B	3-1	27	9	0	0	0	27	8	5	0	7	10	2	2	1	0	0	0	2	103	23.3
B	3-2	25	9	0	0	0	35	8	5	0	6	10	1	1	0	0	0	0	2	103	21.8
B	4-1	28	9	0	0	1	26	9	5	0	8	10	1	2	0	0	0	0	2	103	22.5
B	4-2	25	9	0	0	0	33	8	5	0	6	10	1	1	0	0	0	0	2	103	21.9
B	6-1	28	9	0	0	1	26	9	5	0	8	10	1	2	0	0	0	0	2	103	22.5
B	6-2	26	9	0	0	0	28	9	6	0	7	11	1	2	0	0	0	0	2	103	22.9
B	8-1	35	8	0	0	0	23	8	4	0	8	9	1	2	0	0	0	0	2	103	20.9
B	8-2	26	9	0	0	0	30	8	5	0	8	11	1	1	0	0	0	0	2	103	22.6
C	1-1	8	6	0	0	0	20	1	0	0	3	58	1	1	0	0	0	0	3	102	34.0
C	1-2	8	6	0	0	0	19	1	0	0	3	58	1	1	0	0	0	0	3	103	34.6
C	2-1	8	7	0	0	0	20	1	0	0	3	58	1	1	0	0	0	0	1	102	33.2
C	2-2	8	6	0	0	0	19	2	0	0	4	59	1	1	0	0	0	0	1	102	33.3
C	3-1	9	6	0	0	0	18	1	0	0	3	60	1	1	0	0	0	0	1	102	33.3
C	3-2	8	6	0	0	0	18	1	0	0	4	62	1	1	0	0	0	0	1	102	33.9
C	4-1	7	6	0	0	0	18	1	0	0	3	64	0	0	0	0	0	0	1	102	34.2
C	4-2	8	6	0	0	0	18	2	0	0	4	62	1	0	0	0	0	0	1	102	33.8
C	5-1	8	6	0	0	0	17	1	0	0	4	63	0	0	0	0	0	0	1	102	33.8
C	5-2	8	6	0	0	0	19	2	0	0	4	60	1	0	0	0	0	0	1	102	33.2
D	2-1	55	8	0	0	0	22	3	0	0	2	4	2	1	1	0	0	0	3	103	15.3
D	3-1	52	8	0	0	0	24	3	0	0	2	5	1	1	0	0	0	0	3	103	15.5
D	4-1	50	7	0	0	0	22	5	2	0	4	6	1	1	0	0	0	0	2	103	16.0
D	5-1	52	7	0	0	0	21	5	2	0	4	6	1	1	0	0	0	0	2	103	15.7
D	6-1	53	7	0	0	0	20	5	2	0	4	6	1	1	0	0	0	0	2	103	15.7
D	7-1	40	9	0	0	0	27	5	3	0	4	7	1	1	0	0	0	0	2	103	18.3
D	8-1	44	8	0	0	0	25	5	3	0	4	7	1	1	0	0	0	0	2	102	17.6
D	9-1	45	8	0	0	0	24	5	3	0	5	7	1	1	0	0	0	0	2	103	17.4
D	10-1	34	9	0	0	0	29	6	3	0	5	9	1	1	0	0	0	0	2	103	20.1
E	1-1	7	67	0	0	0	17	1	0	0	1	4	1	0	0	0	0	0	2	103	26.2
E	2-1	7	70	0	0	0	16	1	0	0	1	4	0	0	0	0	0	0	1	103	25.9
E	3-1	9	63	0	0	0	20	1	0	0	1	5	1	1	0	0	0	0	1	103	25.3
E	5-1	9	61	0	0	0	21	1	0	0	1	5	1	1	0	0	0	0	1	103	25.0
E	6-1	9	61	0	0	0	21	1	0	0	1	5	1	1	0	0	0	0	1	103	25.0
E	7-1	10	56	0	0	0	24	1	0	0	1	5	1	1	0	0	0	0	1	103	24.6
LTS	1	17	11	0	0	1	32	10	6	0	6	12	2	2	0	0	0	0	1	103	24.8
LTS	4	17	10	0	0	1	31	10	7	0	9	12	1	1	0	0	0	0	1	103	24.9
LTS	5	18	9	0	0	0	32	8	5	0	9	14	2	1	0	0	0	0	1	103	24.9
LTS	7	22	9	0	0	0	28	8	5	0	7	18	1	1	0	0	0	0	1	103	24.4
LTS	8	16	10	0	0	0	40	8	5	0	6	10	1	2	0	0	0	0	2	103	23.8

Condition	Run	Hydrogen (NHV)	Nitrogen (NHV)	Oxygen (NHV)	Carbon Dioxide (NHV)	Carbon Monoxide (NHV)	Methane (NHV)	Ethane (NHV)	Ethylene (NHV)	Acetylene (NHV)	Propane (NHV)	Propylene (NHV)	Iso-Butane (NHV)	Normal Butane (NHV)	I-Butene, Butene-1 (NHV)	Trans-Butene-2 (NHV)	Cis-Butene-2 (NHV)	1,3 Butadiene (NHV)	Pentane-Plus (C5+) (NHV)	Total NHV	Vg NHV Ref
A	1-1	56	0	0	0	0	392	42	5	1	49	192	35	37	11	9	8	2	83	923	914
A	1-2	53	0	0	0	0	399	43	5	1	52	206	33	37	10	8	7	2	63	920	911
A	2-1	53	0	0	0	0	389	42	5	1	53	192	47	39	16	13	11	2	94	959	951
A	2-2	69	0	0	0	1	344	87	38	1	111	115	28	27	6	4	4	2	43	880	870
A	3-1	54	0	0	0	0	394	43	6	1	52	188	39	38	14	11	9	2	87	937	928
A	3-2	68	0	0	0	1	356	81	32	1	103	107	27	26	5	4	4	2	42	860	849
A	4-1	46	0	0	0	0	341	38	5	1	56	234	41	35	15	11	10	2	105	941	932
A	4-2	55	0	0	0	0	398	43	6	1	53	194	34	36	10	8	7	2	67	915	907
A	5-1	44	0	0	0	0	328	36	5	1	46	174	34	32	12	10	9	2	102	835	824
A	6-2	53	0	0	0	0	401	43	5	1	55	199	34	37	10	8	7	2	61	918	909
A	7-1	57	0	0	0	0	387	42	6	1	52	201	33	36	10	8	7	2	52	895	885
A	8-1	54	0	0	0	0	387	41	5	1	50	182	41	38	14	11	10	2	84	921	912
A	8-3	50	0	0	0	0	381	41	5	1	56	215	47	38	16	13	11	2	104	979	972
A	9-1	54	0	0	0	0	399	43	5	1	52	197	34	37	10	8	7	2	67	918	908
A	9-3	48	0	0	0	0	388	41	5	1	54	199	48	32	18	16	13	2	139	1005	999
B	1-1	80	0	0	0	2	231	132	71	1	134	207	44	59	8	6	6	2	59	1042	1037
B	2-1	75	0	0	0	2	236	135	73	1	143	213	45	60	8	6	6	2	56	1060	1056
B	2-2	61	0	0	0	1	311	120	73	1	130	204	39	38	7	5	5	2	54	1051	1046
B	3-1	72	0	0	0	1	232	132	69	1	154	213	57	59	15	11	9	2	86	1114	1110
B	3-2	65	0	0	0	1	302	119	74	1	126	205	38	36	7	5	5	2	53	1041	1036
B	4-1	74	0	0	0	2	230	137	73	1	168	210	43	54	9	6	6	2	65	1079	1075
B	4-2	66	0	0	0	1	290	119	71	1	139	204	40	39	7	5	5	2	56	1047	1042
B	6-1	74	0	0	0	2	231	134	74	1	175	214	41	49	8	6	6	2	61	1077	1073
B	6-2	68	0	0	0	2	245	136	81	1	165	238	40	45	8	5	5	2	56	1097	1093
B	8-1	92	0	0	0	1	203	125	63	1	176	188	40	47	8	6	5	2	67	1025	1019
B	8-2	67	0	0	0	1	259	129	74	1	167	230	38	43	7	5	5	2	56	1086	1082
C	1-1	21	0	0	0	0	172	21	3	1	70	1218	17	17	7	6	6	2	109	1671	1683
C	1-2	21	0	0	0	0	164	23	4	1	77	1217	29	20	12	10	9	2	116	1704	1717
C	2-1	22	0	0	0	0	177	22	4	1	73	1222	16	18	6	5	5	2	50	1624	1636
C	2-2	22	0	0	0	0	170	25	4	1	82	1240	16	16	6	5	5	2	36	1631	1643
C	3-1	24	0	0	0	0	162	21	3	1	76	1263	15	15	6	5	5	2	39	1638	1650
C	3-2	20	0	0	0	0	158	23	4	1	83	1299	16	15	6	5	5	2	32	1669	1682
C	4-1	19	0	0	0	0	154	19	3	1	77	1341	13	9	6	5	5	2	30	1684	1697
C	4-2	21	0	0	0	0	159	24	4	1	82	1297	15	13	6	5	5	2	30	1663	1676
C	5-1	22	0	0	0	0	152	19	3	1	78	1322	14	10	6	5	5	2	31	1669	1683
C	5-2	22	0	0	0	0	169	25	4	1	81	1255	15	12	6	5	5	2	29	1630	1642
D	2-1	144	0	0	0	0	189	39	4	1	56	93	50	35	16	13	11	2	111	763	750
D	3-1	137	0	0	0	0	212	40	4	1	55	102	43	34	13	11	10	2	102	767	755
D	4-1	133	0	0	0	1	190	77	31	1	91	127	35	37	8	6	5	2	66	810	799
D	5-1	136	0	0	0	1	185	76	30	1	93	121	34	36	7	6	6	2	66	800	789
D	6-1	138	0	0	0	1	177	76	30	1	93	127	35	37	8	6	5	2	70	805	794
D	7-1	107	0	0	0	1	233	85	38	1	97	157	36	40	8	6	6	2	70	889	879
D	8-1	116	0	0	0	1	217	83	36	1	96	147	36	40	8	7	6	2	69	864	853
D	9-1	118	0	0	0	1	212	84	36	1	102	143	35	39	7	6	6	2	67	859	849
D	10-1	89	0	0	0	1	253	98	47	1	117	192	37	43	8	7	6	2	61	963	955
E	1-1	19	0	0	0	0	152	18	4	1	22	85	16	14	7	6	6	2	63	413	390
E	2-1	18	0	0	0	0	141	17	3	1	20	77	14	12	6	5	5	2	39	360	337
E	3-1	23	0	0	0	0	176	20	4	1	25	98	17	16	6	5	5	2	34	432	411
E	5-1	24	0	0	0	0	186	21	4	1	26	98	18	18	6	5	5	2	33	447	426
E	6-1	24	0	0	0	0	187	21	4	1	26	100	18	18	6	5	5	2	32	449	428
E	7-1	26	0	0	0	0	212	23	4	1	28	112	19	19	6	5	5	2	34	497	477
LTS	1	44	0	0	0	2	283	148	93	1	144	262	47	59	10	7	6	2	48	1158	1155
LTS	4	46	0	0	0	2	272	158	94	1	192	252	40	42	7	5	5	2	49	1167	1166
LTS	5	48	0	0	0	1	279	128	76	1	202	293	46	43	10	7	6	2	45	1187	1186
LTS	7	58	0	0	0	1	242	124	70	1	157	374	37	40	8	6	5	2	44	1168	1167
LTS	8	41	0	0	0	1	350	132	76	1	142	218	38	45	9	6	6	2	60	1128	1124

A.4 Personnel Involved with Flare Performance Test

Marathon Petroleum Company, LP

Jim Wilkins
Bill Ewing
Emily Barron
Honor Sheard
Keith Boyd
Bryan Duryee
Chris Bowman
Nicholas Sagonowsky
Crystal Davis
Ruth Cade
Lucy Thurston
Joe Marra
Thomas Roman
Hank Weimer
John Van Oenen
Tim Price
Tim Sipple
Gary Lincks
Brian Wilt
Trisha Ethridge

Clean Air Engineering, Inc.

Daniel Roesler
Scott Evans
Volker Schmid
Jim Wright

Industrial Monitor and Control Corporation (IMACC)

Dr. Robert Spellicy
Mark Sloss

John Zink Company, LLC

Jim Franklin
Zach Kodesh

A.5 Minute Data of Runs

Minute data spreadsheets and charts are located on the digital media provided with this report.

A.6 Video Camera Descriptions

During the test program, a total of seven video cameras recorded flare activity from the lot and road locations (see Section 2.4.3 for location information). At the beginning of the test program, four infrared cameras and two visible light cameras were used. However, one of the infrared cameras became unusable after the first day, so it was replaced by another type of infrared camera for the remainder of the test program. This appendix describes the video cameras used. Appendix A.7 contains the video taken by these cameras.

NEC/Mikron TH5104

This infrared camera was used as an aiming camera for the PFTIR at the lot location. It was mounted on the PFTIR telescope. The PFTIR operator used the image from this camera to aim the instrument. An examination of this video stream gives an indication of PFTIR aiming accuracy. Figure A.6-1 shows an example image from this camera. The crosshair (added for this report) shows the area analyzed by the lot PFTIR (see Section 2.4.3 for road and lot location descriptions).

Figure A.6-1: Image from NEC/Mikron TH5104

Agema Thermovision 510

This infrared camera was an aiming camera for the PFTIR at the road location. It was mounted on the PFTIR telescope. The PFTIR operator used the image from this camera to aim the instrument. An examination of this video stream gives an indication of the PFTIR aiming accuracy. Figure A.6-2 shows an example image from this camera. The image quality of this aiming camera is much lower than the lot location aiming camera. Because of decreasing image quality, the camera became unusable after the first day of testing. It was replaced by a FLIR A320 camera at the road location. The FLIR A320 camera became the road location aiming camera for the rest of the test program.

Figure A.6-2: Image from Agema Thermovision 510

FLIR A320

This infrared camera was used as a stationary thermal camera at both lot and road locations. It captured a general thermal view of the flare during the test program. It has a broad spectral range from 7.5 to 13 microns (1333 to 769 wavenumbers). The temperature scale on the camera was not calibrated for transparent gases, so any temperatures shown were considered relative indicators only. Figure A.6-3 shows an example image from the FLIR A320 camera. At the end of the first day of testing the aiming camera at the road location became unusable, so the FLIR A320 camera at that location replaced the old aiming camera and was mounted on the PFTIR at the road location. The FLIR A320 at the road location was used as the PFTIR aiming camera for the remainder of the test program. Figure A.6-4 shows an example image of the FLIR A320 camera being used as the aiming camera at the road location. A FLIR GasFindIR camera was used for the stationary thermal camera at the road location after the FLIR A320 camera was moved to the aiming camera mount.

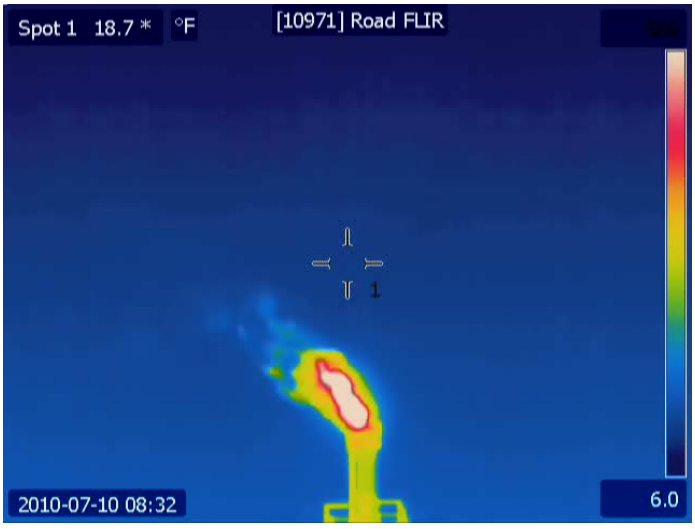

Figure A.6-3: Image from FLIR A320 – Lot Location Stationary

Figure A.6-4: Image from FLIR A320 – Road Location Aiming

FLIR GasFindIR

This infrared camera replaced the stationary FLIR A320 camera at the road location after the FLIR A320 was moved to the aiming mount at the end of the first day. The GasFindIR camera operates in a spectral range of 3 to 4 microns (3333 to 2000 wavenumbers) and is mainly used for leak detection. It is not designed as a general thermal image camera. Figure A.6-5 shows an example image from the GasFindIR camera at the road location. Note that much of the flare flame overexposes the camera, creating a washed out image. This camera replaced the FLIR A320 when the FLIR replaced the malfunctioning aiming camera at the road location.

Figure A.6-5: Image from FLIR GasFindIR

Axis Q1755

This visible light camera was used as a stationary visual camera at both the road and lot locations. The HD cameras provided a detailed visible light image of the flare operation. The purpose of the Axis Q1755 cameras was to provide a visual image corresponding to the PFTIR locations during testing. Figure A.6-6 shows an example image from the Axis Q1755 camera.

Figure A.6-6: Image from Axis Q1755 – Lot Location

A.7 Video of Runs

Videos of runs are located on the digital media provided with this report.

A.8 PFTIR Raw Data and Spectra

PFTIR raw data and spectra are located on the digital media provided with this report.

A.9 Flare Visual Rating Data Sheets

Scanned copies are located on the digital media provided with this report.

A.10 Gas Calibration Sheets for Field Hot Cell Checks

Scanned gas certification sheets and gas mixer log files are located on the digital media provided with this report.

A.11 CEMS Calibration Records for FCCU Stack

FCCU CEMS calibration spreadsheets are located on the digital media provided with this report.